AN INTEGRATIVE BIOPHYSICAL AND BIOANALYTICAL APPROACH FOR INVESTIGATING THE MITOCHONDRIAL LABILE IRON POOL

A Dissertation

by

MICHAEL JOHN MOORE

Submitted to the Office of Graduate and Professional Studies of
Texas A&M University
in partial fulfillment of the requirements for the degree of

DOCTOR OF PHILOSOPHY

Chair of Committee,	Paul A. Lindahl
Committee Members,	David P. Barondeau
	Vishal M. Gohil
	Frank M. Raushel
Head of Department,	Simon North

August 2017

Major Subject: Chemistry

ABSTRACT

Mitochondria contain a low-molecular-mass (LMM) pool of weakly bound iron complexes, called the labile iron pool (LIP). Although its composition and biological function remain largely uncharacterized, the LIP has been implicated in cellular iron metabolism and disease pathogenesis. In this dissertation, results obtained from Mössbauer, EPR, and UV-Vis studies were integrated with LC-ICP-MS data to investigate the chemical nature of the mitochondrial LIP.

LMM Fe, Mn, Cu, Zn, and Co complexes were detected in yeast and mammalian mitochondria. Such complexes were reproducibly observed and hypothesized to metalate mitochondrial apo-metalloproteins. The approximate mass of each complex was estimated along with its mitochondrial concentration. The predominant LMM Fe species detected in mitochondria had a mass of ~580 Da (called Fe_{580}) and was present in both yeast and mammalian mitochondria. Increasing the Fe concentration in the medium increased the intensity of Fe_{580}. Interestingly, the mitochondrial concentration of Fe_{580} was ~100 μM, which was consistent with previous estimates of the mitochondrial LIP. Thus, Fe_{580} was hypothesized as the cytosolic iron species that is imported into mitochondria to form the LIP. Treatment with metal chelators demonstrated that Fe_{580} was labile.

A yeast strain lacking mitochondrial Fe importers, Mrs3/4, was characterized using biophysical and bioanalytical methods (ΔΔ). Respiring Fe-deficient ΔΔ cells exhibited a "slow-growth" phenotype that was ameliorated under Fe-sufficient conditions. ΔΔ cells accumulated more Fe than wild-type (WT) cells, even under Fe-sufficient conditions,

indicating Fe dysregulation. ΔΔ cells accumulated NHHS Fe^{II} and Fe^{III} in the cytosol and vacuoles, respectively. Fe-deficient ΔΔ mitochondria accumulated Fe^{III} oxyhydroxide nanoparticles and were devoid of central doublet ($[Fe_4S_4]^{2+}$ and LS Fe^{II} hemes), whereas Fe-sufficient ΔΔ mitochondria contained comparable levels of central doublet but less NHHS Fe^{II} relative to WT. This suggested the mitochondrial NHHS Fe^{II} pool was reduced in Fe-sufficient ΔΔ cells. Fe_{580} was absent in Fe-deficient ΔΔ mitochondria but present under Fe-sufficient conditions. Two candidate masses {664.46 and 665.46 amu} and {685.39 and 686.39 amu} were determined for Fe_{580}. Viewed comprehensively, this study provides strong evidence that the mitochondrial NHHS Fe^{II} pool is composed predominantly of Fe_{580} and that the size of this pool controls cellular Fe homeostasis.

DEDICATION

To the world's best parents, Donna and Gregory Moore, for putting up with my shenanigans over the years and for always answering my phone calls.

ACKNOWLEDGEMENTS

The completion of this dissertation would not have been possible without generous assistance and support from several valued individuals. Above all, I owe an enormous debt of gratitude to my research advisor, Dr. Paul A. Lindahl, for welcoming me into his laboratory and providing me with every opportunity, advantage, and resource to succeed in my academic endeavors. I could not have asked for a better, more patient advisor to help guide me through the Ph.D. process. From the very beginning, he gave me the freedom to explore various projects, encouraged me through times of difficulty, and made himself available whenever I needed direction or advice. To say I have benefited a great deal from learning under his tutelage would be an understatement. I would also like to thank my committee members—Dr. Frank Raushel, Dr. David Barondeau, and Dr. Vishal Gohil—for sharing their time, expertise, feedback, and insightful suggestions with me over the course of this research.

I would like to extend many thanks to past and present members of the Lindahl Lab, for their camaraderie, intellectual input, and overwhelming moral support throughout the years. I am particularly grateful to the following people: to former lab mates, Drs. Mrinmoy Chakrabarti, Allison Cockrell, Jinkyu Park, and Nema Jhurry, for their help in learning experimental techniques and procedures and for always being receptive to my questions, especially during my salad days with the group; to my REU mentor, Dr. Gregory Holmes-Hampton, for teaching me the precious art of isolating mitochondria; to my graduate school mentor and former colleague, Dr. Sean McCormick, for taking the

time to educate me on the ins and outs of the LC-ICP-MS system; and to current group members, Josh, Trang, Nate, Cody, and Joel, for their help with lab chores, constructive ideas in group meetings, and positive words of encouragement. It has been an honor and a privilege working with each of you, and I wish all of you the best of luck in life (and science)!

In addition, I would like to thank the outstanding administrative and support staff of the Texas A&M Department of Chemistry for their dedicated service and professionalism throughout the years, which made life as a graduate student that much easier. Thanks to collaborators, Dr. Andrew Dancis and Dr. Doyong Kim, for their valuable contributions to this dissertation. Thank you to the entire Lindahl family for extending such gracious hospitality to me during their awesome dinner parties. I would like to express special thanks to all my friends—the old ones back home and the new ones here in Texas—for always keeping my spirits high and for the good times, great adventures, and amazing memories we shared along the way.

Thank you to my girlfriend, Ngoc Huynh, for loving me the past three years and most importantly, for lending me her computer to write this dissertation after mine crashed. I also want to thank Ngoc's family in Austin, Minh and Carl Graves and Thien Huynh, for their love and generous hospitality and for feeding me every other weekend.

Thank you to my family for their constant love and encouragement, especially my wonderful parents, Donna and Gregory Moore, who served as my sounding board, editors, and support system through it all. You both mean the moon to me!

CONTRIBUTORS AND FUNDING SOURCES

Contributors

This work was supervised by a dissertation committee consisting of Professor Paul A. Lindahl and Professors David P. Barondeau and Frank M. Raushel of the Department of Chemistry and Professor Vishal M. Gohil of the Department of Biochemistry and Biophysics.

The *Saccharomyces cerevisiae* wild-type (WT) BY4741 strain used in Chapter III and the WT W303 and Mrs3/4 double-deletion (ΔΔ) strains used in Chapter IV were generously provided by Dr. Andrew Dancis (University of Pennsylvania). The LC-ICP-MS system employed in Chapter III and IV was designed and built by a previous lab member, Dr. Sean McCormick (Ferris State University). In addition, Dr. McCormick analyzed LC-ICP-MS data and prepared the figures and tables in Chapter III. Mössbauer and EPR spectra in Chapter IV were simulated and analyzed by a current lab member, Mr. Joshua Wofford (Texas A&M University). Mr. Wofford also prepared the Mössbauer and EPR figures in Chapter IV, calibrated and maintained the Mössbauer spectrometers, and assisted with the collection of EPR and Mössbauer data. ESI-MS spectra in Chapter IV were collected by Dr. Doyong Kim (Texas A&M University).

All other work conducted for the dissertation was completed by the student independently.

Funding Sources

This work was made possible in part by the National Institutes of Health under Grant Number GM084266 and the Robert A. Welch Foundation under Grant Number A1170. Its contents are solely the responsibility of the authors and do not necessarily represent the official views of the National Institutes of Health or the Robert A. Welch Foundation. Graduate study was supported by a Heep Fellowship from the Texas A&M University Institute for Advanced Study.

NOMENCLATURE

AD	Alzheimer's disease
ADP	adenine diphosphate
Afg3	ATPase family gene 3
AMP	adenine monophosphate
Atm1	ABC transporter of the mitochondrion
ATP	adenine triphosphate
BPS	Bathophenanthroline disulfonate
Ccc1	Fe transport protein on the vacuolar membrane
CIA	cytosolic iron-sulfur cluster assembly
CD	central doublet
Cu_L	a 13 kDa nonproteinaceous Cu species found in mitochondria
CV	column-volume
DDDI	double-distilled and deionized
DTT	dithiothreitol
EGTA	ethylene glycol tetraacetic acid
ERV1	essential for respiration and viability
ESI-MS	electrospray ionization mass spectrometry
EPR	electron paramagnetic resonance
Fe_{cyt}	cytosolic iron
Fe_{med}	iron contained in the growth medium

FTS	flow-through solution
GSH	glutathione (reduced)
GSSG	glutathione disulfide (oxidized)
HMM	high-molecular-mass (> 10 kDa)
Hot13	helper of Tim
HS	high-spin
ICP-MS	inductively coupled plasma mass spectrometry
IM	inner membrane of mitochondria
IMS	intermembrane space
ISC	iron-sulfur cluster
LC	liquid chromatography
LC-ICP-MS	a system consisting of an LC interfaced online to an ICP-MS
LIP	labile iron pool
LMM	low-molecular-mass (< 10 kDa)
LMP	labile metal pool
LS	low-spin
mARC1/2	mitochondrial amidoxime reducing components isoforms 1 and 2
MAS1/2	β and α subunits of MPP
Mia40	mitochondrial intermembrane space import and assembly
MB	Mössbauer
MCF	mitochondrial carrier family
Moco	molybdopterin cofactor

MPP	mitochondrial processing peptidase
Mrs3/4	Mrs3 and Mrs4 (two homologous Fe importers on the IM)
MUT	methyl-malonyl-CoA
NP	ferric oxyhydroxide nanoparticles
NHHS	non-heme high-spin
OD_{600}	optical density measured at 600 nm
OM	outer membrane of mitochondria
PD	Parkinson's disease
Phen	1,10-phenanthroline
PLP	pyridoxal 5'-phosphate
PMSF	phenylmethanesulfonylfluoride
RT	room temperature
ROS	reactive oxygen species
SEC	size-exclusion chromatography
SME	soluble mitochondrial extract
SO	sulfite oxidase
Sod	superoxide dismutase
Tim	translocase of the inner membrane
Tom	translocase of the outer membrane
UV-Vis	ultraviolet-visible
VDAC	voltage-dependent anion channel
V_0	void volume

V_e	elution volume
WT	wild-type
$WT1_{BPS}$	Wild-type cells grown on 25 μM BPS + 1 μM Fe
WT1	Wild-type cells grown on 1 μM Fe
WT10	Wild-type cells grown on 1 μM Fe
WT40	Wild-type cells grown on 1 μM Fe
YL0	yeast, low OD_{600}, injected following preparation (t = 0)
YL5	yeast, low OD_{600}, injected 5 days after preparation (t = 5)
YH0	yeast, high OD_{600}, injected following preparation (t = 0)
YH5	yeast, high OD_{600}, injected 5 days after preparation (t = 5)
YRL0	yeast, respiring, low OD_{600}, injected following preparation (t = 0)
YPD	standard rich growth medium for yeast containing glucose
YPAD	rich growth medium for yeast containing glucose and adenine
α	exponential growth rate
δ	isomer shift
ΔE_Q	quadrupole splitting
ΔΔ	Mrs3/4 double-deletion mutant yeast strain
$\Delta\Delta 1_{BPS}$	Mrs3/4 double-deletion cells grown on 25 μM BPS + 1 μM Fe
ΔΔ1	Mrs3/4 double-deletion cells grown on 1 μM Fe
ΔΔ10	Mrs3/4 double-deletion cells grown on 10 μM Fe
ΔΔ40	Mrs3/4 double-deletion cells grown on 40 μM Fe

TABLE OF CONTENTS

Page

ABSTRACT ii

DEDICATION iv

ACKNOWLEDGEMENTS v

CONTRIBUTORS AND FUNDING SOURCES vii

NOMENCLATURE ix

TABLE OF CONTENTS xiii

LIST OF FIGURES xvi

LIST OF TABLES xviii

CHAPTER

I INTRODUCTION AND LITERATURE REVIEW 1

Mitochondria as "Hubs" of Metal Metabolism 1
Labile Metal Pools within Mitochondria 5
Evaluation of Current Research Strategies 6
Implications in Disease Pathogenesis 9
Low-Molecular-Mass Metal Complexes in Mitochondria 11
Copper 12
Zinc 15
Manganese 19
Cobalt 22
Molybdenum 22
Iron 24
Objectives 28

II MATERIALS AND METHODS 30

Biophysical Methods Used 30
Mössbauer Spectroscopy 31
EPR Spectroscopy 33

UV-Vis Spectroscopy 35
Inductively Coupled Plasma Mass Spectrometry 36
Application of LC-ICP-MS System for Bioanalytical Studies 37
Chemicals, Buffers, and Standards 40
Yeast Strains and Media 41
Growth and Preparation of Whole Cell Samples 44
Isolation of Mitochondria 45
Preparation of LMM Mitochondrial Flow-Through Solutions 49
ESI-MS Experiment 52
Metal Concentration Analysis 52

III DETECTION OF LABILE LOW-MOLECULAR-MASS TRANSITION METAL COMPLEXES IN MITOCHONDRIA 54

Introduction 54
Results 57
LC-ICP-MS Characterization of FTSs 63
Phosphorus 66
Sulfur 67
Zinc 67
Manganese 69
Iron 71
Copper 73
Cobalt 76
Molybdenum 76
Lability of LMM Metal Complexes 78
Discussion 78

IV AN INTEGRATIVE ANALYSIS OF *MRS3*Δ*MRS4*Δ SACCHAROMYCES CEREVISIAE UNDER IRON-DEFICIENT AND IRON-SUFFICIENT CONDITIONS 91

Introduction 91
Results 94
The ΔΔ Slow-Growth Phenotype 94
Iron Concentrations in ΔΔ Cells and Mitochondria 97
Mössbauer Spectra of Whole Cells and Isolated Mitochondria 98
UV-Vis and EPR Investigations 106
LC-ICP-MS of ΔΔ Mitochondrial FTSs 110
Electrospray Ionization Mass Spectrometry (ESI-MS) of Fe_{580} 112
Relationship Between Fe_{1100} and Fe_{580} 112
Effect of Mrs3/4 Deletion on Other Metals 114
Discussion 119

V CONCLUSIONS AND FUTURE WORK 125

Conclusions 125
Future Work 130

REFERENCES 133

LIST OF FIGURES

Page

Figure II-1 Calibration curve for determining molecular masses based on the migration through size-exclusion column. 38

Figure II-2 Verification of Mrs3/4 double-deletion (ΔΔ) yeast strain. 43

Figure III-1 Phosphorus chromatograms of LMM mitochondrial FTSs. 64

Figure III-2 Sulfur chromatograms of LMM mitochondrial FTSs. 68

Figure III-3 Zinc chromatograms of LMM mitochondrial FTSs. 68

Figure III-4 Manganese chromatograms of LMM mitochondrial FTSs. 70

Figure III-5 Iron chromatograms of LMM mitochondrial FTSs. 72

Figure III-6 Copper chromatograms of LMM mitochondrial FTSs. 74

Figure III-7 Cobalt chromatograms of LMM mitochondrial FTSs. 77

Figure III-8 Molybdenum chromatograms of LMM mitochondrial FTSs. 77

Figure III-9 Lability of LMM metal complexes. 79

Figure III-10 Model of LMM metal complex speciation in yeast and mammalian mitochondria. 80

Figure IV-1 Growth rates of WT and ΔΔ cells. 95

Figure IV-2 Mössbauer spectra of respiring whole cells. 100

Figure IV-3 Mössbauer spectra of mitochondria isolated from ΔΔ and WT cells. 102

Figure IV-4 UV-Vis spectra of mitochondria isolated from respiring WT and ΔΔ cells. 107

Figure IV-5 X-band EPR spectra of respiring ΔΔ and WT cells. 108

Figure IV-6 Iron chromatograms of LMM FTSs prepared from WT and and ΔΔ mitochondrial extracts. 111

Figure IV-7 Electrospray ionization mass spectrometry of Fe_{580}-containing LC fractions. 113

Figure IV-8 Relationship between Fe_{1100} and Fe_{580}. 115

Figure IV-9 Copper chromatograms of LMM FTSs prepared from WT and and ΔΔ mitochondrial extracts. 116

Figure IV-10 Manganese chromatograms of LMM FTSs prepared from WT and and ΔΔ mitochondrial extracts. 117

Figure IV-11 Zinc chromatograms of LMM FTSs prepared from WT and and ΔΔ mitochondrial extracts. 118

LIST OF TABLES

Page

Table II-1 Compounds used for calibrating the size-exclusion columns. 39

Table III-1 Nomenclature of LC batches. 58

Table III-2 Concentrations of selected elements in isolated mitochondria. 60

Table III-3 Average concentrations of selected elements in mitochondria. 61

Table III-4 Concentrations of selected elements present as LMM species in isolated mitochondria. 62

Table III-5 LMM metal complexes and P and S compounds in mitochondria. 65

Table IV-1 Metal concentrations in whole cells and isolated mitochondria. 96

Table IV-2 Summary of Fe percentages and concentrations determined by Mössbauer spectroscopy. 99

CHAPTER I

INTRODUCTION AND LITERATURE REVIEW*

Mitochondria as "Hubs" of Metal Metabolism

Mitochondria are fundamental organelles found in almost all eukaryotic cells. In addition to their prominent and well-established role in cellular energy transduction, mitochondria serve as major "traffic hubs" for an array of transition metals. Redox-active transition metals, including iron, copper, manganese, cobalt, and molybdenum (as well as redox-inactive zinc) are typically bound at the active sites of enzymes where they help catalyze diverse biochemical reactions. Their excellent catalytic properties derive from (a) the availability of d orbitals to participate in redox chemistry and bonding, (b) the abundance of coordination sites that can accommodate and orient multiple substrates, and (c) the weakness of coordinate bonds that promotes facile binding and release of substrates, intermediates, and products. Metals also serve as integral structural and functional components in a large class of proteins, called metalloproteins.

A significant number of metalloproteins and enzymes are distributed throughout the mitochondria. These organelles contain respiratory complexes and respiration-related proteins that are packed with iron-sulfur clusters (ISCs) and heme centers. In fact, both ISC assembly and the Fe insertion step of heme biosynthesis occur within this subcellular

---

* Adapted with permission from Paul A. Lindahl and Michael J. Moore (2016) Labile Low-Molecular-Mass Metal Complexes in Mitochondria: Trials and Tribulations of a Burgeoning Field, *Biochemistry 55*, 4140–4153. Copyright 2016 American Chemical Society.

compartment.[1] Mitochondria house copper-containing proteins such as cytochrome c oxidase, Cu/Zn superoxide dismutase (Cu/Zn Sod1), and the many chaperones that shuttle Cu to these two enzymes during their assembly.[2,3] Mitochondria possess an important manganese-containing enzyme, namely superoxide dismutase (MnSod2).[4] Mammalian mitochondria also contain arginase II, a dimanganese enzyme.[5,6] Approximately 15% of the cobalt in mammalian cells is localized to mitochondria,[7] most of which is bound at the active site of methyl-malonyl-CoA mutase (MUT). A small portion of mitochondrial Co is coordinated to trafficking proteins that install adenosylcobalamin into apo-MUT. Mammalian mitochondria contain three molybdenum metalloenzymes, including sulfite oxidase and mitochondrial amidoxime reducing component isoforms 1 and 2 (mARC1 and -2, respectively).[8] Mitochondria house numerous zinc-containing proteins, the best known of which include Cu/Zn Sod1 and cytochrome c oxidase.[3,9,10] In yeast, alcohol dehydrogenase III (ADH3) is a Zn metalloenzyme that is involved in NAD(P)H redox balance and the ethanol–acetaldehyde shuttle under anaerobic conditions.[11,12] Zn-bound MST1 is a mitochondrial threonyl-tRNA synthetase that aminoacylates two tRNAs.[25] D-lactate dehydrogenase is a Zn-containing enzyme that catalyzes the oxidation of lactate to pyruvate,[13] and the Zn-dependent enzyme glyoxalase II promotes the hydrolysis of S-D-lactoylglutathione into glutathione and D-lactate within the matrix.[14] α-Isopropylmalate synthase I and II are Zn enzymes that catalyze the first step of leucine biosynthesis.[15] Both of these enzymes are regulated by the Zn-dependent reversible inactivation by coenzyme A, which links leucine biosynthesis to mitochondrial energy metabolism.[16] Zn-bound MST1 is a mitochondrial threonyl-tRNA synthetase that aminoacylates two tRNAs.[17]

Virtually all mitochondrial proteins are encoded in the nucleus, synthesized on ribosomes in the cytosol, and imported into mitochondria via protein translocation machines.[18,19] Many nascent unfolded proteins are threaded through the TOM (translocase of the outer mitochondrial membrane) complex and then sorted according to their final intramitochondrial destinations.[20] The imported proteins that are targeted for the matrix typically contain a presequence that is cleaved by mitochondrial processing peptidase (MPP), a reaction that triggers protein folding. Numerous Zn-containing metalloproteases are involved in these processes. Mas1/2 is the MPP metalloendopeptidase that cleaves presequences from the majority of imported mitochondrial proteins.[21] Oct1 is a matrix intermediate metallopeptidase that cleaves destabilizing N-terminal residues of some proteins after cleavage by MPP.[22] Afg3 is a subunit of the ATP-dependent m-AAA metalloprotease found in the inner membrane of mitochondria (IM).[21] Yme1 is the Zn-containing catalytic subunit of the i-AAA metalloprotease complex; this IM enzyme helps degrade unfolded or misfolded mitochondrial proteins.[23] Cym1 and Prd1 are lysine-specific metalloproteases that degrade proteins and presequences.[22] Other Zn-containing proteins are involved in protein import or folding. ZIM17 (zinc finger motif protein of 17 kDa) helps import and fold proteins entering the matrix.[24] MDJ1 stimulates the ATPase activity of the Hsp70 protein Ssc1p and helps fold or refold proteins in the matrix. This Zn-containing protein helps form mitochondrial nucleoids and maintain mtDNA stability.[25] Zn-containing TIM9 and TIM10 (translocases of the inner mitochondrial membrane) form a hexameric complex in the intermembrane space (IMS) that delivers hydrophobic proteins to the TIM22 complex for insertion into the IM.[26] Binding of Zn to

Cys residues stabilizes these proteins and prevents oxidation to disulfides. Newly imported IMS proteins TIM10, TIM12, and TIM13 bind Zn and interact with Mia40 for folding and oxidation.[27] Mia40 is an IMS protein that coordinates Zn.[28] The Zn bound to these small TIM proteins may be transferred onto Mia40 during oxidation (a process that traps these proteins in the IMS). Zn bound to reduced Mia40 may inhibit its reoxidation by Erv1. IMS protein Hot13 may remove Zn from Mia40 to aid in its reoxidation.[29] However, the small TIM proteins may not be importable with Zn bound, suggesting an alternative role for Hot13.[30]

The folding of nascent apo-metalloproteins within the matrix is typically accompanied by the incorporation of metal ions or centers. The question is how these metals reach the matrix. Metals en route to the matrix must first pass across the outer membrane of mitochondria (OM), which may occur via simple diffusion through the hydrophilic pores of VDACs (voltage-dependent anion channels). VDACs, also known as porins, are integral membrane proteins that constitute ~30% of the OM surface area,[31] creating pores with diameters of 2 – 3 nm.[32] Metabolites with masses of less than ~5000 Da, including water, ions, ATP/ADP, and perhaps metal species, can freely diffuse through VDACs, whereas import of larger compounds is regulated. In contrast to the OM, the IM is notoriously impermeable to most small metabolites and ions, such that even protons are unable to diffuse across it under normal conditions. In all likelihood, metal ions are translocated from the IMS into the matrix by specific transport proteins embedded in the IM.[3,33] Similar issues arise for metalloproteins targeted to other mitochondrial locations; specific metal complexes must be used, and there must be distinct transport

systems that guide them to the appropriate location within the organelle so that they can metalate their targets. Thus, metalation reactions in the IMS are likely different from those in the matrix, which may be especially important for Zn and Cu trafficking.

Labile Metal Pools within Mitochondria

The discovery of metallochaperone proteins in the 1990s suggested that upon entering the cell, transition metals are trafficked to their respective target proteins by being passed from one metallochaperone to another, like a baton handed from one runner to the next in a relay race. In addition to metallochaperones, cells utilize a variety of proteins that modulate metal homeostasis and delivery to apoproteins, including metal storage proteins,[34] metal-sensing proteins,[35] and metal-inserting enzymes.[36] Thus, aqueous metal complexes (sometimes erroneously called "free" metal ions) or other non-protein-bound metal complexes were not thought to exist in cells.[37-39] However, this view has evolved over the years because of the detection of labile metal pools (LMPs) within cells and mitochondria.

Labile metal pools are defined as collections of endogenous metal ions bound weakly to various low-affinity nonproteinaceous ligands. Such pools have been termed "bioavailable pools," "chelatable pools," or "exchangeable pools" (often interchangeably) throughout the literature. The first documented mention of a labile metal pool appeared in a 1949 report by Greenburg and Wintrobe,[40] and was further described by Jacobs,[41] as a transient intracellular iron pool that exists as a metabolic intermediate between iron uptake from the extracellular environment and iron incorporation into iron-containing

compounds. Since then, labile pools of iron,[42] zinc,[43] and copper[44] have been identified in mitochondria. Mitochondrial LMPs are thought to exist because of the continuous demand for metals to be available for the biosynthesis of metal-containing proteins and enzymes, inducing metal ion uptake from the cytosol into the matrix compartment. The concentration of the metals in such pools is relatively low (micromolar to nanomolar range), accounting for only a minor fraction of the total mitochondrial metal content. As such, the majority of metals in mitochondria are tightly associated with metalloproteins. Concentrations of LMPs may be important in regulating cellular metal homeostasis via metal-sensing proteins under metal-deficient and -sufficient states.[35]

Many of the details concerning the nature, structural composition, and physiological role of LMPs remain obscure. As a result, the number of metal compounds constituting LMPs as well as the identities of endogenous ligands are unknown. Although their exact cellular functions are uncharacterized, LMPs likely participate in trafficking, regulation, signaling, and/or storage of metal ions.[45,46] Given their lability (and low concentrations in mitochondria), determining the structures and functions of the metal complexes that compose these pools has been, and continues to be, a considerable challenge.

Evaluation of Current Research Strategies

Two general strategies, in combination with genetic and spectroscopic methods, have been used to investigate labile metal pools in mitochondria. The most popular strategy entails custom-designed chelators that are localized to mitochondria and bind

specifically (or at least preferentially) to a particular metal. These chelator-based sensors, or probes, must be hydrophilic enough to be soluble in aqueous regions of the cell, yet lipophilic enough to traverse membranes. Satisfying these criteria is a formidable endeavor that requires considerable synthetic abilities. Fluorescence associated with these molecular probes either increases, decreases, or shifts upon metal coordination. A key property of most fluorescent probes is that the signal response is ratiometric and affords an estimation of the labile metal concentration. The major advantage of this strategy is that it is relatively non-disruptive with respect to the integrity of the cell itself, which is particularly useful for monitoring dynamic changes to LMPs in live, intact biological samples (e.g., tissues, cells, or isolated organelles). Also, this method provides valuable *in vivo* snapshots of LMPs with high spatial and temporal resolution. Custom-engineered chelator sensors are highly tunable and designed to probe a dynamic range of concentrations. As sensors become more specific and sophisticated, they will become more helpful in understanding the cellular function of LMPs.

The alternative strategy for investigating LMPs is to fractionate and identify individual metal complexes via liquid chromatography (LC). LC is an effective bioanalytical technique that offers several different mechanisms of chemical separation. Different types of LC can be combined to yield separations with higher degrees of purity. The application of inductively coupled plasma mass spectrometry (ICP-MS) allows for sensitive detection of various transition metals in complex sample matrices over a dynamic concentration range. This approach is the most direct method to characterize metal complexes and is limited to those that do not decompose during chromatographic workup.

Evidence of decomposition would include chromatography peaks corresponding to aqueous ("free") metal ions or adherence to the column.

Both approaches have contributed valuable insights to the current understanding of labile metal pools in biological systems, yet each has shortcomings. A significant limitation of the chelator-based method is that the ligands associated with an endogenous metal complex are inevitably displaced when the probe coordinates the metal. Thus, chemical characterization of such complexes has not been possible and does not seem possible moving forward. Moreover, a given chelator will almost certainly interact with numerous labile metal species, perhaps including sites that are typically considered nonlabile, e.g., metalloprotein active sites. Different chelators (or even the same chelator reacting under different conditions) undoubtedly detect different LMPs. Some of these problems have been demonstrated recently with Zn sensors,[47] and other fundamental questions remain unanswered. For example, do probes targeted to mitochondria interact with labile metal centers in the cytosol en route to their target? Might the resulting metal-bound probes enter mitochondria and thus be counted (erroneously) as evidence of a mitochondrial pool? Is the concentration of the chelator that ultimately localizes to the mitochondria sufficient such that the endogenous concentration of labile metal (rather than of the chelator itself) dictates the extent of reaction and thus the observed pool size? Many of these questions have been raised,[45,47,48] but they must be settled experimentally before confidence can be placed in the results obtained by this approach.

A major drawback of the chromatography-based strategy is that the structural integrity of cells and organelles are compromised during the isolation of metal complexes.

As a result, cellular contents are mixed together, which can promote side reactions involving these labile metals, giving rise to artifacts. Thus, LC peaks observed in chromatograms might be artifacts of the isolation procedure. Past LC studies of metal complexes have been plagued with a lack of demonstrated reproducibility in chromatograms, which is a serious concern. Unfortunately, metal complexes are difficult to isolate because of their lability and low concentrations. There is also a lack of commercially available technologies (e.g., chromatography columns) designed and optimized to help isolate these complexes from biological extracts. Another problem is that isolated mitochondria may not be pure, and contaminating species from other cellular compartments can confuse analyses. Typically, the purity of these organelles is assessed by microscopy and Western blots. Ascertaining the cellular function of a metal complex that has been isolated from mitochondria is difficult. However, additional information can be obtained by fractionating mitochondria into subcomponents.[49]

Overall, the chelator-based strategy may be better suited for addressing functional aspects of LMPs, whereas the chromatography-based approach may be better suited for cataloging and chemically characterizing individual metal complexes that compose LMPs. Ultimately, complementary insights from both approaches will be needed to adequately characterize LMPs and to elucidate their physiological roles.

Implications in Disease Pathogenesis

Disruption of metal ion homeostasis in the mitochondria has been implicated in the pathogenesis of several human diseases and disorders. In particular, perturbations in

the concentrations of LMPs may be linked with pathological consequences. At the cellular level, excessive concentrations of labile redox-active metals such as iron, copper, and cobalt can induce oxidative stress in living systems by generating ROS (reactive oxygen species) like hydrogen peroxide and superoxide radical. ROS are toxic to the cell because of their propensity to destroy critical biomolecules including proteins,[50] DNA,[51] and lipids.[52] Metal-induced oxidative stress has been associated with triggering the onset of ageing and cancer. The deleterious potential of metals can be nullified by stimulating their incorporation into the active sites of recipient apoproteins. Clearly, adequate levels of bioavailable metal pools are required for the efficient metalation of mitochondrial proteins and enzymes. With this in mind, diminished concentrations of LMPs can lead to detrimental mismetalation of protein targets, leading to their inactivation. These damaging effects caused by misregulation of homeostatic concentrations of LMPs are suspected factors in disease progression.

Elevated levels of labile zinc, copper, and iron pools are suspected to play a significant role in causing neurodegenerative disorders such as Alzheimer's disease (AD) and Parkinson's disease (PD).[53-56] Increased levels of zinc may induce the aggregation of beta amyloid plaques in the brain, which happens to be one of the most prominent characteristics associated with AD.[57] Misregulation of copper and iron pools is thought to contribute in the pathogenesis of AD and PD. Excess levels of these labile metals are connected with the formation of metal-bound protein aggregates that facilitate the accumulation of beta amyloid plaques in AD[58] and Lewy bodies in PD.[59,60] Aside from neurodegenerative conditions, disruption of iron homeostasis is considered to participate

in cancer formation and pathogenesis of cardiovascular diseases via ROS-mediated toxicity.[61] For instance, the labile iron pool may play a role in the development of atherosclerosis—one of the leading risk factors for coronary heart disease—by catalyzing the production of ROS, which can oxidize low density lipoproteins forming the plaque deposits within arterial walls.[62]

Labile metal pools have long been suspected to play key roles in the etiology and progression of various diseases. Their link to disease has been predominantly based on the general mechanism that LMPs, when present in excess levels, are able to generate ROS known to induce extensive cellular damage. However, after decades of research on these pools, no studies have successfully established a direct causative link to disease pathogenesis. Elucidating the roles and molecular complexes associated with LMPs will therefore be instrumental to understanding how they participate in pathology. Such investigations into the chemical nature of bioavailable metal pools offer significant potential for clinical therapeutic applications.

Low-Molecular-Mass Metal Complexes in Mitochondria

Mitochondrial labile metal pools are thought to be comprised of low-molecular-mass (LMM) metal complexes—defined here as having masses of less than 10 kDa—that are, for the most part, nonproteinaceous. Simple monodentate ligands tend to exchange rapidly when coordinated to first-row d-block metal ions. For example, aqueous Mn^{II}, Fe^{II}, Co^{II}, Cu^{II}, and Zn^{II} complexes have water-exchange rates ranging from 10^6 to 10^9 sec^{-1}.[63] Unfortunately, this lability makes isolating and characterizing such complexes difficult.

Ligand-exchange kinetics are slowed dramatically when metals coordinate to large polydentate ligands (e.g., protein metal binding sites). As a result, most metals bound in proteins are relatively inert except for the open coordination sites to which substrates bind. Non-protein-bound LMM metal complexes tend to be more labile, though there are exceptions to this tendency. For instance, metals that are bound to metallochaperone carrier proteins must be sufficiently labile to facilitate delivery to downstream intracellular targets. Also, some metalloenzymes contain labile metal centers.[64] Other exceptions are siderophores, LMM organic chelating agents secreted by certain microorganisms to sequester trace amounts of Fe^{III} from the environment.[65] These LMM iron complexes are generally inert, except at low pH.

In this review, we detail recent discoveries and highlight current controversies surrounding labile LMM metal complexes in mitochondrial biochemistry.

Copper

Initial studies by Winge, Cobine, and co-workers concluded that 70 – 85% of mitochondrial Cu is associated with a LMM complex found in the matrix called CuL.[44,66] An elaborate isolation procedure is employed to purify CuL. Cellular extracts are treated with 100% methanol. The resulting extracts are dried and resuspended in aqueous solutions before being loaded onto an anion-exchange column. Fractions containing the CuL apo ligand are dried and resuspended in water prior to injection onto a C18 reverse-phase column. Ligand-containing fractions elute in the middle of a methanol gradient and are subsequently screened for fluorescence.[67] Cu^{I} is added to fractions containing the

purified apo ligand, resulting in the formation of CuL as indicated by fluorescence quenching. The material obtained from this rather involved procedure, defined as CuL, is soluble, anionic, and stable to boiling and migrates on size-exclusion columns like a globular protein with a mass of 13,000 Da.[44] However, CuL exhibits no absorption at 280 nm and is unaffected by proteinase K treatment, suggesting that it is nonproteinaceous. In terms of biological significance, Winge and Cobine view the CuL pool as a reservoir or "dynamic rheostat" that is used to buffer intracellular copper levels. They hypothesize that the Cu in CuL is ligated by small metabolites such as organic acids or nucleotides. They suggest that the CuL ligand prevents mitochondrial Cu from damaging ISCs that are generated in the matrix.

These researchers hypothesize that CuL is originally produced in the cytosol and imported into the matrix by Pic2[67] and Mrs3,[68] both of which are MCF members. They conclude that Pic2 mediates the transport of Cu into the matrix, which is supported by the observation that Δpic2 cells exhibit a growth phenotype on synthetic Cu-deficient nonfermentable medium (whereas growth on Cu-sufficient media shows no phenotype). Moreover, increasing the amount of silver ions in the growth medium, which directly compete with Cu ions, exacerbates the growth defect. The rate of Cu uptake in Δpic2 mitochondria is nearly half that for wild-type (WT) mitochondria. Consistent with this, the concentration of Cu within mitochondria from Δpic2 cells is only ~70% relative to that in WT mitochondria. Together, these results infer the existence of an alternative mitochondrial Cu transport protein, presumably Mrs3.[68]

Other aspects of mitochondrial copper metabolism occur in the IMS.[69] During assembly of cytochrome c oxidase, Cu is transported into the IMS where it is incorporated into the Cu_B and Cu_A sites of the enzyme using a variety of required ancillary proteins. Metalation of Cu/Zn Sod1 also occurs within the IMS and is mediated by the Cu chaperone Ccs1.[4] The form of Cu that enters the IMS and the compartment from which it enters remain unresolved. Winge and Cobine conclude that CuL is shuttled into the IMS from the matrix by an unidentified IM carrier.[66,68] However, with a mass of 13,000 Da, CuL is too large to diffuse through a carrier protein channel.[70] Another possibility is that Cu from the cytosol is directed into the IMS by Cox17, a soluble 8 kDa protein containing a Cu^I center coordinated by three conserved cysteines.[71-75] Indeed, this protein is found in both the IMS and cytosol.[73] However, Cox17 is translocated into the IMS by the Mia40 oxidative folding pathway, meaning that it arrives in the IMS as an unfolded apoprotein.[76,77] Moreover, Maxfield et al. demonstrated that tethering Cox17 to the IM affords normal cytochrome c oxidase activity,[78] indicating that it does not import Cu from the cytosol. The Cu trafficking pathway downstream of Cox17 is better characterized. Cox17 supplies Cu to Cox11 (34 kDa) and Sco1 (33 kDa) through specific protein-protein interactions. Other small soluble Cu binding IMS proteins involved in the metalation of cytochrome c oxidase include Cox19 (11 kDa) and Coa6 (12 kDa).[79,80]

Labile Cu pools in mitochondria have been detected by chelator-based sensors. Yang et al.[81] used a membrane-permeable copper-selective fluorescent probe along with X-ray fluorescence microscopy to detect and characterize a labile pool of low-coordinate Cu^I with sulfur-based ligands in mitochondria of fibroblasts that had been pretreated with

a high concentration of $CuCl_2$. Cu-based signals were nearly undetectable in samples that were not treated in this manner, which raises concern that newly imported copper arising from the Cu treatment was detected, rather than endogenous Cu in the organelle. Nevertheless, the authors concluded that their results "strongly support" the presence of an endogenous labile Cu pool within the mitochondrial matrix. In this case, substantial amounts of the Cu matrix pool should have also been found in mitochondria of cells grown on medium that was not spiked with Cu, a condition for which Yang et al. detected little Cu intensity.[81]

Better evidence of endogenous labile Cu in mitochondria is provided by Dodani et al.,[82] who similarly employed a mitochondrially-targeted Cu sensor to detect labile copper pools within the organelle. Fluorescence increased 34% in live, intact cells that had been incubated in high concentrations of $CuCl_2$. Conversely, emission decreased 36% after a strong Cu chelator had been added, which presumably entered the mitochondria and coordinated endogenous Cu in the organelle. Giuffrida et al. developed a water-soluble highly selective fluorescent Cu^I probe that is specific for mitochondria.[83] No significant effects on cell viability were observed after neuroblastoma cells had been treated with large doses of this chelator. This confirms that the sensor does not damage the cell, but it also raises doubts that it chelates a form of Cu that is physiologically relevant.

Zinc

Winge, Eide, and co-workers have also detected and isolated a cationic LMM Zn pool in mitochondrial extracts.[84] The pool is stable to boiling and proteinase K digestion,

suggesting that it is not proteinaceous. Under Zn-sufficient growth conditions, approximately half of mitochondrial Zn is soluble, and a significant portion of this comprises the Zn pool. When cells are grown on high-Zn medium, the size of the pool increases significantly. Reducing the size of the pool (by genetically inserting a Zn-requiring alcohol dehydrogenase apoprotein into the matrix, which then incorporates Zn from the pool during metalation) causes cells to have difficulty respiring. This suggests that the Zn pool is required for respiration.

Labile Zn pools in mitochondria have also been identified using fluorescent probes. Tomat et al.[85] synthesized a Zn-sensitive chelator that was targeted to the mitochondria of HeLa cells. In their study, they observed a dramatic increase in fluorescence intensity after cells were treated with 10 – 50 μM $ZnCl_2$. Sensi et al. detected a pool of labile Zn ions in mitochondria from mammalian neuronal cells.[43] This pool was in dynamic exchange with a labile cytosolic Zn pool, and its size increased in cells grown on medium supplemented with Zn.[43,86] High levels of cytosolic Zn induce loss of mitochondrial membrane potential ($\Delta\Psi_m$), perhaps by opening IM channels or pores. Malaiyandi et al. used sensors to monitor the uptake of exogenously added Zn in the matrix of mitochondria isolated from rat brains.[87] Zn^{2+} was imported via a Ca^{2+} uniporter in a process that required $\Delta\Psi_m$. Zn^{2+} can also be imported into mitochondria via ZnT-type IM transporters, e.g., ZnT2 in mammalian systems.[9,87-91]

In the study by Malaiyandi et al., targeted mitochondria exhibited a weak fluorescent response, inferring low endogenous levels of labile Zn.[100 87] Treatment with Zn caused a sudden increase in emission, which indicated an increase in the size of the

labile Zn pool. Emission quickly returned to baseline levels, suggesting that mitochondria can rapidly export excess Zn, perhaps via the ZIP8 transporter in mammals.[91] Zn enters mitochondria only when supraphysiological amounts are added. $\Delta\Psi_m$ decreases when mitochondria are treated with high levels of Zn, presumably because Zn binds to the exterior of the organelle.[92] The effect of Zn on the mitochondrial permeability transition pore differs from that of calcium.[93,94]

High concentrations of mitochondrial Zn, obtained by either incubating isolated mitochondria in solutions spiked with excess Zn or using genetic strains that disrupt Fe metabolism, can have deleterious effects. Fe^{III} nanoparticles accumulate in the mitochondria of yeast cells lacking the frataxin homologue (Yfh1), which also contain deficient amounts of ISCs and hemes.[95] What is less commonly realized is that Zn-protoporphyrin IX accumulates in mitochondria from this same strain.[96,97] This probably occurs because mitochondrial Fe^{II}, which in WT cells is used by ferrochelatase to metalate protoporphyrin IX, has been converted into oxidized nanoparticles that cannot be installed. Under these conditions, Zn^{II} can substitute for Fe^{II} in the ferrochelatase reaction. The mismetalation of Zn does not arise because of excess Zn^{II}; in fact, Δyfh1 cells import only a fraction of the Zn imported by WT cells.[98] Rather, misincorporation arises because of the scarcity of Fe^{II}.[88] Accordingly, Zn-protoporphyrin is also observed in Fe-deficient cells.[88,96,97,99] Curiously, excess $ZnSO_4$ in the medium (a) prevents the accumulation of Fe in mitochondria of Δyfh1 cells, (b) increases the growth rate of this strain, and (c) mitigates ROS damage. Surprisingly, these responses are not caused by an increase in ISC or heme synthesis, which makes them difficult to explain. Accumulation of Fe in ISC mutants is

thought to arise from insufficient ISC (and/or heme) biosynthesis. Lower-than-normal ISC/heme biosynthetic activities are thought to diminish the rate of export of X-S, the unknown sulfur-containing product that is a cytosolic signaling molecule for these mitochondrial processes. X-S has been posited to regulate cellular Fe import via a signaling pathway involving glutaredoxins and the transcription factors Aft1/2.[100] The fact that Zn added to the exterior of mitochondria suppresses this regulatory mechanism implies that it can functionally substitute for X-S, but how this might work is not obvious. Excess Zn inhibits the TCA cycle, decreases the rate of respiration, inhibits the respiratory electron transport chain,[101] and stimulates ROS production.[43,86] Gazaryan et al. found that picomolar concentrations of aqueous Zn inhibit α-ketoglutarate dependent mitochondrial respiration by inhibiting lipoamide dehydrogenase.[115 102] Perhaps these inhibitory effects indirectly regulate Fe import.

Also involved in mitochondrial Zn metabolism is Mzm1, a soluble 14 kDa protein found in the matrix that helps maintain the labile Zn pool in the matrix and stabilize respiratory complex III.[84,103] Δmzm1 mutant cells grow poorly on nonfermentable carbon sources when Zn is limited in the growth medium. Mitochondria isolated from these cells contain decreased amounts of Zn, but not Fe, Cu, Mn, or Mg. They also exhibit decreased respiratory complex III activity. Zn is also critical for autophagy.[104] Zn deficiency induces apoptosis by activating the mitochondrial cell death pathway.[88]

The concentration of labile Zn in mitochondria is reported to be extraordinarily low.[37] McCranor et al.[105] used a FRET-based biosensor derived from carbonic anhydrase II variants that were targeted to the matrix of mitochondria of mammalian cells. The

biosensor was exquisitely sensitive to and specific for labile Zn. They reported a labile Zn concentration in the matrix of ~0.15 pM! When cells were deprived of glucose and O_2 for 3 h and then reperfused in O_2, there was an initial surge in labile mitochondrial Zn (as cytosolic levels declined); mitochondrial Zn levels returned to normal after reperfusion for 2 h. In another study, Park et al.[106] used a genetically encoded protein-based Zn sensor that was targeted to mitochondria to measure the labile Zn concentration in the organelle. Zn binding induced a conformational change that was monitored by FRET. They reported a concentration of 0.14 pM for labile Zn, far lower than the concentration of the labile Zn pool in the cytosol.

Manganese

MnSod2 is directed to the mitochondrial matrix by an N-terminal targeting sequence.[107] Once inside the matrix and once the targeting sequence has been clipped, the resulting apoprotein folds with help from Hsp60/Hsp10.[108,109] In the absence of its targeting sequence, apo-Sod2 is neither folded nor metalated, suggesting that metalation occurs during folding of Sod2.

How cytosolic Mn is transported into the matrix for metalation is unknown. As a member of the MCF, Mtm1 was initially considered to be a Mn transporter and was thus named the manganese trafficking factor for mitochondrial Sod2 because cells lacking it exhibit low Sod2 activity.[98,110] Contrary to the behavior expected for this role, the concentration of Mn in the matrix was higher in Δmtm1 mutants than in WT cells. Attention turned to iron when the absence of Mtm1 was found to cause Fe to accumulate

in the matrix. Iron accumulation along with the propensity of bacterial MnSods (e.g., in *Escherichia coli* MnSod) to misincorporate Fe seemed to explain the diminished MnSod2-based activity in the Δmtm1 yeast strain. The results of initial chromatography studies of Sod2 supported the misincorporation hypothesis.[111] Namely, when Δmtm1 soluble extracts were chromatographed, most of the eluted Fe comigrated with Sod2. In chromatographs of WT extracts, most of the eluted Mn comigrated with Sod2.

An X-ray absorption spectroscopy study[112] subsequently demonstrated that the vast majority of Fe that accumulated in Δmtm1 mitochondria had not misincorporated into apo-Sod2. A corresponding Mössbauer study revealed that mitochondrial Fe accumulated as Fe^{III} oxyhydroxide nanoparticles,[113] similar to the Fe accumulation phenotypes observed in ISC mutants such as Yah1-depleted or Atm1-depleted mitochondria.[114,115] Moreover, little of the Fe that accumulated in Δmtm1 mitochondria was in a form (i.e., Fe^{II}) that could be misincorporated. Another surprise was that Fe did not accumulate in Δmtm1 cells grown anaerobically, but they did have low Sod2 activity. This indicated that the two phenomena, Fe accumulation and low Sod2 activity, were independent.[113]

Previously, Park et al. used an LC-ICP-MS system in an effort to detect misincorporated Fe Sod2. In chromatograms of extracts from Δmtm1 versus WT cells, they observed reduced protein and activity levels of MnSod2 but no increase in putative FeSod2 features.[113] Quantitative accounting of Mn concentrations and Sod2 protein levels revealed that the majority of Sod2 protein was missing in soluble fractions, suggesting that apo-Sod2 proteins in mitochondria lacking Mtm1 are less stable toward folding and metalation with Mn.

Supporting this new hypothesis was a LMM Mn species whose concentration was increased in Δmtm1 mitochondrial extracts, as would be expected if apo-Sod2 was unfolded and unstable and could not be metalated. The LMM Mn species (called Mn_{2-3}) was estimated to have a molecular mass of 2000 – 3000 Da. Mn_{2-3} was also present in WT cells, but at a concentration of just 1 μM (12% of mitochondrial Mn). In Δmtm1 mitochondria, the corresponding concentration was 22 μM (80% of mitochondrial Mn). In WT mitochondria from cells supplemented with excess $MnCl_2$, the concentration of Mn_{2-3} increased to 23 μM (there was no change in MnSod2 levels). Because MnSod2 was the only Mn-containing peak in chromatograms and Mn_{2-3} was the only LMM Mn species observed, Park et al. hypothesized that Mn_{2-3} was imported into the matrix through an unknown IM transporter and that this complex was used to metalate apo-Sod2. They further hypothesized that Mtm1 imports a species that is required for the maturation, activity, or stability of apo-Sod2, and that there is a competition of maturation and metalation versus misfolding and degradation. A recent study by Whittaker et al.[116] reveals that Mtm1 binds pyridoxal 5'-phosphate (PLP) with micromolar affinity, prompting them to conclude that Mtm1 transports PLP into the matrix. Consistent with this, PLP-dependent proteins in Δmtm1 mitochondria lack this coenzyme. Heme and ISC biosynthetic pathways depend on PLP, explaining the connection between Mtm1 and mitochondrial Fe metabolism, but how a deficiency in PLP translates into a decline in Sod2 activity in Δmtm1 cells remains a mystery; the case would be settled if mitochondria were found to contain a PLP-dependent protein that mediates the folding, maturation, and/or metalation of apo-Sod2.

Cobalt

Cobalt enters mammalian cells in the form of cobalamin, which is then transported to various intracellular locations. The cobalamin delivered to mammalian mitochondria is used to metalate apo-MUT, the only known Co-containing enzyme in this organelle.[117] However, the mitochondrial cobalamin transporter on the IM remains obscure. Once co(II)balamin reaches the matrix, it binds ATP:cob(I)alamin adenosyltransferase (MMAB), is reduced to the Co(I)balamin state, and then accepts a 5-deoxyadenosyl group from ATP.[118] MMAB then incorporates the resulting adenosylcob(III)alamin into apo-MUT.[119] MMAA, a GTPase "gatekeeping G-protein chaperone," binds MMAB and apo-MUT to regulate the installation of adenosylcob(III)alamin.[120]

Molybdenum

The mechanism by which sulfite oxidase (SO) is assembled in the IMS of mammalian mitochondria and then metalated with the molybdopterin cofactor (Moco) and heme centers has been investigated.[121] Mitochondrial localization is dictated by an N-terminal sequence that targets this protein to the IMS via the TOM complex. Upon being imported into the IMS, the targeting sequence is cleaved by mitochondrial IM peptidase, followed by the incorporation of Moco into the apo-SO protein, which initiates folding and traps the enzyme within the IMS. SO also contains heme b, but this cofactor does not play a major role in folding or trapping. How Moco is shuttled across the OM is unclear; it might pass through a transporter or just diffuse through VDAC pores. The assembly of molybdopterin requires the coordinated action of multiple enzymes in the cytosol,[122] such

that Moco is likely installed as a complete unit into mitochondrial Mo enzymes. Moco is unstable in protein-free solutions,[123] suggesting that its translocation into the IMS coincides with its insertion into apo-SO.[121] A pool of free, non-protein-bound Moco was detected in mitochondria, which might be an intermediate in the installation process.

Two Mo-containing enzymes, mARC1 and mARC2, are associated with the OM of mammalian mitochondria where they function with cytochrome b_5, NADH, and NADH-cytochrome b_5 reductase to reduce various N-hydroxylated compounds and convert nitrite ion into nitric oxide.[124-126] Both mARC1/2 proteins are small (6 – 22 kDa) and possess broad substrate specificity. Developmental expression profiles reveal distinct differences between the two isoforms, suggesting that their expression is controlled by independent regulatory mechanisms. mARC2 is only expressed in adult livers where it is involved in lipogenesis and is regulated by nutritional status. This protein may have dual localization in mitochondria and peroxisomes. mARC1 is expressed in both adult and fetal tissues.[127] It has characteristics of a typical OM protein in which the C-terminal catalytic domain is exposed to cytosol and the N-terminal domain points towards the IMS.[128] Moco in the SO family of molybdenum hydroxylases contains a Mo center coordinated by a cysteine thiolate and two oxo groups. Moco in mARC1/2 is of the SO type,[129] suggesting that the Moco unit, which is installed in both SO and mARC1/2, originates from a common source.

Iron

The most prominent mitochondrial transporters of transition metals are mitoferrins 1 and 2. Counterparts of mitoferrin 1/2, called Mrs3 and Mrs4, are present in yeast. These homologous proteins are high-affinity iron transporters situated in the IM.[130-133] They are members of the mitochondrial carrier family (MCF), which includes 53 proteins in humans and 35 proteins in yeast.[134] The physiological differences between mitoferrin 1 and 2 (or Mrs3/4) pairs have yet to be fully established. Mitoferrin 1 is an essential iron importer for developing erythrocytes, whereas mitoferrin 2 may be required for heme and ISC assembly in nonerythroid cells.[130] The iron transported through these high-affinity importers is ultimately utilized in the biosynthesis of ISC and heme cofactors.[99,135] Indeed, the majority of Fe that accumulates in mitochondria of ISC mutants (e.g., frataxin-deficient cells) passes through these carrier proteins.

Rim2, another MCF protein, translocates Fe ions and pyrimidine nucleotides.[136,137] In the absence of Mrs3/4, Rim2 has been shown to mediate the import of Fe into the matrix. Interestingly, the extent of ISC biogenesis is diminished in yeast cells that lack Mrs3/4 and Rim2 but not in cells lacking only Rim2. This implies that Rim2 is a backup low-affinity Fe importer. The non-lethality of the Mrs3/4 and Rim2 triple deletion strain implies an additional route of Fe import into mitochondria.

The Fe complexes that are recognized by these mitochondrial import proteins have not been identified. In general, MCF members transport a variety of chemically diverse substrates across the IM, such as nucleotides, amino acids, keto/carboxylic acids, phosphate ions, and cofactors. Although the structures of many MCF members, including

the mitoferrins, have not been determined, their sequences are similar enough that an approximate structure can be estimated. Mitochondrial carrier proteins have basket-shaped structures. The bottoms of these structures face the matrix side and are structurally stabilized by salt bridge networks. They have a common substrate binding site located at the midpoint of the IM.[138] Mitoferrins possess three conserved His ligands that are spatially arranged like steps of a spiral staircase to shuttle Fe^{II} ions across the membrane,[139] along with three conserved Asp/Glu residues that may participate in metal transport. Mitoferrins do not belong to any established class of MCF proteins, so their substrates are unlikely to be similar to those listed above. Nevertheless, their substrates must be small enough to fit through the narrow channels in these proteins. This excludes large metallochaperones from consideration as substrates and suggests that LMM metal complexes may serve such roles.

An early study by Tangerås et al.[140] identified a labile Fe pool in mitochondria isolated from rat livers. In their study, extracts were treated with bathophenanthroline sulfonate (BPS), a chelating agent that turns red when coordinated to Fe^{II}, thereby permitting quantification of the labile Fe^{II} concentration in their samples. Their findings suggest that ~25% of mitochondrial Fe is labile and primarily located in the matrix. In a later study, Petrat et al.[141,142] used membrane-permeable chelators to detect and quantify a labile Fe pool within mitochondria of intact whole cells. They incubated cells with fluorescent probes that penetrated into mitochondria and quenched in response to binding Fe. Subsequent treatment with a more powerful chelator removed all of the Fe bound to the sensor, concomitantly restoring the fluorescent signal. The difference in emission was

then quantified, affording labile Fe concentrations of 5 – 17 μM in rat mitochondria.[42] Mitochondria contain ~700 μM Fe,[62] so the labile Fe fraction, as quantified, corresponds to 1 – 2% of mitochondrial iron, far less than what was determined by Tangerås and co-workers. Petrat et al. postulated that the higher concentration reported in the earlier study was artifactual.[141,142]

More recently, we examined mitochondria isolated from fermenting and respiring yeast cells using Mössbauer spectroscopy,[143] which can distinguish various groups of Fe-containing species, including hemes, ISCs, and non-heme Fe. They discovered that ~20% of the iron in fermenting mitochondria (~150 μM) is present as non-heme high-spin (NHHS) Fe^{II}.[144] Membrane-impermeable chelators were unable to access this pool of iron unless mitochondria were disrupted by sonication or treated with detergent. By contrast, membrane-permeable Phen selectively chelated the NHHS Fe^{II} ions without perturbing the other Fe-containing species in the organelle. In independent studies, Lutz et al.[145] and Pandey et al.[146] developed assays for monitoring ISC biogenesis in intact mitochondria. These investigators found that treating isolated mitochondria with Phen inhibits ISC activity. They concluded that mitochondria contain a pool of labile Fe that is used as feedstock for ISC assembly. When considered with our Mössbauer results showing that NHHS Fe^{II} is selectively chelated by phen, it becomes evident that this pool of NHHS Fe^{II} is used as feedstock for ISC assembly and that it is probably transported through mitoferrin carriers.

The same pool might also be feedstock for heme biosynthesis, but further studies are required to establish this. Lange et al. concluded that Fe in the matrix is not used for

insertion into porphyrin and that Fe is supplied to ferrochelatase directly from the IM.[147] However, the subsequent structure of ferrochelatase revealed that the Fe^{II} binding site is exposed to the matrix, implying that heme Fe is contributed by a pool in this subcompartment.[148] Dancis and co-workers performed experiments demonstrating that most Fe^{II} ions used in heme biosynthesis enter the matrix through the IM mitoferrins, Mrs3/4.[99]

The coordination chemistry of iron and glutathione (GSH) may be relevant to this issue. GSH represents about ~90% of cellular LMM sulfur-containing species,[149] with 10-15% of that located in mitochondria.[150] The concentration of GSH in mitochondria is very high (10 – 14 mM).[151,152] Hider and Kong argue that an Fe^{II}(GSH) adduct is the major LMM Fe complex in the cytosol based on a high stability constant for the complex and the abundance of GSH within the cytosol.[153] A similar argument could be made for LMM Fe^{II}(GSH) adducts in the mitochondrial matrix. Citrate, another metabolite present in the matrix at high concentrations, should also be considered as a potential ligand for LMM metal complexes.[152,154]

Another aspect of iron:GSH metabolism occurring in yeast mitochondria involves the IM protein Atm1 (ABCB7 in humans). Atm1 exports a poorly defined LMM sulfur-containing species called X-S, which is used as feedstock for ISC assembly in the cytosol and as a signaling molecule that regulates the import of iron into the cell and mitochondria. The Atm1 structure has either GSH, GSSG (glutathione disulfide), or GSSH (glutathione peroxide) bound, suggesting that it catalyzes the export of these or similar molecules (e.g., the trisulfide GSSSG) into the cytosol.[155,156] GSH also coordinates Fe_2S_2 clusters, and the

$[Fe_2S_2(GS)_4]^{2-}$ complex has been proposed to be present in mitochondria and exported by Atm1.[157]

Objectives

Research in the Lindahl Lab is aimed at understanding fundamentals of iron metabolism in cells. This involves studying important iron-related cellular processes such as trafficking, homeostasis, and regulation. One of the biggest mysteries in the field of iron metabolism, standing at the nexus of these three research areas, is the mitochondrial labile iron pool (LIP). The presence of this compartmentalized endogenous pool of iron has been predominantly established with fluorescent chelator probes. Furthermore, Holmes-Hampton et al. identified a pool of non-heme high-spin (NHHS) Fe^{II} localized within yeast mitochondria via Mössbauer spectroscopy.[144] Aside from this, however, the chemical nature of the LIP remains largely uncharacterized. The primary objective of this dissertation was to implement an integrative biophysical and bioanalytical approach to investigate the mitochondrial LIP.

The iron pool is widely considered to consist of labile iron complexes weakly coordinated to nonproteinaceous LMM ligands. This is rationalized based on size restrictions imposed by the channels of essential transport proteins situated in the OM and IM. The objective in chapter III of this dissertation was to establish the presence of LMM iron complexes (i.e. < 10 kDa) in mitochondria. Additionally, we evaluated the presence of such iron species in mammalian mitochondria. LMM complexes containing other biologically relevant elements such as manganese, zinc, copper, cobalt, molybdenum,

phosphorus, and sulfur were also studied. To accomplish this goal, we utilized a bioanalytical approach involving size-exclusion chromatography (SEC) for separation and isolation of LMM complexes in mitochondria in combination with ICP-MS for multi-element detection and analysis. Moreover, this online LC-ICP-MS system was encapsulated in a refrigerated anaerobic glove box to reduce ligand-exchange and prevent oxidation of LMM iron/metal complexes. McCormick et al. used this system to detect and catalog distinct LMM metal complexes in the mouse brain and to determine their approximate molecular masses and concentrations.[158]

In *Saccharomyces cerevisiae*, two homologous proteins belonging to the mitochondrial carrier family (MCF) termed Mrs3 and Mrs4 (Mrs3/4) mediate iron uptake across the IM.[131,133] These proteins are essential for importing cytosolic iron into the matrix under iron-limiting conditions.[132] In addition, the iron transported by Mrs3/4 is ultimately utilized in the biosynthesis of ISCs and heme cofactors.[99] The identity of the endogenous iron complex transported by Mrs3/4 has not been identified. We hypothesized that Mrs3/4 import a LMM iron complex that composes a large portion of the mitochondrial labile iron pool. This hypothesis was investigated in further detail in chapter IV of this dissertation using a Mrs3/4 double-deletion (ΔΔ) mutant yeast strain. We employed biophysical techniques including Mössbauer, EPR, and UV-Vis spectroscopies to probe the iron content, distribution, and speciation in respiring Mrs3/4-deficient whole cells and isolated mitochondria. Finally, ΔΔ mitochondria were analyzed for LMM iron complexes with the aforementioned LC-ICP-MS system.

CHAPTER II

MATERIALS AND METHODS*

Biophysical Methods Used

The application of molecular genetics and biochemistry has promoted a greater understanding of iron metabolism in eukaryotic cells. In particular, such methodology has proven valuable for identifying key players involved in iron uptake, trafficking, storage, and homeostasis. Conventionally, this has been accomplished by characterizing phenotypes resulting from genetic manipulation (e.g., deletion or mutation) of a protein or enzyme of interest. Biophysical techniques have also been employed for characterization but mainly in the context of isolated protein studies.

In Chapter IV of this dissertation, several biophysical methods were used to investigate the mitochondrial labile iron pool from a systems-level perspective. The principal technique used for biophysical analysis was Mössbauer spectroscopy, while electron paramagnetic resonance (EPR) and ultraviolet-visible (UV-Vis) spectroscopy were utilized as auxiliary tools. Inductively coupled plasma mass spectrometry (ICP-MS) was employed to measure absolute metal concentrations. Clues obtained from each of these methods were integrated to form a "big picture" of the distribution and speciation of iron in whole cells and isolated mitochondria.

---

* Adapted with permission from Sean P. McCormick, Michael J. Moore, and Paul A. Lindahl (2015) Detection of Labile Low-Molecular-Mass Transition Metal Complexes in Mitochondria, *Biochemistry 54*, 3442–3453. Copyright 2015 American Chemical Society.

Mössbauer Spectroscopy

Mössbauer (MB) spectroscopy is one of the most powerful methods for investigating intracellular iron trafficking and metabolism. The principles behind MB spectroscopy, which is more specifically described as recoilless nuclear gamma-ray resonance, were discovered in 1958 by the physicist, Rudolf Mössbauer.[159] In this technique, nuclei in samples absorb gammy ray photons emitted from a radioactive source and undergo transitions to an excited nuclear spin state. The energy of emitted gamma ray photons is altered via the Doppler Effect by moving the source towards and away from the fixed sample. Typical MB spectra are plotted with the absorption intensity (or percent effect) on the y-axis and the velocity of the moving source (in units of mm/s) on the x-axis. There are only a few elements that are MB active, which requires using specific radioactive sources.

With respect to iron, MB spectroscopy can only detect ^{57}Fe (I=1/2), which is 2% naturally abundant. Thus, samples analyzed via MB must be enriched in this specific iron isotope. Gamma radiation is supplied by a radioactive ^{57}Co source, which releases a 14.4 keV photon that is absorbed by ^{57}Fe nuclei in samples. This energy induces a nuclear transition from a ground state (I=1/2) to the first excited state (I=3/2). There are six allowed transitions for ^{57}Fe nuclei dictated by the selection rules for Mössbauer.[160] MB can detect individual iron centers in isolated proteins. MB can also resolve groups of iron species in whole cells or isolated organelles. Examples of such groups include high-spin (HS) and low-spin (LS) hemes, oxidized and reduced ISCs, mononuclear non-heme Fe^{II} and Fe^{III} species, and ferric oxyhydroxide nanoparticles (NP).

Groups of Fe species are distinguished in MB spectra by spectral patterns along with unique parameters called isomer shift (δ) and quadrupole splitting (ΔE_Q). Common spectral patterns include a two-line quadrupole doublet and a six-line sextet. The former arises due to an interaction between a quadrupole moment and an electric field gradient (EFG), while the latter occurs because of magnetic hyperfine splitting. The isomer shift (δ) corresponds to the deviation (positive or negative) of the MB transition from zero velocity in a given spectra. This parameter is based on the difference of s-electron density in the nucleus and contributes valuable information regarding the oxidation state of iron. Fe^{II} species contain more d electrons than Fe^{III} species, resulting in more shielding and less s-electron density in Fe^{II} nuclei. In general, ferrous species have larger values of δ than ferric species. All δ values are determined relative to an α-Fe foil calibration standard. Quadrupole splitting (ΔE_Q) corresponds to the difference in energy between the two lines of a quadrupole doublet and is dependent on the symmetry of an EFG around an iron nucleus. The δ of quadrupole doublets is measured relative to the midpoint of the two spectral lines. The magnitude of ΔE_Q increases when the symmetry of the electronic charge distribution decreases. Typically, HS Fe^{II} species have larger ΔE_Q values than HS Fe^{III} species. This is due to the fact that the electronic structure of a HS Fe^{II} system is less symmetric than a HS Fe^{III} system, in which there are 5 d electrons equally distributed in discrete orbitals.

There are a few drawbacks associated with Mössbauer spectroscopy. First, the time spent collecting Mössbauer spectra is dependent on the level of ^{57}Fe enrichment in samples. As a result, samples with low micromolar concentrations may involve 100 – 250

hours of data collection. Second, Mössbauer is an expensive technique due to costly prices related to operating and maintaining the instruments as well as purchasing radioactive sources and pure ^{57}Fe. Lastly, MB is rather esoteric and practical for studying only a handful of elements, and in terms of biological systems, it is restricted exclusively to iron analyses.

One of the major strengths of MB spectroscopy is that it detects all the ^{57}Fe in a sample, making it extremely effective at examining iron content in complex systems. In addition, simulations of MB spectra yield the relative percentages of groups of Fe species. Pairing these percentages with the absolute concentration of ^{57}Fe obtained via ICP-MS allows for absolute concentrations of groups of Fe species to be determined. MB spectroscopy supplies a plethora of chemical information about iron that cannot be matched by any other non-disruptive method.

Low temperature, low field (5 K, 0.05 T) Mössbauer spectra in Chapter IV were obtained using a model MS4 WRC spectrometer (SEE Co., Edina, Minnesota). Spectra were simulated with WMOSS software and calibrated at room temperature (RT) with α-Fe foil as described[114]. Applied magnetic fields were parallel relative to the γ-radiation.

EPR Spectroscopy

Electron paramagnetic resonance (EPR) spectroscopy is an effective and sensitive technique for studying species that contain unpaired electrons. Therefore, EPR can be applied to detect many transition metals in conjunction with iron. This biophysical tool probes for transitions within the ground state spin manifold by sweeping an externally

applied magnetic field and using a fixed frequency of microwave radiation. Increasing the magnetic field strength results in a linear increase in the energy difference between these two states,[160] and when the transition energy matches the supplied energy of microwaves, resonant absorption occurs. Detected signals in EPR spectra are typically plotted as the first derivative of the electronic spin absorption.[160] Common paramagnetic species are characterized in EPR analysis with signature measurements called g-values. G-values are unique proportionality factors that can be calculated from the equation: $g\beta B = h\nu$, where β is the Bohr magneton, B is the magnetic field, h is Planck's constant, and ν is the frequency of the microwaves.

Similar to Mössbauer, EPR spectroscopy is useful because it is a non-disruptive method of studying biological samples. However, EPR is more sensitive than Mössbauer and is capable of detecting half-integer spin systems in the low micromolar concentration range. Signals can be quantitated using spin standards with a known concentration and analytical software. A major limitation of EPR is that metal species with no unpaired electrons, also known as diamagnetic species (S=0), are left undetected in samples. This limited coverage of EPR for probing all the iron species in samples like intact cells or isolated mitochondria can be somewhat overcome by integrating it with data obtained from Mössbauer and UV-Vis analysis. EPR and Mössbauer have synergies such that the analysis of a sample can be strengthened significantly when both methods of analysis are used. EPR-active iron-containing species will exhibit magnetic hyperfine interactions in low-temperature Mössbauer spectra (in the slow-relaxation limit) and a quadrupole doublet at high temperature (in the fast-relaxation limit). The EPR spectra can provide

crucial parameters used in the spin Hamiltonian such as S, D, and E/D. These same parameters can then be assumed when simulating magnetic Mössbauer spectra.

EPR spectra in Chapter IV were collected at either 4.2 or 10 K using an X-band ELEXSYS spectrometer (Bruker Biospin Corp., Billerica, MA).

UV-Vis Spectroscopy

UV-Vis spectroscopy plays an important role in detecting and quantifying ISCs and heme centers, primarily in isolated mitochondria. Heme centers in the reduced form exhibit three characteristic bands, termed the α, β, and γ (Soret) bands. UV-Vis is able to resolve heme a, b, and c based on their unique α band wavelengths, which are ~605, ~565, ~550 nm, respectively.[161] These signature UV-Vis bands disappear whenever the heme centers are oxidized. Two different ISCs can be detected using UV-Vis, including [Fe_4S_4] and [Fe_2S_2], which display distinct features at ~410 and ~430 nm, respectively.[162,163] In contrast to heme centers, UV-Vis bands of ISCs diminish when the clusters become reduced.

Known extinction coefficients of heme a, b, and c can be used to calculate the concentrations of individual heme components.[164] The major advantage of UV-Vis spectroscopy is its ability to resolve each of these heme centers. Mössbauer spectroscopy is unable to differentiate between low-spin (LS) hemes and [Fe_4S_4] clusters. Thus, UV-Vis analysis contributes information regarding heme concentrations that can be integrated with Mössbauer and EPR data. A serious limitation of UV-Vis spectroscopy is its poor

coverage of different iron species. Many iron centers are left undetected in UV-Vis spectra and is the main reason why UV-Vis can only be utilized as a complementary method.

UV-Vis spectra in Chapter IV were recorded at RT under anaerobic conditions using a Hitachi U-3310 spectrometer (Tokyo, Japan) equipped with a Head-on photomultiplier tube.

Inductively Coupled Plasma Mass Spectrometry

ICP-MS is an effective analytical tool that is used to measure highly accurate metal concentrations in whole cells and isolated mitochondria. This technique is very sensitive and is able to detect most elements including transition metals in concentrations as low as 10 parts per trillion (ppt). This low detection limit makes it suitable for quantifying the trace metal content in complex biological systems, such as tissues, cells, and organelles. This method also has a large dynamic linear range with an upper detection limit in the high parts per million (ppm). ICP-MS is able to rapidly analyze a broad spectrum of elements and has detection limits that are 100-fold better than optical emission techniques. Detection via ICP-MS is based on mass which makes it useful for distinguishing different isotopes of a given element (e.g., ^{56}Fe and ^{57}Fe). However, despite its utility ICP-MS is unable to differentiate between oxidized and reduced forms of metal species.

ICP-MS is used in these studies for its ability to quantify metal content in biological samples. More importantly, ICP-MS is able to quantify total concentrations of ^{57}Fe in whole cells or isolated mitochondria, which can complement data obtained from Mössbauer analysis. As discussed previously, Mössbauer requires samples to be enriched

with ^{57}Fe. Since ^{57}Fe is the only iron isotope that is detected by Mössbauer, percentages of iron species in simulations can be used for estimating absolute concentrations of such species in samples. Results obtained by ICP-MS analysis are useful for characterizing iron phenotypes in mutant strains. Thus, ICP-MS can be utilized in two different capacities: as a precise tool for determining metal content in complex sample matrices and as a mutli-element detector when connected to an LC setup.

Application of LC-ICP-MS System for Bioanalytical Studies

Bioanalytical studies were conducted using a liquid chromatography (LC) system interfaced with an online inductively coupled plasma mass spectrometer (ICP-MS). The LC-ICP-MS system was utilized to study LMM metal complexes (< 10 kDa) in mitochondrial extracts. Separation of LMM complexes by size-exclusion chromatography (SEC) was achieved with two Superdex peptide columns, which were suitable for resolving peptides and nonproteinaceous metal species with masses between 0.2 and 10 kDa. This setup was able to fractionate LMM complexes by molecular weight. Metal complexes that eluted from the LC column were directed into the ICP-MS for detection. Approximate masses of detected complexes were estimated by calibrating size-exclusion columns with a series of standards (Figure II-1 and Table II-1).

The online LC-ICP-MS system was not only optimized to identify endogenous LMM metal species but also to isolate and preserve them for downstream characterization methods. Eluate could be split so that a small portion was sent to the ICP-MS for metal analysis while the remainder was sent to a fraction collector. This experimental setup was

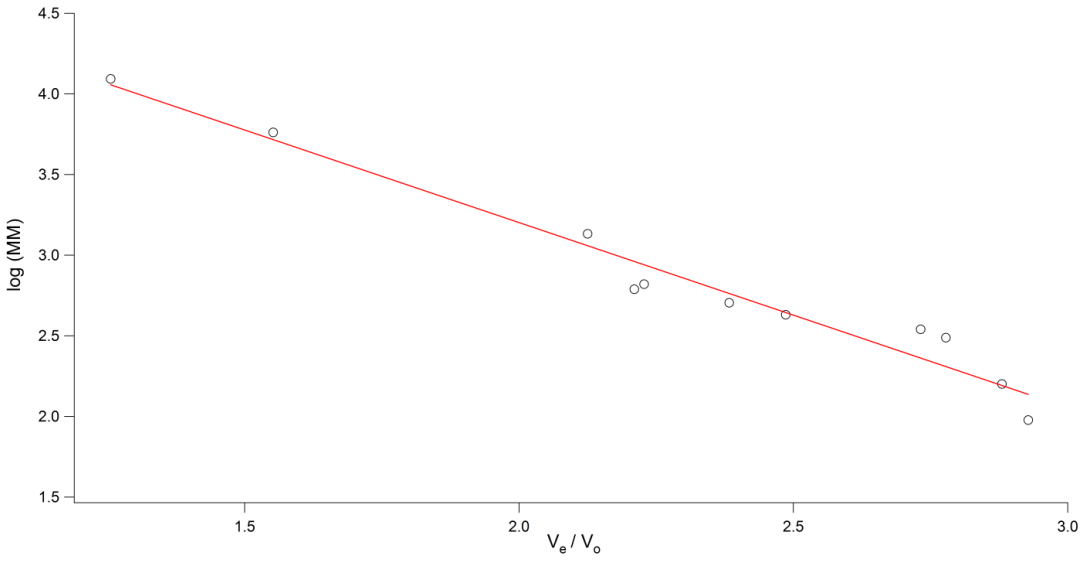

Figure II-1. Calibration curve for determining molecular masses based on the migration through the size-exclusion column. Open circles represent the compounds listed in Table II-1. The best-fit line through the data (solid line) has a slope of -1.142 and an intercept of 5.473. The R^2 for the fit was 0.966, and V_0 was 15.32 mL.

Table II-1. Compounds used for calibrating the size-exclusion columns. V_0 determined to be 15.3 mL using Blue Dextran (Fisher Sci.). [a]from a previous study.[158]

Compound	Source	Method of Detection	Molecular Weight (Da)	Log(MW)	Elution Volume (mL)	V_e/V_o
P_i (PO_4^{3-})	Fisher Sci.	ICP-MS (P)	95	1.978	44.8	2.92
Molybdate (MoO_4^{3-})	Sigma Aldrich	ICP-MS (Mo)	159	2.201	44.1[a]	2.88
Glutathione (GSH)	Sigma Aldrich	ICP-MS (S)	307.32	2.488	42.5[a]	2.77
AMP	Fisher Sci.	ICP-MS (P)	347	2.540	41.8[a]	2.73
ADP	Fisher Sci.	ICP-MS (P)	427.2	2.631	38.0[a]	2.48
ATP	Fisher Sci.	ICP-MS (P)	507.18	2.705	36.5	2.38
Oxidized Glutathione (GSSG)	Sigma Aldrich	ICP-MS (S)	614.64	2.789	33.8	2.21
Inositol Hexaphosphate	Sigma Aldrich	ICP-MS (P)	660	2.820	34.1[a]	2.22
Cyanocobalamin	Fisher Sci.	ICP-MS (Co)	1,355	3.132	32.5	2.12
Insulin (equine)	Fisher Sci.	UV (280 nm)	5777	3.761	23.7[a]	1.55
Cytochrome C (*S. cerevisiae*)	Sigma Aldrich	ICP-MS (Fe)	12,384	4.093	19.2	1.25

novel because the entire system, excluding the ICP-MS, was encapsulated inside a refrigerated anaerobic N_2-atmosphere glove box (≤ 5 ppm O_2, 10˚C). This approach was pioneered to prevent the oxidation of metal centers and to reduce the rate of ligand-exchange and only applied to metal species that did not decompose during the course of the experiment. Evidence of decomposition would include chromatograms exhibiting peaks that correspond to masses of aqueous ("free") metal ions (<200 Da).

Chemicals, Buffers, and Standards

Deionized (DI) water was prepared using a Barnstead B-Pure™ water purification system. High purity double-distilled-and-deionized (DDDI) water was generated using a Teflon sub-boiling still (Savillex DST-1000). DI water was used to prepare media and mitochondrial isolation buffers, while DDDI water was used in LC running buffers and any experiments involving ICP-MS. ^{57}Fe metal powder was purchased from Isoflex (San Francisco, California). Ar (99.998%), N_2 (99.999%), and O_2 (99.6%) compressed gas cylinders were purchased from Praxair (Bryan, Texas).

For mitochondrial isolations, the following buffers were used: SP buffer (1.2 M sorbitol, 20 mM KH_2PO_4, 1 mM EGTA, pH 7.4); Tris buffer (100 mM Tris-HCl, 1 mM EGTA, pH 9.4); SH buffer (0.6 M sorbitol, 20 mM HEPES, 1 mM EGTA, pH 7.4); PBS buffer (137 mM NaCl, 10 mM Phosphate, 2.7 mM KCl, pH 7.4); and mitochondrial isolation buffer, or MIB, (225 mM D-mannitol, 75 mM sucrose, 5 mM HEPES, 1 mM EGTA, and 1 mM PMSF, pH 7.4). Regarding online LC-ICP-MS experiments, two running buffers were used: 50 mM Tris-HCl (pH 7.4) in Chapter III and 20 mM

ammonium bicarbonate (pH 8.5) in Chapter IV. All buffers were degassed on a Schlenk line and purged with 99.998% Ar gas for at least 3 cycles immediately prior to use.

Primary and secondary elemental calibration standards used in offline ICP-MS concentration analysis were obtained from Inorganic Ventures (Christiansburg, Virginia). Size-exclusion columns used in LC-ICP-MS analysis were calibrated with a series of 11 known standards (Table II-1). Sodium phosphate (PO_4^{3-}), adenosine-5'-monophosphate (AMP) disodium salt, adenosine-5'-diphosphate (ADP) monosodium salt, adenosine-5'-triphosphate (ATP) disodium salt, cyanocobalamin, and insulin (equine) were purchased from Fisher Scientific (Pittsburgh, Pennsylvania). Cytochrome c (*Saccharomyces cerevisiae*), inositol hexaphosphate, oxidized glutathione (GSSG), reduced glutathione (GSH), and sodium molybdate (MoO_4^{3-}) were purchased from Sigma Aldrich (St. Louis, Missouri).

Yeast Strains and Media

Saccharomyces cerevisiae strain BY4741 (*MATα*, *ura3Δ0, leu2Δ0, met15Δ0, his3Δ1*) was used in Chapter III of this dissertation. Wild-type (WT) BY4741 cells were grown on standard yeast peptone agar plates with 2% glucose (YPD) for 3–4 days. YPD plates consisted of 2% glucose, 2% Bacto peptone, 2% Bacto agar, and 1% yeast extract (percentages in w/v). Colonies were inoculated into minimal medium containing 2% (w/v) glucose, 5 g/L ammonium sulfate, 1.7 g/L YNB (lacking ammonium sulfate and copper sulfate), 100 mg/L leucine, 50 mg/L adenine hemisulfate dihydrate, 20 mg/L uracil, 20mg/L histidine, 20 mg/L methionine, and 50 mg/L tryptophan. The endogenous metal

ion concentrations of minimal medium were: 10 μM Zn, 2 μM Mn, 2 μM Co, 0.3 μM Fe, 0.2 μM Cu, 5 nM Mo (n=2). For standard growth, Cu^{II} sulfate and $^{57}Fe^{III}$ citrate were added to the medium to final concentrations of 1 and 10 μM, respectively. In two metal supplementation experiments, 10 μM Cu^{II} sulfate or 100 μM Fe^{III} citrate was added to standard medium. In two other supplementation experiments, 100 μM $Zn(acetate)_2$ or 20 μM $MnCl_2$ (final concentrations) was added.

The Mrs3/4 double-deletion (ΔΔ) mutant strain used in Chapter IV was derived from a WT *S. cerevisiae* W303 strain (*MAT*α, *ura3-1*, *ade2-1*, *trp1-1*, *his3-11, 15*, *leu2-3, 112*). Deletion of *MRS3* and *MRS4* in the ΔΔ strain was confirmed via PCR analysis (Figure II-2). WT and ΔΔ cells were grown on YPAD agar plates for 3 days at 30 °C. YPAD plates consisted of 2% glucose, 2% Bacto peptone, 2% Bacto agar, 1% yeast extract, and 0.01% adenine (percentages in w/v). Cells were taken from plates and grown under respiring conditions in liquid minimal medium containing 3% (v/v) glycerol, 1% (v/v) ethanol, 5 g/L ammonium sulfate, 1.7 g/L YNB (lacking ammonium sulfate and copper sulfate), 100 mg/L leucine, 50 mg/L adenine hemisulfate dihydrate, 20 mg/L histidine, 20 mg/L uracil, 50 mg/L tryptophan, and 1 μM copper sulfate. A 40 mM stock solution of $^{57}Fe^{III}$ citrate (pH ~5) was prepared as described (*1*) and added to the growth medium to achieve final concentrations of 1, 10, and 40 μM. For BPS-treated medium, bathophenanthrolinedisulfonic acid (BPS), a strong Fe^{II} chelator, was added to a final concentration of 25 μM, followed by supplementation with 1 μM (final concentration) $^{57}Fe^{III}$ citrate. Taking into account the endogenous [Fe] in minimal medium was ~7 μM,

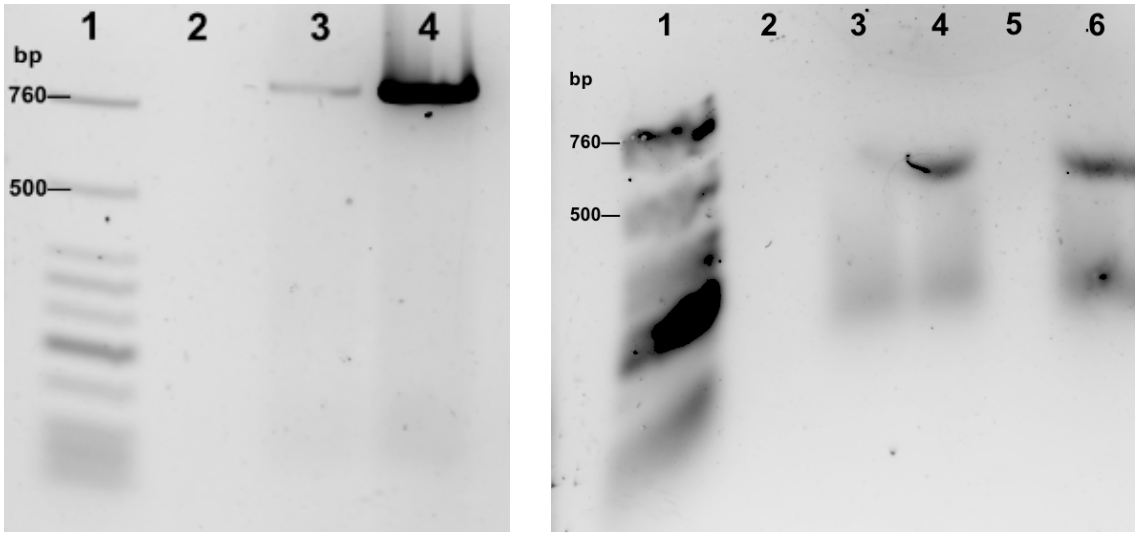

Figure II-2. Verification of Mrs3/4 double-deletion (ΔΔ) yeast strain. Agarose gel (2%) of WT cell extract (left image) and ΔΔ cell extract (right image). DNA was extracted from 50 mL cultures grown on minimal medium containing 40 μM Fe and harvested at OD_{600}= 0.8. Left image: Lane 1, DNA ladder with the sizes (in bp) of relevant markers indicated on the side; Lane 2, blank; Lane 3, *MRS3*; Lane 4, *MRS4*. The bands at ~800 bp correspond to the PCR products of WT DNA (*MRS3* and *MRS4*). Right image: Lane 1, DNA ladder; Lane 2, blank; Lane 3, Δ*MRS3*; Lane 4, Δ*MRS3* (twice as much loaded as in Lane 3); Lane 5, blank; Lane 6, Δ*MRS4* (same amount loaded as in Lane 4). The bands at ~500 bp correspond to the PCR products of ΔΔ DNA (Δ*MRS3* and Δ*MRS4*).

this afforded a molar excess of BPS. All yeast strains were generously provided by Dr. Andrew Dancis (University of Pennsylvania) and stored at -80˚C in YPAD medium containing 15% glycerol.

Growth and Preparation of Whole Cell Samples

Growth of yeast cells was monitored by measuring optical density at 600 nm (OD_{600}) with a Thermo Spectronic Genesys 6 spectrophotometer (Thermo Electronic Corporation, Waltham, MA). For all yeast experiments, frozen cell stocks were streaked out on YPAD plates and incubated for 3 days at 30˚C. Single colonies were inoculated into 50 mL of minimal medium. At OD_{600}= 0.8 ± 0.1, 50 mL cultures were transferred into 1 L of minimal medium. 50 mL and 1 L cell cultures were grown in baffled flasks at 30˚C with constant shaking. Growth curves shown in Chapter IV were obtained by recording OD_{600} values of 1 L cultures at various time points starting from the time of inoculation (t=0) until cells reached stationary phase.

For yeast mitochondrial isolations, 1 L cell cultures (OD_{600}= 0.8) were used to inoculate 24 L of minimal medium in a custom-built iron-free glass/titanium water-jacketed bioreactor with O_2 gas bubbled through the medium (~1 L/min) and a temperature-controlled water-jacket set at 30˚C. For most batches, cells were harvested in exponential growth phase at OD_{600}= 0.8 (1 cm pathlength). Other batches were harvested at OD_{600}= 1.2 – 1.6 when cells were transitioning into postexponential growth mode. At the start of each harvest, the bioreactor was set to 5˚C.

Whole cell samples were prepared aerobically. When cells reached OD_{600}= 0.8, 1 L cultures were centrifuged at 5000g for 5 minutes (Sorvall Evolution RC centrifuge, SLC-6000 rotor). Cells were washed 3× with unbuffered 1 mM EGTA and then 3× with distilled water. Cells were subsequently packed into EPR tubes and Mössbauer cups and frozen in liquid nitrogen (N_2) for further biophysical analysis.

Isolation of Mitochondria

At OD_{600}= 0.8, 24 L cultures of yeast cells were transferred into numerous 1 L centrifuge bottles using a transfer line and peristaltic pump and pelleted at 5000g for 5 minutes (Sorvall Evolution RC centrifuge, SLC-6000 rotor). Supernatants were discarded, and cell pellets were resuspended in distilled (DI) water using a rubber policeman. Resulting cell suspensions were consolidated into one centrifuge bottle. This bottle was centrifuged at 5000g for 5 minutes. The supernatant was discarded, and the weight of the cell pellet was measured and recorded. Typically, a 24 L culture at OD_{600}= 0.8 yielded a ~50 g cell pellet. The centrifuge bottle containing the weighed cell pellet was brought into an anaerobic glove box (~5 ppm O_2, 5˚C) unsealed. The cell pellet was resuspended in ~500 mL of degassed Tris buffer (pH 9.4) inside the glove box. Dithiothreitol (DTT) was brought into the glove box, dissolved in ~10 mL of Tris buffer, and immediately added to the cell suspension to a final concentration of 10 mM. For a 500 mL solution, this required 0.7708 g of DTT. Once the DTT was added, the resulting suspension was sealed tightly, removed from the glove box, and incubated inside a rotary shaker at 30˚C for 12 minutes. Cells were then pelleted at 5000g for 5 minutes and brought inside the glove box. The

supernatant was discarded, and the cell pellet was resuspended with ~500 mL of degassed SP buffer (pH 7.4). The centrifuge bottle was removed from the glove box and centrifuged at 5000g for 5 minutes. Cells were brought into the glove box, and the supernatant was discarded. The cell pellet was then resuspended in SP buffer (~500 mL) and a 1 mL aliquot of the resulting cell suspension was removed and placed in an Eppendorf tube. Lyticase (Sigma-Aldrich, L2524) was brought into the glove box, dissolved in ~10 mL of SP buffer, and immediately added to the cell suspension. The amount of lyticase added (in units of mg) was based off the mass of the cell pellet and calculated using the following formula:

mg of lyticase = (mass of cells in g) × (1000 U/g of cells) × (mg of lyticase/3949 U)

After the addition of lyticase, a 1 mL aliquot of the cell suspension was pipetted into an Eppendorf tube. Cells were removed from the glove box and incubated in a rotary shaker at 30˚C until spheroplasts formed. Aliquots taken before and after the addition of lyticase were used to monitor the formation of spheroplasts. Spheroplast formation was indicated by a 20 – 30% decrease in OD_{600} of 1:100 dilutions of lyticase-treated cells in water. Typically, a 20 – 30% decrease was reached in 1 – 2 hours. Following this decrease, spheroplasts were centrifuged at 5000g for 5 minutes and brought inside the glove box. At this stage, the spheroplast should be *loose and handled gently*. The supernatant was discarded and the spheroplast pellet was resuspended with SP buffer (~500 mL). The cell suspension was removed from the glove box and centrifuged at 5000g for 5 minutes. Spheroplasts were brought into the glove box, and the supernatant was discarded. The spheroplast pellet was resuspended in a 1:1 solution of degassed 2xSH buffer (pH 7.4) and H_2O containing 1 mM PMSF. In general, 100 mL of 2xSH was added first, followed by

100 mL of H_2O containing 1 mM PMSF. The resulting suspension (~200 mL) was homogenized inside the glove box using 25 strokes from a Dounce homogenizer (Type B pestle), which could only accommodate ~40 mL of spheroplast suspension. Thus, 5 – 6 rounds of homogenization were required. Homogenates were placed into a 250 mL centrifuge bottle, sealed tightly, and removed from the glove box. Homogenates were pelleted at 2000g for 5 minutes (GSA rotor) to remove cell debris. The pellet formed from this centrifugation was *extremely loose and required delicate handling*. The centrifuge bottle was brought inside the glove box, and the *supernatant* was *retained* in another 250 mL centrifuge bottle. The cell debris pellet was resuspended in ~150 mL of degassed SH buffer (pH 7.4). The resulting suspension was homogenized using only 10 strokes, removed from the glove box, and centrifuged at 2000g for 5 minutes. The centrifuge bottle was brought into the glove box, and the supernatant was combined with the supernatant from the previous homogenization step. The pooled supernatants were taken out of the glove box and centrifuged at 12000g for 10 minutes. The resulting pellet was referred to as "crude" mitochondria and was *handled delicately*. The centrifuge bottle was brought inside the glove box, and the supernatant was discarded. "Crude" mitochondria were resuspended in a ~10 mL of SH buffer and gently layered on top of discontinuous density gradients. Each density gradient was composed of 10 mL of 14.5% (w/v) Histodenz overlayed on top of 10 mL of 18.5% (w/v) Histodenz. Both solutions of Histodenz were prepared using SH buffer. Typically, 4 – 6 density gradients were made, and the "crude" mitochondrial suspension was distributed equally among them (roughly 2 – 3 mL of crude suspension per gradient). After crude mitochondria were pipetted onto density gradients,

they were sealed in ultracentrifuge inserts and removed from the glove box. Density gradients were spun at 150,000g for 1 hour in a Beckman Coulter Optima 90K ultracentrifuge (SW 32 Ti rotor). Ultracentrifuge inserts were brought into the glove box, and the less dense material floating at the top of gradients was removed with a glass pipette and discarded. Mitochondria were collected at the interface between the 14.5 and 18.5% Histodenz solutions using a glass pipette and placed in a new ultracentrifuge tube. Mitochondria were rinsed with 5 – 10 mL of SH buffer, sealed in an ultracentrifuge insert, and removed from the glove box. Mitochondria were pelleted in the ultracentrifuge at 12000g for 10 minutes. The insert was brought back into the glove box, and the resulting pellet was referred to as isolated mitochondria.

In Chapter IV, isolated yeast mitochondria were packed into EPR tubes or Mössbauer cups and frozen in liquid N_2 for subsequent analysis as described.[165] For UV-Vis studies, mitochondrial EPR samples were thawed anaerobically inside a glove box. Once thawed, samples were transferred into 3.5" EPR tubes and placed in ultracentrifuge inserts before being removed from the glove box. Mitochondrial samples were pelleted in the ultracentrifuge (SW 32 Ti rotor) at 12000g for 10 minutes. Samples were brought into the glove box and diluted 1:1 with SH buffer and transferred to custom 2 mm path length quartz UV-Vis cuvettes (NSG Precision Cells, Inc., Farmingdale, New York). Volumes of packed mitochondria were determined as described.[165] Cuvettes were sealed with a rubber septum and removed from the glove box for UV-Vis analysis.

Human Jurkat cells were grown on 10 μM Fe^{III} citrate, and mitochondria were anaerobically isolated as described.[166] Briefly, Jurkat cells were washed with PBS buffer

(pH 7.4) containing 1 mM EGTA, resuspended in mitochondrial isolation buffer (pH 7.4), and lysed by nitrogen cavitation. Cell lysate was strained, followed by centrifugation (Sorvall Evolution RC centrifuge, SLC-6000 rotor) at 800g for 10 minutes. Supernatant was saved and centrifuged at 9000g for 30 minutes. The mitochondrial pellet was resuspended in ~2 mL of MIB and pipetted on top of four Histodenz density gradients. Each gradient was composed of 3 mL of 35% Histodenz, 3 mL of 17% Histodenz, and 7.5 mL of 5% Histodenz. All Histodenz solutions were prepared using MIB. Density gradients were spun in an ultracentrifuge at 45000g for 1 hour (SW 32 Ti rotor). Mitochondria were pipetted from the 17-35% Histodenz interface and washed with MIB and frozen in liquid N_2. This sample was thawed anaerobically inside a glove box and injected into the online LC-ICP-MS system.

C57BL/6 mice were raised, and organs were dissected as described.[167] Mitochondria isolated from mouse brain and liver tissues used in Chapter III were prepared as described.[168] Samples were retrieved from liquid N_2 dewars, thawed anaerobically inside a glove box, and subjected to LC-ICP-MS analysis.

Preparation of LMM Mitochondrial Flow-Through Solutions

Isolated mitochondria were washed two or three times in 50 mM Tris (pH 7.4). For yeast and mammalian mitochondria, 82% and 65% of the packed volume of the isolated organelle were previously determined to be due, respectively, to the mitochondria themselves.[165,169] Assuming these packing efficiencies, pellets were resuspended in 1.0 mL of the same buffer but with 2% Triton X-100. This typically afforded a final volume

of 1.4 mL. After being incubated for 15 min while being constantly vortexed, the solution was centrifuged at 12000g for 15 min. The resulting supernatant, called the soluble mitochondrial extract (SME), typically constituted all but ~50 μL of the solution volume. The SME was transferred to an Amicon stirred cell concentrator containing a 10 kDa cutoff membrane, and the flow-through solution (FTS) was collected. Relative to concentrations in intact isolated yeast mitochondria, both SME and FTS were typically 4 times more dilute [1.4/(0.4×0.82) ≈ 4].

For each batch, 75 μL aliquots of the SMEs and FTSs were placed in 15 mL nitric acid-rinsed screw-capped polypropylene tubes. Samples were incubated with 100 μL of concentrated trace metal grade nitric acid, sealed with plastic electrical tape, digested for 12 h at 90˚C, and then diluted with water to 10 mL. Resulting solutions were analyzed by ICP-MS. Concentrations were calibrated using primary P, S, Mn, ^{56}Fe, ^{57}Fe, Co, Cu, and Zn standards (Inorganic Ventures, 5000 μg of metal/L each). Secondary standards (0, 10, 50, and 100 μg/L for each metal and 0, 1000, 5000, and 10000 μg/L for P and S) were used for calibration.

LC-ICP-MS experiments were performed in a refrigerated anaerobic glove box (MBraun Labmaster) at 10˚C and ~5 ppm of O_2. FTSs (500 μL) were injected onto two 10 × 300 mm Superdex peptide columns (GE Healthcare Life Sciences, Product No. 17517601) connected in series. The resulting double-length column was equilibrated with 50 mM Tris-HCl (pH 7.4) in Chapter III and 20 mM ammonium bicarbonate (pH 8.5) in Chapter IV. After injection, the running buffer was pumped through the column at a rate of 0.350 mL/min for 166 min using an Agilent Bioinert high-performance liquid

chromatography system (Tokyo, Japan) with titanium pump heads and all-PEEK tubing. The total elution volume (58 mL) corresponded to 2 column volumes (CVs), as determined using Blue Dextran. The eluent passed through a diode array UV-vis detector and into the nebulizer of an Agilent 7700x ICP-MS. The ICP-MS detected ^{31}P, ^{34}S, ^{55}Mn, ^{56}Fe, ^{57}Fe, ^{59}Co, ^{63}Cu, ^{66}Zn, and ^{95}Mo in He collision mode with a dwell time of 0.1 s. After every other run, columns were cleaned with 10 CVs of a chelator cocktail.[158]

The metal concentration corresponding to each peak in the chromatograms was determined as follows. The column was replaced with tubing, and 500 μL of the same elemental standards were injected onto the "phantom column". The resulting "eluent" flowed into the ICP-MS, affording a chromatogram, for each element, composed of a single peak. Each area:concentration ratio was obtained by dividing the integrated areas under the peak by the concentration of the standard injected.

A second method for determining metal concentrations was also used to evaluate the fraction of metal ions that adsorbed onto the column. Areas associated with each peak were determined by fitting. Each peak area was divided by the sum of all areas in the chromatogram. The resulting fractions reflected the proportion of each metal associated with a particular peak. The sum of these areas was assumed to correspond to the total concentration of the metal in the FTS.

If no metals adsorbed onto the column during a run, the concentrations obtained by the second method would equal those obtained by the first. In practice, the two differed by <10%, indicating that the vast majority of the metals in the FTSs eluted from the column.

ESI-MS Experiment

Mitochondria were isolated from cells grown on medium containing an approximate 1:1 molar ratio of ^{56}Fe:^{57}Fe (40 μM total). FTS (500 μL) was injected onto two Superdex peptide columns connected in series, and the eluent (flow rate = 0.35 mL/min) was split via a micro splitter valve (Upchurch Scientific, USA) with ~30% directed to the ICP-MS and ~70% directed to an Agilent 1260 Infinity Analytical-scale Fraction Collector (Agilent, Tokyo, Japan). 700 μL fractions were collected in 96 Deep Well plates, and those selected for ESI-MS analysis were anaerobically frozen in liquid N_2. ESI-MS spectra were acquired in positive ion mode using an Orbitrap Fusion Tribrid mass spectrometer (Thermo Scientific) equipped with a HESI source. Sample was injected at 5 μL/min, and the spray potential was set to 3 kV. Sheath gas, Aux gas, and Sweep gas were set at 3, 2, and 1 (arbitrary units), respectively. Acquired ESI-MS data was interrogated using Thermo Excalibur software.

Metal Concentration Analysis

Metal concentrations of whole cells or isolated mitochondria in Chapter IV were analyzed by offline ICP-MS (Agilent Model 7700x). After collecting Mössbauer spectra, samples were thawed and packed into EPR tubes to measure sample volumes (ca. 200 – 300 μL) and then diluted with 250 μL of high purity DDDI water. 50, 75, and 100 μL aliquots from the resulting suspensions were transferred to 15 mL screw-top polypropylene Falcon tubes, digested with 250 μL of concentrated trace metal grade nitric acid, and heated overnight (~16 hours) at 90˚C. Digested samples were diluted with high

purity DDDI H_2O to a final volume of 8.0 mL. Reported metal concentrations of whole cells and mitochondria were calibrated as described and corrected using previously reported packing efficiencies of 0.70 for whole cells and 0.77 for mitochondria.

CHAPTER III

DETECTION OF LABILE LOW-MOLECULAR-MASS TRANSITION METAL COMPLEXES IN MITOCHONDRIA*

Introduction

Many transition metal complexes are labile, meaning that their coordinating ligands are weakly bound and rapidly exchanging with other ligands in solution. This behavior adds a significant challenge to the isolation, identification, and characterization of such labile metal pools (LMPs) in cells.[170] These pools have been detected by incubating live, intact cells with custom-designed fluorescence-based chelators, also known as sensors or probes.[171] Chelator probes penetrate cell membranes and coordinate the metal ions that compose such pools; they can also be targeted to specific organelles within the cell. Binding metal ions either enhances or quenches the fluorescence properties of the probes, thereby reporting on the existence and size of such pools.

The use of chelator probes has dramatically improved our awareness of LMPs in cells, yet many details, including the composition, structure, and function of the metal pools, remain unknown. LMPs likely participate in metal ion trafficking, regulation, signaling, and storage and release. Such processes require that metals coordinate ligands weakly enough such that the metals can be transferred from one species to another, or that

---

* Reproduced with permission from Sean P. McCormick, Michael J. Moore, and Paul A. Lindahl (2015) Detection of Labile Low-Molecular-Mass Transition Metal Complexes in Mitochondria, *Biochemistry 54*, 3442–3453. Copyright 2015 American Chemical Society.

the metals can dynamically bind to regulatory sites in a concentration-sensitive manner. These processes play vital roles in metal ion metabolism and are often altered in metal-associated diseases. These considerations motivate our efforts to identify and characterize LMPs, the challenges associated with their lability notwithstanding.

The benefits of detecting LMPs in live, intact cells and organelles using fluorescence-based probes are counterbalanced by the fact that the sought-after complexes are destroyed during detection; i.e., the endogenous ligands associated with LMPs dissociate when the probe coordinates the metal. This is a major disadvantage because the ligand environment dictates many properties of these complexes. Also, the binding strength required to chelate a particular metal ion pool is unknown such that stronger probes might overestimate the size of a pool and weaker ones might underestimate it. LMPs may be heterogeneous, with more than one metal complex contributing. Probes are often championed as being specific for a particular metal ion, but they actually need to be specific for a particular metal ion complex, a far more difficult requirement. Deciphering the molecular-level function of each complex that composes a heterogeneous LMP based solely on the overall chelation properties of the pool seems virtually impossible.

Ligand-exchange rates of LMPs are likely to be fast, but if they were faster than the rates of relevant biochemical reactions, e.g., binding of a complex to a receptor, the complexes would lack a defined shape, a requirement of receptor recognition. With such extreme fluxionality, how could cells use such complexes in trafficking, regulation, signaling, or storage? Would not their coordination sites become available for deleterious

Fenton and Haber–Weiss reactions? Should not there have been a selective advantage to minimize such chaos?

Motivated by these considerations, we hypothesized that the rates of ligand exchange associated with LMPs are actually slow enough for individual metal complexes to be isolated. Perhaps exchange rates have been reduced during evolution by the use of polydentate ligands and donor atoms that afford relatively strong metal-ligand binding interactions.

With the goal of isolating labile metal complexes, we have designed a refrigerated anaerobic liquid chromatography system interfaced with an online inductively coupled plasma mass spectrometer. Our LC-ICP-MS system can split a portion of the eluent to the ICP-MS for detection and send the remainder to a fraction collector. This arrangement allows us to detect, isolate, and eventually characterize the complexes that compose LMPs.

In this study, we have focused on LMPs in mitochondria isolated from fermenting *Saccharomyces cerevisiae* cells. LMPs were assumed to be composed of metal complexes with masses of <10 kDa, rationalized as follows. Most mitochondrial metalloproteins are encoded by nuclear DNA and imported into mitochondria as unfolded polypeptides threaded through the TOM/TIM protein complexes on the outer and inner membranes (OM and IM, respectively).[172] Once in the matrix, a signal sequence is typically clipped, and the apo-metalloprotein folds and is metalated. Metalloproteins encoded by mtDNA are probably metalated by similar mechanisms. In either case, most of the metal ions used in metalation must be transported into the matrix. Because the IM is "tight," these metal

ions must enter the matrix through channel-containing IM transport proteins, thereby excluding high-molecular-mass (HMM) species.[3,88] Metal donors must be small enough to pass through pores in the OM, which is limited to masses of less than ~3 kDa.[173] Metalloproteins that localize to the IMS might be metalated by metal complexes that enter the IMS via the OM.[28] However, the Cu ions that metalate IMS metalloproteins have been proposed to pass from the cytosol to the matrix and then to the IMS.[157]

Here we report detection of LMM P, S, Mn, Fe, Co, Cu, Zn, and Mo species, some of which probably function to metalate mitochondrial apo-metalloproteins. We assessed the reproducible occurrence of such species, determined their approximate molecular masses, and estimated their concentrations within the organelle. Our results set the stage for more advanced downstream characterizations.

Results

Five independent batches of mitochondria were isolated from WT yeast cells grown on medium supplemented with 10 μM Fe^{III} citrate and 1 μM $CuSO_4$. The cells were harvested at a low OD_{600} of 0.8 during the exponential phase. Aliquots were subjected to the LC-ICP-MS system immediately (at t = 0) after mitochondria were isolated. To highlight these batch-dependent characteristics (Yeast, Low, t = 0), we will refer to the batches as *YL0A*, *YL0B*, *YL0C*, *YL0D,* and *YL0E* (Table III-1). Aliquots of YL0A and YL0B were re-run after being incubated for 5 days in the glove box; those runs will be called *YL5A* and *YL5B*.

Table III-1. Nomenclature of LC batches.

Batch Name	Organism	OD_{600} at harvest	Time of injection	Comments
YL0A	Yeast	0.8	Immediately	Fermenting
YL5A	Yeast	0.8	5 days later	Same batch as YL0A
YL0B	Yeast	0.8	Immediately	Fermenting
YL5B	Yeast	0.8	5 days later	Same batch as YL0B
YL0C	Yeast	0.8	Immediately	Fermenting
YL0D	Yeast	0.8	Immediately	Fermenting (only shown in Figure 6)
YL0E	Yeast	0.8	Immediately	Fermenting (not shown in Figures)
YRL0A	Yeast	0.8	Immediately	Respiring (glycerol) (only in Figure III-6)
YL0Fe	Yeast	0.8	Immediately	Fermenting (extra Fe)
YL0Cu	Yeast	0.8	Immediately	Fermenting (extra Cu)
YL0Zn	Yeast	0.8	Immediately	Fermenting (extra Zn)
YL0Mn	Yeast	0.8	Immediately	Fermenting (extra Mn)
YH0A	Yeast	1.4	Immediately	Fermenting
YH0B	Yeast	1.6	Immediately	Fermenting
YH5B	Yeast	1.5	5 days later	Same batch as YH0B
YH0C	Yeast	1.6	Immediately	Fermenting
Brain	Mouse	From adult mice	Frozen and thawed	See Holmes-Hampton et al.[167]
Jurkat	Human	Described in Jhurry et al.[169]	Frozen and thawed	See Jhurry et al.[169]
Liver	Mouse	From adult mice	Frozen and thawed	See Chakrabarti et al.[168]

Four other batches were prepared from WT yeast cells grown on the same medium but spiked one at a time with 100 μM Fe, 10 μM Cu, 100 μM Zn, and 20 μM Mn. These batches will be called *YL0Fe*, *YL0Cu*, *YL0Zn*, and *YL0Mn*, respectively. Three other batches were harvested at higher culture densities (postexponential phase), including *YH0A*, *YH0B*, and *YH0C*. An aliquot of YH0B was re-run 5 days after it was initially prepared, generating trace *YH5B*. A batch prepared under respiring (glycerol) conditions will be called *YRL0A*. Three other batches of mitochondria were prepared, including one each from mouse brain, human Jurkat cells, and mouse liver.

Concentrations of selected elements in isolated mitochondria are listed in Table III-2; rounded averages are in Table III-3. Previous studies[115,143,174] afforded comparable yeast mitochondrial metal concentrations. Concentrations for mammalian mitochondria were similar except for that of Mo, which was ~4 times higher than in the yeast organelle. Increasing Mn, Fe, Cu, and Zn concentrations 10-fold in the yeast growth medium, one at a time, significantly increased the concentration of that element in isolated mitochondria. The concentrations of the other detected elements, whose concentrations were not increased in the medium, were unaffected. This sensitivity between the medium and mitochondrial metal ion concentrations must be mediated by changes in cytosolic metal ion levels, but the pathways involved are unknown. The absence of secondary perturbations suggests that the homeostatic systems regulating the concentrations of these metals in mitochondria are largely independent of each other.

The concentrations of the LMM forms of these elements in mitochondria are listed in Table III-4, with averages again listed in Table III-3. No significant differences between

Table III-2. Concentrations of selected elements in isolated mitochondria. Reported values are concentrations in SMEs multiplied by dilution factors (average dilution factor was 3.5 ± 0.2). Numbers shaded in grey and red were not included in averages (the values in grey were high because the medium was supplemented with extra metal; the value in red was presumed to be high due to the presence of nanoparticles. Numbers shaded in blue, from batches grown to high OD_{600}, were separated from unshaded values in the column, from batches grown to low OD_{600}.

Figure Legend	P (mM)	S (mM)	Mn (µM)	Fe (µM)	Co (nM)	Cu (µM)	Zn (µM)	Mo (µM)
YL0A/YL5A	25	5.8	15	420	100	58	290	2
YH0A	30	6.2	18	750	150	78	380	1
YL0B/YL5B	26	6.0	16	480	80	54	310	1
YL0C	25	6.1	15	430	90	48	270	1
YL0Fe	26	6.2	12	780	80	83	280	2
YL0Cu	23	6.0	13	410	60	140	240	2
YL0Zn	28	6.0	14	460	60	35	480	1
YL0Mn	29	6.0	25	460	50	64	250	2
YL0D	25	6.1	14	430	90	63	260	1
YH0B/YH5B	29	6.4	20	720	120	80	360	1
YH0C	29	6.3	18	770	100	92	340	2
YL0E	26	6.2	17	410	80	56	280	1
YRL0A	32	6.8	19	620	110	120	320	2
Brain	33	7.9	13	380	60	25	210	5
Jurkat	28	7.9	18	1,000	120	120	220	6
Liver	34	8.6	16	420	80	21	320	8

Table III-3. Average concentrations of selected elements in mitochondria. The top group of rows refers to total mitochondrial concentrations. The second group refers to previous reports of metal concentrations in fermenting yeast mitochondria. The third group refers to LMM species only. The bottom group indicates the percent of each selected element that is found in mitochondria as LMM species (based on data from this study). [a]The Fe concentration from ref 115 (1190 μM) was excluded. [b]The Cu concentration from ref 175 (220 μM) was excluded because those cells were grown under respiration conditions where cytochrome c oxidase levels are higher. In the Mo column, Y refers to yeast and M to mammalian mitochondria. Numbers in the bottom two rows are given as percentages, not concentrations.

	P (mM)	**S (mM)**	**Mn (μM)**	**Fe (μM)**	**Co (nM)**	**Cu (μM)**	**Zn (μM)**	**Mo (μM)**
Average (HMM+LMM)	28	6.6	16	530	89	71	300	1.4Y;6.3M
Standard Deviation	3	0.9	3	150	27	34	60	0.4Y;1.2M
10-fold M	---	---	25	780	---	140	480	---
Previous Average (HMM+LMM)[115,143,174,175]	---	---	20	630[a]	---	70[b]	280	---
Standard Deviation	---	---	9	100	---	28	38	---
Average (LMM)	24	5.4	3.1	116	65	32	140	0.02Y;1M
Standard Deviation	3	0.6	1.0	32	18	9	21	5Y;0M
10-fold M	---	---	8	170	---	120	280	---
% LMM	86	82	19	22	73	45	47	1.5Y;16M
Standard Deviation	5	5	6	6	14	20	6	0.9Y;3M

Table III-4. Concentrations of selected elements present as LMM species in isolated mitochondria. Numbers shaded in grey were not included in averages. Values in tables are concentrations of FTSs multiplied by the same dilution factors used in Table III-2.

Figure Legend	P (mM)	S (mM)	Mn (µM)	Fe (µM)	Co (nM)	Cu (µM)	Zn (µM)	Mo (nM)
YL0A/YL5A	20.2	4.8	2	110	55	24	120	20
YH0A	27.5	5.5	4	120	85	30	160	20
YL0B/YL5B	21.5	4.9	3	100	45	26	130	30
YL0C	21.0	5.0	2	120	55	24	120	20
YL0Fe	21.4	5.3	3	170	72	21	120	20
YL0Cu	19.7	5.5	2	100	58	120	120	10
YL0Zn	21.2	5.0	2	120	49	27	280	20
YL0Mn	23.3	4.9	8	110	45	20	120	20
YL0D	22.1	5.1	3	110	60	26	120	20
YH0B/YH5B	24.6	5.4	3	150	95	34	180	30
YH0C	26.2	5.2	3	160	80	32	160	20
YL0E	20.6	4.8	2	100	50	28	130	20
YRL0A	29	5.4	2	150	75	50	160	30
Brain	26.7	6.3	4	50	50	3	110	1,000
Jurkat	26.2	6.5	4	110	100	22	110	1,000
Liver	28.4	6.4	3	60	72	5	120	1,000

yeast and mammalian mitochondria were observed except that the average concentration of LMM Mo in mammalian mitochondria was 50 times higher than in yeast. Approximately 80% of P, S, and Co in mitochondria were LMM, while only 20% of Mn and Fe were LMM. Nearly half of the Cu in mitochondria was in the form of LMM complexes. However, some LMM Co and Cu may not be physiologically relevant (see below), lowering these percentage estimates. In mammalian mitochondria, ~16% of Mo in the organelle was present in LMM forms. Nearly half of mitochondrial Zn ions was LMM. Atkinson et al.[84] reported that nearly half of the Zn in sonicated yeast mitochondrial homogenates was soluble; the two results together suggest that most soluble Zn in mitochondria is LMM.

LC-ICP-MS Characterization of FTSs

Mitochondrial FTSs were subjected to anaerobic liquid chromatography. Eluents were monitored for LMM P, S, Mn, Fe, Co, Cu, Zn and Mo using an online ICP-MS. The abscissas for all chromatograms (Figures III-1 – III-8) were adjusted slightly (±0.3 mL) to align two particular phosphorus peaks [Figure III-1, P_{1000} and P_{800} (see below)]. Plots of all of the other monitored elements in the same run were adjusted identically (i.e., based on the P alignment).

Concentrations of the reproducibly observed LMM species are listed in Table III-5. HMM peaks were often observed at elution volumes near the void volume (15.3 mL). Such peaks were used in concentration determinations but were not analyzed for molecular

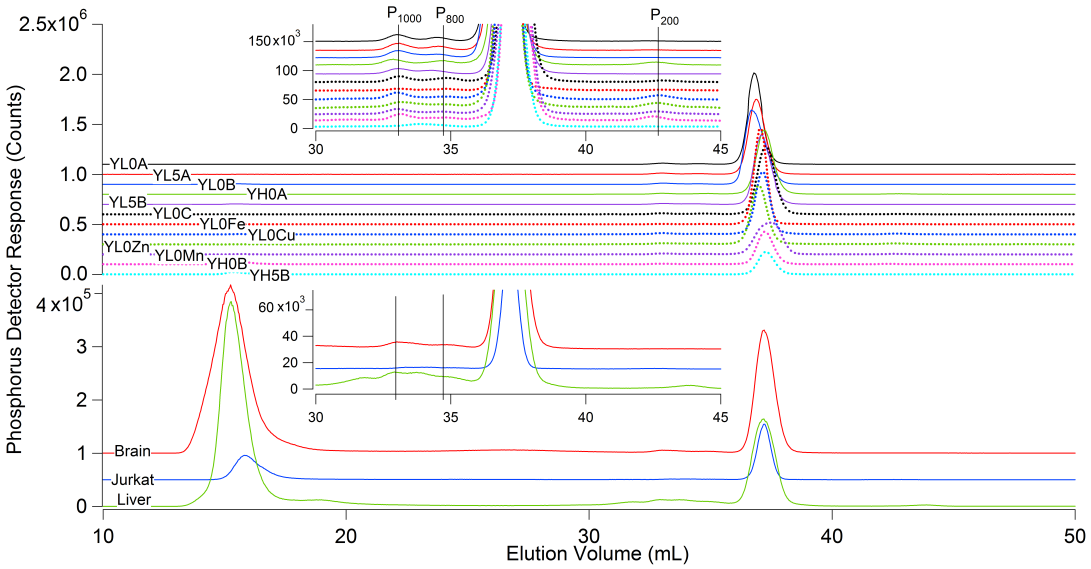

Figure III-1. Phosphorus chromatograms of LMM mitochondrial FTSs.

Table III-5. LMM metal complexes and P and S compounds in mitochondria. Values were obtained by fitting to Gaussian functions as described in the text.[158] ND means not detected. The *R* value indicates the confidence in yeast traces only.

Peak Name	Center (mL)	Width (mL)	Molecular Mass (Da)	[yeast] (μM)	[mouse] (μM)	[Jurkat] (μM)	*R* value (%)
P_{1000}	33.4 ± 0.2	0.9 ± 0.1	1000 ± 200	400 ± 100	500	400	100
P_{800}	34.6 ± 0.1	1.3 ± 0.2	800 ± 200	300 ± 100	400	400	100
P_{520}	37.1 ± 0.2	0.7 ± 0.1	520 ± 100	20000 ± 4000	24000	24000	100
P_{200}	42.7 ± 0.2	1.4 ± 0.1	200 ± 50	230 ± 140	100	100	80
S_{1100}	32.8 ± 0.3	1.0 ± 0.1	1100 ± 150	4900 ± 40	6300	6300	100
S_{780}	34.8 ± 0.1	1.4 ± 0.5	780 ± 200	500 ± 400	ND	ND	60
Mn_{2000}	30.5 ± 0.2	1.2 ± 0.1	2000 ± 200	ND	2	3.5	ND
Mn_{1100}	32.6 ± 0.1	0.9 ± 0.1	1100 ± 160	1.9 ± 0.2	2	0.5	100
Fe_{1500}	30.8 ± 0.1	0.8 ± 0.2	1500 ± 300	ND	15	ND	ND
Fe_{1100}	32.7 ± 0.1	1.3 ± 0.2	1100 ± 250	6 ± 2	10	ND	80
Fe_{870}	34.1 ± 0.5	0.7 ± 0.1	870 ± 100	12 ± 9	2	ND	60
Fe_{680}	35.6 ± 0.4	1.1 ± 0.4	680 ± 130	20 ± 10	2	ND	50
Fe_{580}	36.6 ± 0.3	1.4 ± 0.1	575 ± 150	90 ± 20	26	110	100
Fe_{200}	43.3 ± 0.2	1.2 ± 0.8	200 ± 40	2 ± 1	1	ND	90
Co_{1500}	30.8 ± 0.3	0.8 ± 0.2	1500 ± 300	ND	0.01	0.02	90
Co_{1200}	32.3 ± 0.2	0.9 ± 0.1	1200 ± 180	0.03 ± 0.02	0.04	0.04	90
Co_{840}	34.3 ± 0.3	1.7 ± 0.6	840 ± 270	0.02 ± 0.01	0.01	0.02	90
Co_{450}	38.2 ± 0.5	2.4 ± 0.9	450 ± 200	0.013 ± 0.002	ND	ND	70
Co_{340}	39.8 ± 0.2	1.8 ± 0.4	340 ± 100	0.006 ± 0.004	ND	ND	90
Co_{300}	41.1 ± 0.4	2.0 ± 1.5	300 ± 10	0.002 ± 0.001	ND	ND	80
Cu_{5000}	23.1 ± 0.1	1.4 ± 0.2	5000 ± 1000	16 ± 7	ND	ND	90
Zn_{1500}	30.8 ± 0.2	0.7 ± 0.1	1500 ± 200	ND	8	6	ND
Zn_{1200}	32.2 ± 0.2	0.6 ± 0.2	1150 ± 100	110 ± 20	100	100	100
Zn_{900}	34.1 ± 0.1	1.8 ± 1.3	900 ± 300	6 ± 1	ND	ND	100
Mo_{730}	35.0 ± 0.1	0.7 ± 0.1	730 ± 100	ND	0.4	0.3	100

mass because the species that migrated in this region were not sufficiently well resolved to allow for accurate molecular mass determinations.

Phosphorus

Yeast mitochondrial FTSs exhibited four major LMM P species with approximate masses of 1000, 800, 520, and 200 Da (Figure III-1 and Table III-5). We will refer to these as P_{1000}, P_{800}, P_{520}, and P_{200}, respectively. P_{520} exhibited the greatest intensity, followed distantly by P_{1000}, P_{800}, and P_{200}. The concentration of P_{520} in isolated mitochondria was approximately 20 mM. It essentially comigrated with ATP (507 Da). Thus, the majority of the P_{520} peak was assigned to ATP, with ADP (427 Da) thought to contribute to the broadening on the low-mass side of the peak. If this is assumed, the concentration of P_{520} in mitochondria would be ~7 mM (20/3). Yeast mitochondria reportedly contain 7.8 mM ATP.[176] This supports our assignment and adds confidence that our methods of estimating concentrations and masses were reasonably accurate.

P_{1000}, P_{800}, and P_{200} were not assigned. However, the apparent masses of P_{800} and P_{200} were similar to those of NADPH (744 Da) and pyrophosphate (174 Da). If these assignments were correct, the concentration of these species in mitochondria would be 100 and 200 μM, respectively. Reported concentrations of NADPH in mitochondria and cytosol range between 45 and 235 μM,[177] which are in the same ballpark.

The P content of mammalian mitochondria was similar to that of yeast; P_{520} again dominated, and the same minor-intensity species were evident. In the P chromatogram of mitochondria from Jurkat cells, the same minor-intensity peaks were present, but their

intensities were lower than in the other mammalian samples. The chromatograms of liver and brain mitochondrial FTSs exhibited additional P-containing species that were not assigned.

Sulfur

Mitochondrial FTSs consisted of two major S peaks, corresponding to masses of 1100 and 780 Da (Figure III-2 and Table III-5). S_{1100} dominated and was reproducibly present at concentrations near 5 mM. The presence of S_{780} was more sporadic. Surprisingly, neither species comigrated with glutathione (GSH, 307 Da) or glutathione disulfide (GSSG, 612 Da); further studies are needed to explain this given the abundance of glutathione in mitochondria. Authentic GSSG migrated in accordance with its mass, including in a run of FTS spiked with GSSG. Authentic GSH appears to oxidize as it migrates through the column, but the details of this are under investigation.

Zinc

Yeast mitochondrial FTSs exhibited an intense Zn peak corresponding to a mass of 1200 Da (Figure III-3 and Table III-5). The concentration of Zn_{1200} in yeast mitochondria was 110 μM, nearly half of the total Zn in the organelle and almost all of the soluble Zn. The same species was in FTSs from mammalian mitochondria. A minor-intensity species with a mass of ~900 Da (Zn_{900}) was in yeast mitochondria at a concentration of ~1 μM. Mitochondria from yeast grown on medium containing 10-fold more Zn than normal exhibited a 2.5-fold increase in the intensity of Zn_{1200} whereas the

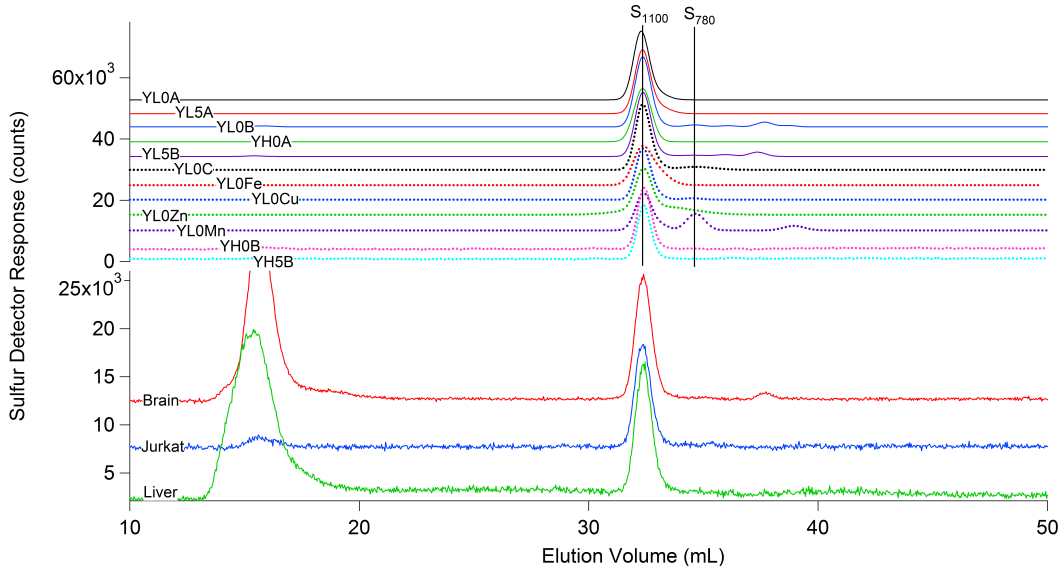

Figure III-2. Sulfur chromatograms of LMM mitochondrial FTSs.

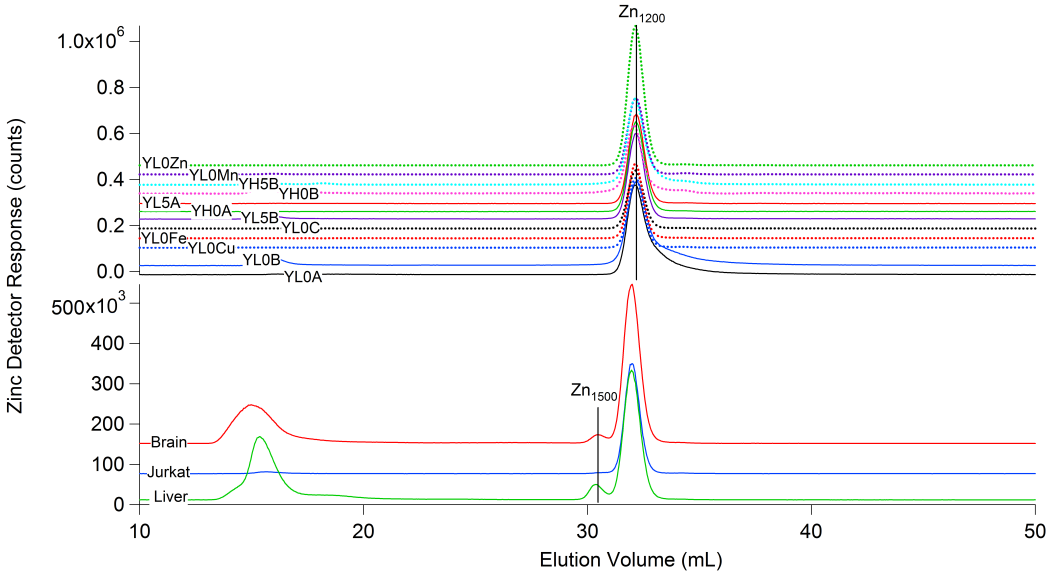

Figure III-3. Zinc chromatograms of LMM mitochondrial FTSs.

intensities for the other peaks were not significantly affected. A higher-mass species (Zn_{1500}) was detected in mitochondria from brain and liver but not yeast.

Manganese

A single LMM Mn species with a mass of 1100 Da (Mn_{1100}) dominated the chromatograms of fermenting yeast mitochondrial FTSs (Figure III-4 and Table III-5). A minority species of higher mass (Mn_{2000}) was in some FTSs. The concentration of Mn_{1100} in yeast mitochondria was ~2 μM, while that of Mn_{2000} was 23-fold lower. The Mn_{1100} concentration increased 4-fold in mitochondrial FTS from yeast cells grown in media containing 10-fold normal Mn; the concentration of Mn_{2000} also increased, albeit more modestly.

Both Mn_{2000} and Mn_{1100} were in mitochondrial FTSs from human cells and mouse tissues, but the relative intensities differed significantly from those in yeast. In mitochondria from Jurkat cells, Mn_{2000} represented ~95% of the Mn in the organelle, with minor contributions from Mn_{1100}. The concentrations of these two species in mitochondria from mouse brain and liver were more balanced, affording concentrations of 1 – 2 μM each. We previously observed a single LMM Mn species in yeast mitochondria with a mass between 2000 and 3000 Da.[113] Such a species was not observed currently in fermenting yeast mitochondria but was observed in our one batch of respiring yeast mitochondria (YRL01). A systematic study is required, but we currently suspect metabolism-dependent effects.

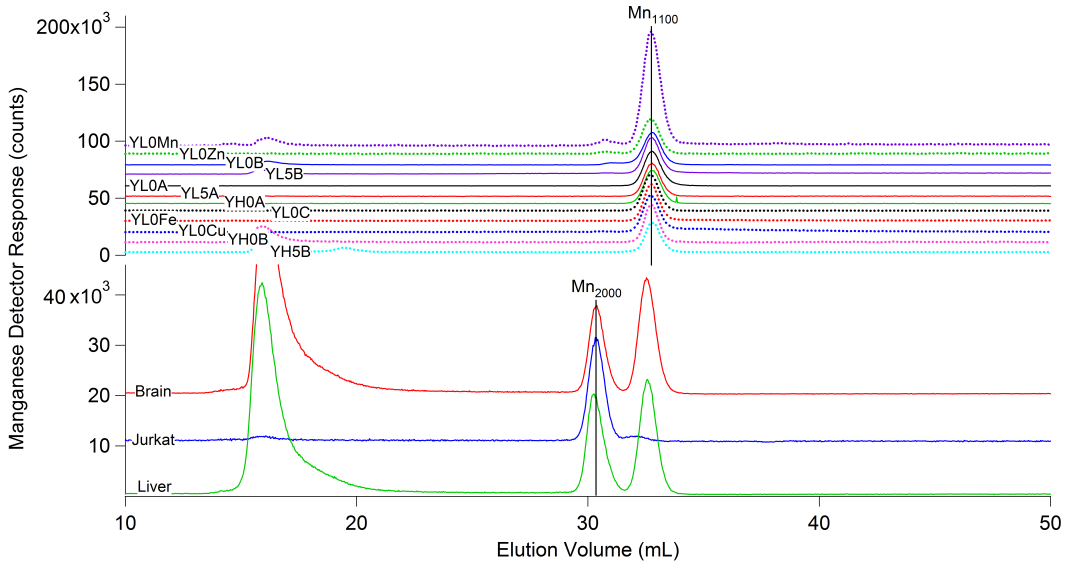

Figure III-4. Manganese chromatograms of LMM mitochondrial FTSs.

Iron

Yeast mitochondrial FTSs exhibited two major Fe species (Fe_{580} and Fe_{1100}), with either species dominating depending on (a) the mode of growth of the cells at the time of harvesting and (b) whether the FTS was chromatographed immediately after it was prepared or 5 days later. Mitochondrial FTSs isolated from cells harvested during exponential growth and run immediately exhibited Fe_{580} (Figure III-5 and Table III-5). A low-intensity peak corresponding to a higher-mass species (Fe_{1100}) was also evident. The chromatogram from mitochondrial FTS obtained from cells grown on medium containing 100 μM Fe^{III} citrate (rather than the standard 10 μM) exhibited a 1.7-fold increase in the intensity of the Fe_{580} peak.

Fe-detected chromatograms of FTSs isolated from cells harvested during the postexponential growth phase and run immediately after isolation were dominated by Fe_{1100}. Fe_{580} was present but at a reduced intensity. Unexpectedly, when a FTS dominated by Fe_{1100} was left in a refrigerated glove box for 5 days, the resulting chromatogram was dominated by Fe_{580}, with Fe_{1100} downgraded to a minor component. In that chromatogram, another Fe-containing species with an intermediate mass was also evident. For reasons that we don't understand, trace YL0Mn exhibited a more highly resolved species with a mass of 870 Da (Fe_{870}) (Figure III-5). During incubation, Fe_{1100} may convert into Fe_{580} via intermediate Fe_{870}. The only other Fe species present exhibited a very low intensity peak associated with a mass of 200 Da. Because hexaqua Fe has a mass of ~160 Da, we assign Fe_{200} as such. The concentration of Fe_{200} in our isolated mitochondria samples was 1 – 3 μM, which we regard as an upper limit of what it might be in intact mitochondria (one-

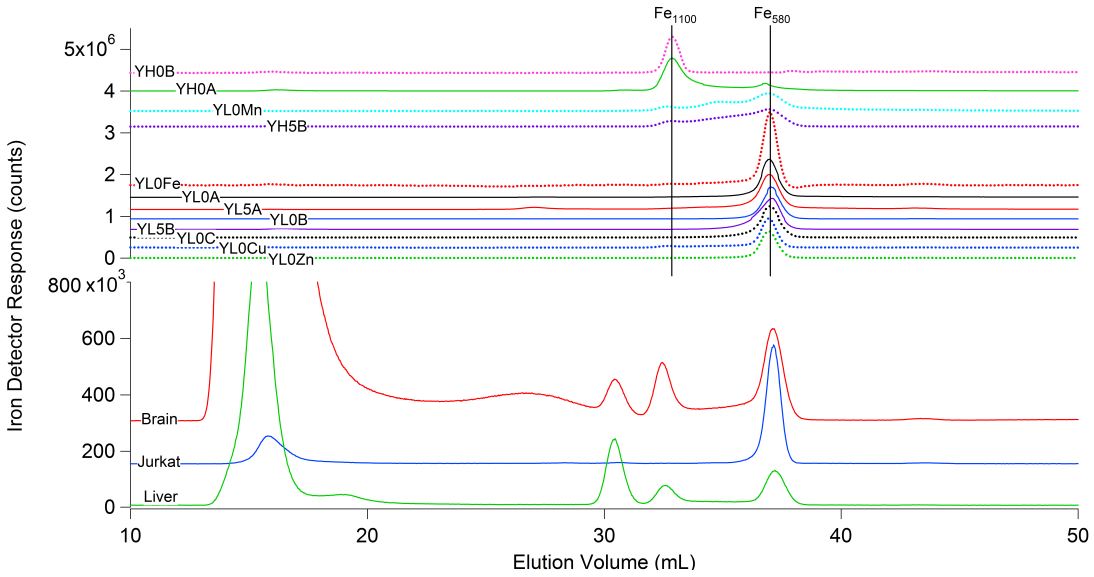

Figure III-5. Iron chromatograms of LMM mitochondrial FTSs.

half of 1% of the Fe in mitochondria). Fe_{200} may be an artifact of the isolation procedure, with healthy mitochondria devoid of this species.

Iron chromatograms of FTSs from mitochondria isolated from mammalian cells and tissues were similar to those of yeast, but with additional peaks. The chromatogram of FTS from mitochondria of Jurkat cells was similar to that of yeast harvested during the exponential growth phase, with Fe_{580} dominating. The chromatogram from mouse tissues also exhibited Fe_{580}, but intense peaks corresponding to masses of 2000 and 1200 Da (Fe_{2000} and Fe_{1200}, respectively) were also observed. Fe_{2000} was not present in yeast mitochondria. Fe_{1200} in mouse mitochondria may or may not correspond to Fe_{1100} in yeast mitochondria; the two migrated near each other, but they did not comigrate. Concentrations of Fe_{2000} and Fe_{1100}/Fe_{1200} in mammalian mitochondria were ~10 μM each.

Copper

FTSs from mammalian mitochondria exhibited Cu peaks near or slightly beyond the 10 kDa cutoff (Figure III-6, top panel). The observed intensities of Cu species with masses of >10 kDa may be less than proportional to their actual concentration in mitochondria, as some of these species may have been retained by the cutoff membrane. These cutoffs are not exact, such that some proportion of higher-mass Cu species also passes into the FTS, as observed. Also, our size-exclusion column has some resolving power beyond 10 kDa. For example, cytochrome c (Table II-1, 12384 Da) fell nicely on the calibration line (Figure II-1), although its mass is beyond the formal resolving limit of the column. Thus, a Cu complex with a mass of ~13 kDa would be detected and resolved

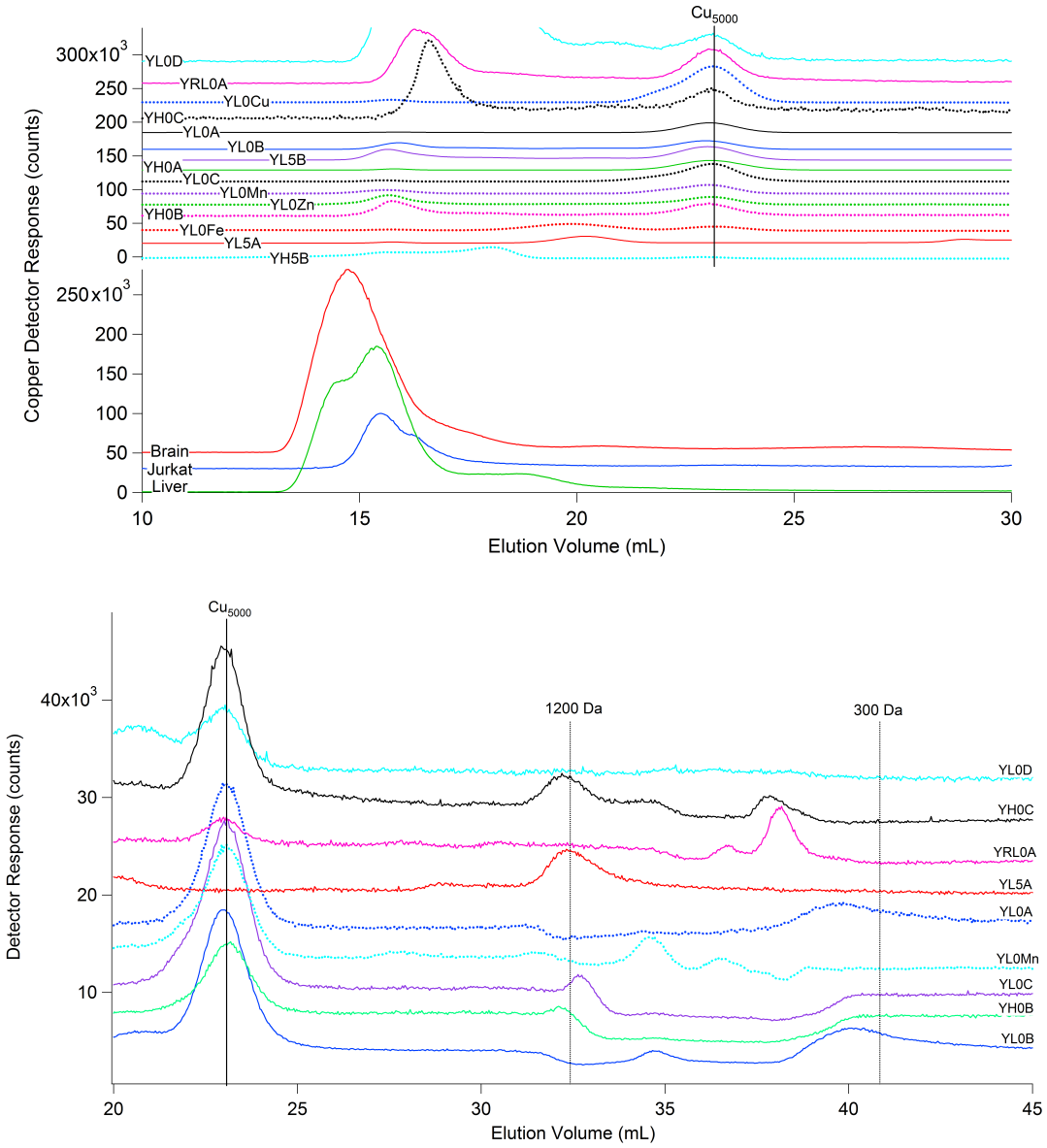

Figure III-6. Copper chromatograms of LMM mitochondrial FTSs.

by our experiment; indeed, such features are observed in FTSs from mammalian mitochondria.

The region between 10000 and 2000 Da exhibited the greatest reproducibility (Figure III-6, top panel). Cu-detected chromatograms of the FTS of mitochondria from yeast cells were dominated by a peak corresponding to a mass of 5000 Da; the corresponding concentration was ~16 μM. Cu_{5000} accounted for ~60% of the Cu in the FTS and ~20% of Cu in yeast mitochondria. With a mass of 5000 Da, Cu_{5000} might be proteinaceous. The intensity of this species increased 4-fold when the Cu concentration in the medium was increased 10-fold. Curiously, the Cu-detected chromatograms of the mammalian system did not exhibit Cu_{5000} or any other peak in 2000–10000 Da region. This was similar to the results of our previous study of mouse brain LMM extracts, in which no LMM Cu species were reproducibly evident but many HMM Cu species (8–48 kDa) were observed.[158]

For mitochondrial FTSs, the region between 200 and 2000 Da exhibited minor-intensity peaks with significant preparation-to-preparation variation (Figure III-6, bottom panel). At the high sensitive required to observe these peaks, some baseline drift is evident. Peaks corresponding to masses of ~300 Da may reflect hydrated Cu ions. The poorer reproducibility and low-intensity character of these LMM Cu-based peaks suggest that some Cu ions may dissociate from their endogenous complexes during mitochondrial isolation, and that the released ions coordinate to various ligands.

Cobalt

The Co-detected chromatograms of mitochondrial FTSs exhibited many peaks between 1200 and 300 Da (Figure III-7 and Table III-5), albeit with more batch-to-batch variability than for most other metals. The concentration of the dominant peak at 1200 Da (Co_{1200}) was 30 nM, 3 orders of magnitude lower than for many other LMM metal species. The similar masses of various cobalamins (1300–1700 Da) suggest that Co_{1200} is a cobalamin. FTS from yeast mitochondria exhibited other Co peaks, corresponding to masses between 840 and 200 Da, but the batch-to-batch variation in the intensity of these peaks was significant. Peaks in the 200 Da region were probably hydrated Co ions. Peaks corresponding to masses between 300 and 800 Da were probably not cobalamins as their masses were too low; their concentrations were in the nanomolar range.

Co chromatograms of mammalian samples were similar to each other, except that the intensities of the Co peaks in the Jurkat sample were very low. FTSs of mammalian mitochondria contained Co_{1200} as well as another cobalamin (Co_{1700}) with a mass of 1700 Da.

Molybdenum

Chromatograms of mammalian mitochondrial FTSs exhibited a single Mo peak (Mo_{730}) at 730 Da (Figure III-8 and Table III-5). No Mo species were detected in fermenting yeast mitochondrial FTSs.

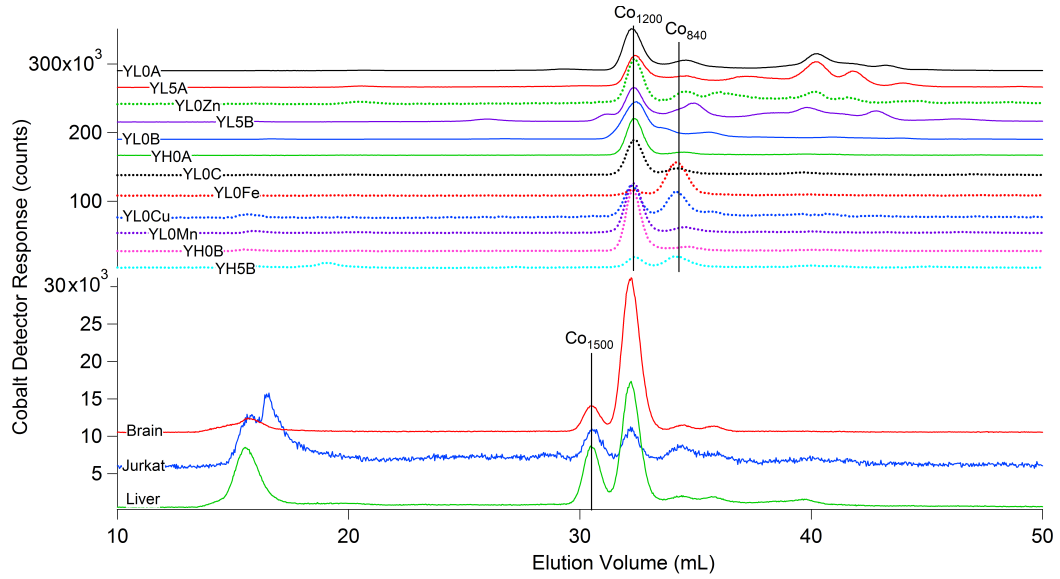

Figure III-7. Cobalt chromatograms of LMM mitochondrial FTSs.

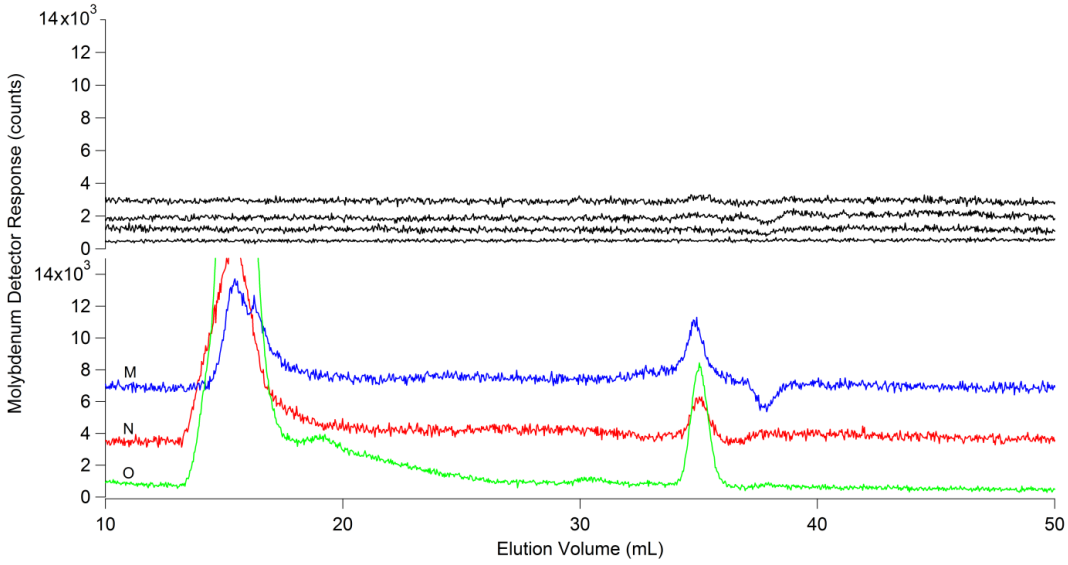

Figure III-8. Molybdenum chromatograms of LMM mitochondrial FTSs. Black traces are representative of those found in FTSs from yeast mitochondria. M) from mice brains, N) from human Jurkat cells, O) from mice livers.

Lability of LMM Metal Complexes

We assessed whether 1,10-phenanthroline (Phen) and bathophenanthroline disulfonate (BPS) could chelate the metal ions in the detected complexes. The FTS from a batch of yeast mitochondria was subjected to the LC-ICP-MS system, and Fe, Zn, Co, Mn, and Cu chromatograms were obtained (Figure III-9, black lines). Fractions containing LMM metal complexes were pooled and treated with BPS, but this had little effect. After being treated with BPS, Phen, and the reductant dithionite, the same pool exhibited chromatograms whose peaks were significantly changed (Figure III-9, red lines). The changes were numerous and dramatic, such that further systematic studies are required to interpret them. It is clear, however, that the dominant LMM metal complexes in yeast mitochondria can be labilized by metal chelators.

Discussion

In this study, we detected numerous LMM P, S, Mn, Fe, Co, Cu, and Zn compounds in mitochondria isolated from yeast and mammalian cells. A LMM Mo complex was detected exclusively in mitochondria from mammalian cells. We cataloged each and estimated their molecular mass and concentration within the organelle. The model of Figure III-10 illustrates the major detected species, including concentrations and suggested locations in the organelle. Most of these metal complexes are presumed to be in the matrix and used to metalate apo-metalloproteins. Cu_{5000} in yeast mitochondria and Mo_{730} in mammalian mitochondria may be located in the IMS. Further studies are required

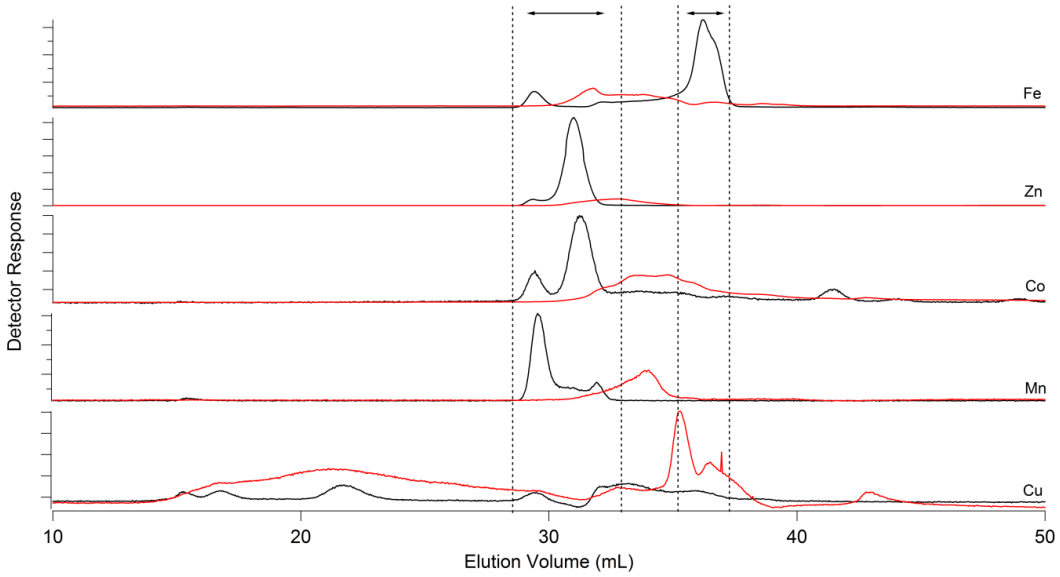

Figure III-9. Lability of LMM metal complexes. The FTS from yeast mitochondria were subjected to the LC-ICP-MS system. Fe, Zn, Co, Mn, and Cu chromatograms were obtained (black lines). Fractions were collected in the two regions which contained the major LMM peaks (two pairs of vertical dashed lines). Those fractions were pooled and treated with BPS (500 µM final concentration). After 15 min, the solutions were centrifuged and half of the supernatant was subjected again to the LC-ICP-MS system. The resulting chromatograms were essentially unchanged. The other half of the supernatant was treated with 1,10-phenanthroline and freshly prepared dithionite (500 and 750 µM, respective final concentrations). The solution was centrifuged again and the supernatant was subjected to the LC-ICP-MS system. Red lines are the resulting traces.

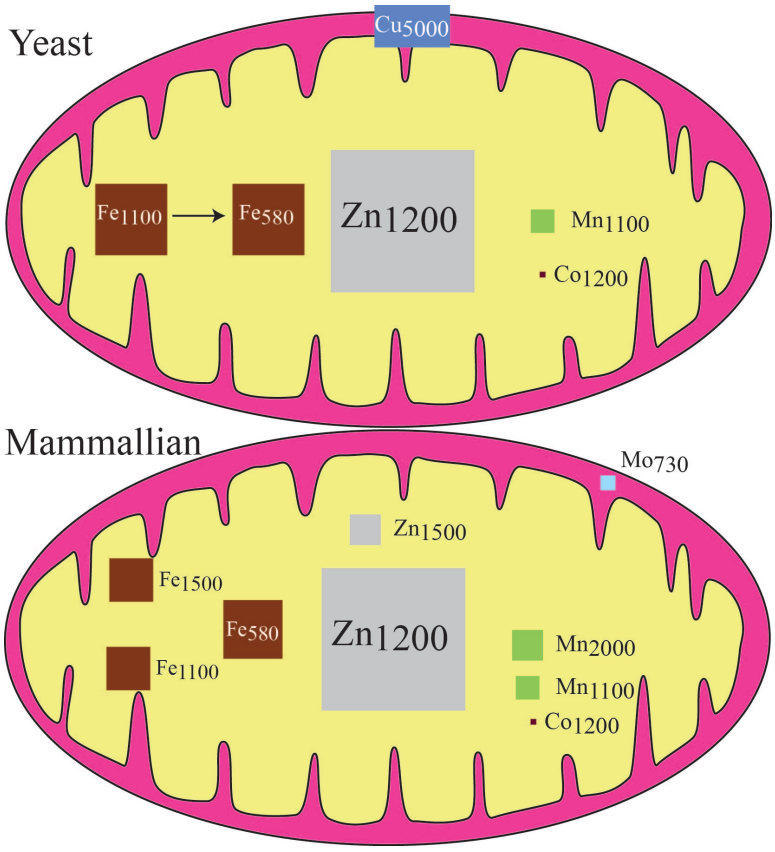

Figure III-10. Model of LMM metal complex speciation in yeast and mammalian mitochondria. The sizes of the colored squares represent the relative concentrations of various LMM species. Other details are given in the text.

to establish their locations, compositions, structures, and biochemical and physiological functions.

We previously detected a single Mn species in yeast mitochondria and proposed that it metalated apo-Sod2.[113] We now assign this role to Mn_{1100} despite a slightly lower mass. Mammalian mitochondria contain a second Mn enzyme, Type II arginase,[178,179] that catalyzes the synthesis of ornithine and may regulate the production of NO by nitric oxide synthase. An enzyme precursor is imported into the matrix where a signal sequence is clipped, and the protein folds and is metalated, perhaps by a second Mn complex in these organelles, Mn_{2000}.

Zn_{1200} in yeast mitochondria and Zn_{1200}, Zn_{900}, and Zn_{1500} in mammalian mitochondria probably compose the labile Zn pool that metallates various mitochondrial Zn proteins.[84] High concentrations of mitochondrial Zn inhibit respiration.[180] Perhaps ferrochelatase installs Zn_{1200} rather than Fe^{II} into protoporphyrin IX.[99] Mitochondria from neuronal cells contain Zn that can be mobilized and released when the IM is depolarized.[43] Mobilized Zn ions may correspond to one or more detected LMM Zn species.

Using fluorescence resonance energy transfer-based sensors, Palmer and co-workers detected labile Zn in mitochondria of HeLa cells.[106] McCranor et al.[105] used human carbonic anhydrase II variants to detect labile Zn in rat mitochondria. Labile Zn was detected in mitochondria from mammalian cells using modified GFP fused to calmodulin.[43,180] Chyan et al.[181] used a synthetic fluorescent probe to detect labile Zn in prostate cells. When the medium was spiked with 50 μM Zn, the fluorescence intensity of the mitochondria in normal cells increased 2.3-fold.

We anticipated that the Zn species detected in our study would be the same as those detected by fluorescence-based methods. However, if the reported concentration of the fluorescence-detected Zn species is accurate, we have not detected them. McCranor et al.[105] concluded that the concentration of labile Zn in mitochondria isolated from a rat cell line was 0.15 pM. Virtually the same concentration was reported for the labile Zn pool in mitochondria of HeLa cells.[106] These concentrations are 1 billion times lower than our estimates for the concentration of Zn_{1200}. Our LC-ICP-MS system simply cannot detect picomolar concentrations (1pM Zn = 0.07 ppt) so our ability to detect Zn species implies that they are present at concentrations greater than hundreds of picomolar.

Another consideration is that the collective volume of mitochondria in cells is just a few percent of the volume of a yeast cell, suggesting a mitochondrial volume of $\sim 10^{-15}$ L. Within this volume, a concentration of 0.15 pM would correspond to 10^{-4} molecules of labile mitochondrial Zn per cell. This implies that just 1 of every 10000 cells would contain mitochondria with a single labile Zn ion, a property that should be easily distinguished from that in which all mitochondria in a cell population uniformly fluoresce when treated with a sensor. As far as we are aware, there have been no reports of stochastic single-molecule fluorescence in these organelles. This implies that each mitochondrion contains a sizable number of labile Zn ions, which implies, in turn, a labile Zn concentration orders of magnitude higher than reported.

In contrast, our Zn results are fully consistent with those of Atkinson et al.,[84] who used LC to detect a LMM cationic Zn pool in the matrix of yeast mitochondria. Their reported pool probably corresponds to Zn_{1200}. The Zn ions in their pool migrate through a

Sephadex G25 column in accordance with a mass slightly lower than that of vitamin B_{12} (1355 Da), within error of the mass of our Zn_{1200}. The size of their Zn pool increases when the growth medium is supplemented with Zn, similar to what we observed with Zn_{1200}. The Zn species composing their pool is cationic (implying ligands that on average are uncharged), resistant to boiling, and inert toward proteinase K digestion (implying that it is nonproteinaceous). This species was proposed to metalate numerous Zn enzymes in the matrix, including alcohol dehydrogenases, Leu9, and cytochrome c oxidase. Depleting this pool (by placing the apo form of a Zn enzyme into the matrix) causes a respiratory growth defect, consistent with Zn_{1200} serving to metalate proteins required for respiration.

Lutz et al.[145] discovered that 1,10-phenanthroline inhibits Fe/S cluster assembly in intact mitochondria. Similar results were obtained by Amutha et al.[182] and Pandey et al.[183] who speculated that mitochondria must contain a pool of Fe that is used as feedstock for Fe/S cluster assembly. Phen was thought to penetrate the matrix and coordinate the pool, making it unavailable for Fe/S cluster assembly. Unaware of those results, Holmes-Hampton et al.[144] performed the same experiment in which Phen was added to intact ^{57}Fe-enriched mitochondria. Using Mössbauer spectroscopy, they discovered a pool of non-heme high-spin (NHHS) Fe^{II} ions that were selectively chelated by phen. When considered with the results of Lutz, Amutha, and Pandey, the pool of NHHS Fe^{II} ions very likely functions as feedstock for Fe/S cluster biosynthesis. The associated Mössbauer parameters indicate an Fe^{II} species with five or six oxygen and nitrogen donors but no sulfurs. This HS $Fe^{II}(O/N)_{5\text{-}6}$ species appears to be in equilibrium with a HS Fe^{III} species and with Fe^{III} oxyhydroxide nanoparticles.[143,144] The concentration of NHHS Fe^{II} that constitutes this

pool depends on the metabolic state of the cells from which the mitochondria are isolated. In fermenting mitochondria, the concentration of the NHHS Fe^{II} was ~150 μM, whereas in respiring mitochondria, it was much lower. Because the concentrations of respiratory complexes are 3 times higher in respiring mitochondria, Morales et al.[143] proposed that this decline was due to an increased rate of Fe/S cluster assembly (and an invariant rate of import of Fe into the pool) under respiration conditions.

Rauen et al.[42] detected a labile Fe pool in mitochondria using rhodamine-based fluorescence sensors and estimated a concentration of ~16 μM.[142] It is intriguing to consider that the same species detected by fluorescence is the NHHS Fe^{II} species detected by Mössbauer spectroscopy and used for Fe/S cluster assembly. The 10-fold disparity in concentration may reflect differences in the cells used or different metabolic conditions.

In this study, we have detected two LMM Fe complexes in mitochondria, Fe_{1100} and Fe_{580}. This contrasts with our previous results in which a single LMM Fe complex with a mass of ~3000 Da was detected in soluble extracts of mitochondria isolated[113] from fermenting yeast cells harvested as they entered postexponential growth. There may have been a systematic error in calibrating masses, but we cannot identify any. More likely, different Fe species may be present, depending on metabolic conditions or preparation methods.

The collective concentration of Fe_{1100} and Fe_{580} in mitochondria was ~100 μM; some chromatograms were dominated by one Fe species, while others were dominated by the other. Fe_{1100} and Fe_{580} appear to be related, as the former transformed into the latter by simply incubation of the FTS for 5 days in a refrigerated inert atmosphere. Although much

remains to be learned regarding this relationship and the function of these species, we tentatively suggest the following model:

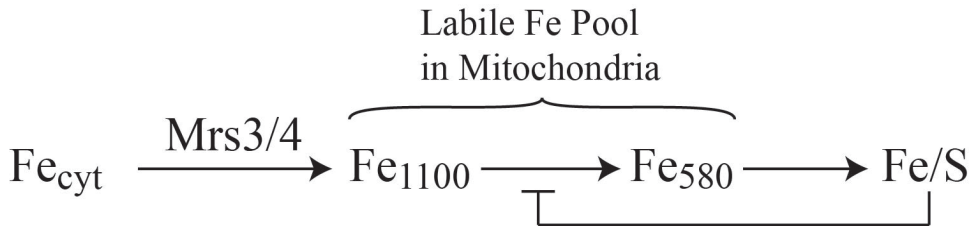

The key feature of this relationship is that the level of Fe/S clusters in the matrix inhibits the conversion of Fe_{1100} to Fe_{580}. During exponential growth, the steady-state level of Fe/S clusters is low because the clusters are quickly being installed into various apoprotein targets. This relieves the inhibition, such that Fe_{1100} levels decline and Fe_{580} levels rise (as observed). As cell growth declines, the steady-state level of Fe/S clusters builds, which strengthens the inhibition of the transforming reaction. Thus, Fe_{1100} accumulates and Fe_{580} declines (as observed). This model must be tested further; it currently serves merely to organize our results. The role of Fe_{1500} in mammalian cells remains unknown.

Curiously, the dominant S, Mn, Zn, and Fe (at high culture density) species in fermenting yeast mitochondria all have molecular masses of ~1100 – 1200 Da. One interesting possibility is that all of these complexes possess a similar coordination environment that includes sulfur as a ligand. Metal glutathione complexes have been proposed as trafficking ligands in eukaryotic cells.[153,157,184] Conceivably, these metal

complexes might be related to $[M(SG)_4]^{2-}$, which would have a mass of ~1300 Da. Further studies are required to evaluate this possibility.

Winge and Cobine reported that 70 – 85% of the Cu in mitochondria is a nonproteinaceous species that serves trafficking and/or metallating functions.[33,44,66] They considered this species (Cu_L) to be "low-molecular weight," but it migrates in accordance with a 13 kDa globular protein.[44] The complex with characteristics most like those of Cu_L is Cu_{5000}. Like that of Cu_{5000}, the concentration of Cu_L is sensitive to the concentration of Cu in the medium; the level of Cu_L increases 6-fold in cells grown in medium supplemented with 500 μM Cu.[44,66] One difference is that Cu_L is found in both yeast and mouse liver mitochondria, while we have detected Cu_{5000} in only yeast mitochondria. More of the Cu ions in mammalian mitochondria are in a HMM form, including some Cu species with masses near 13 kDa.

Cu_{5000} accounted for 22% of the Cu in mitochondria (16 μM out of 71 μM total). Morales et al.[143] estimated that the concentration of cytochrome c oxidase in fermenting yeast mitochondria was ~8 μM, implying ~24 μM Cu (there are three Cu ions per enzyme molecule). Combining these two concentrations (16 + 24 = 40 μM) leaves ~30 μM for all other Cu-binding proteins in mitochondria, including Sco1/2, Cox17, CuZn Sod1, Ccs1, and Cu_L. Cu_L has been estimated to represent 85% of the Cu in yeast mitochondria.[88] In our preparations, this would correspond to 60 μM. The region between 2000 and 200 Da was devoid of any peak with an intensity corresponding to anywhere near 60 μM (observed peaks are roughly $1/100^{th}$ of this concentration).

Many studies have detected labile Cu in mitochondria, all of which have been attributed to Cu_L. Dodani et al.[82] developed a fluorescent sensor (Mito-CS1) that selectively targets the mitochondria of HEK293T cells and human fibroblasts where it binds a labile Cu^I species. Yang et al.[81] used a custom-designed fluorescent sensor along with synchrotron X-ray fluorescence to detect labile Cu in mitochondria. Their data indicate a Cu^I complex with linear or trigonal geometry and primarily sulfur coordination.

Our experiment with Phen suggests that Cu_{5000} is labile, raising the possibility that the fluorescence-detected labile Cu in mitochondria might arise from Cu_{5000} rather than (or in addition to) Cu_L. However, the absence of Cu_{5000} or other LMM Cu species in mitochondria from mammalian cells would seem to argue against this possibility. Also uncertain is whether Cu_{5000} (or Cu_L or some other Cu-trafficking species) is used to metalate cytochrome c oxidase. Cu is thought to be imported into the matrix via Pic2, a mitochondrial carrier family protein.[67] Cu_L in the matrix has also been suggested to metalate the Cu-containing proteins in the IMS,[79] but further studies are required to establish this. Given the size of Cu_{5000}, transporting it across the IM from the matrix to the IMS seems unlikely. The possibility that the Cu used to metalate cytochrome c oxidase travels from the cytosol directly to the IMS should be reconsidered. Cu_{5000} may be just small enough to pass through the pores of the OM. However, further studies are needed to evaluate these ideas.

The concentrations of LMM Co species observed here were very low, leading us to wonder whether they are physiological. They may correspond to cobalamin degradation products, possibly including hydrated Co ions at ~200 Da. Cobalamins are noncovalently

attached to proteins, and tiny quantities may have been released during isolation. Alternatively, the observed species may be trafficking complexes that metalate methyl-malonyl-CoA mutase, the only known cobalamin-containing mitochondrial enzyme.[119] Cobalamins are not synthesized by mammalian cells but are imported as vitamin B_{12}. The mechanism by which B_{12} enters mitochondria involves trafficking proteins CblB, CblC, and CblD.[119]

The presence of a LMM Mo species (Mo_{730}) in mammalian mitochondria and its absence in yeast mitochondria are consistent with the presence of mitochondrial amidoxime reducing components 1 and 2 (mARC1/2) in mammalian mitochondria and the absence of these and any other Mo-containing enzymes in yeast. mARC1/2 are molybdopterin-containing proteins found in the OM of mitochondria,[185] where they catalyze the reduction of NO_2^- to NO and might be involved in a signaling pathway that regulates NADH-dependent hypoxic NO production.[186] The mass of Mo_{730} is within the range of molybdopterins (albeit with two pterin coenzymes coordinated). Mo_{730} may be associated with the metalation of mARC1/2. Alternatively, it may reflect a tiny amount of a molybdopterin released into solution during mitochondrial isolation.

We have used the same LC-ICP-MS system to detect LMM metal complexes in mouse brain homogenates, including complexes found in mitochondria and other regions of the brain.[158] At this early stage of investigation, we have focused solely on identifying common species. We suggest the following correspondences: P_{490}(brain) ≈ P_{520}(mito), S_{940}(brain) ≈ S_{1100}(mito), Fe_{1720}(brain) ≈ Fe_{1500}(mito), Fe_{510}(brain) ≈ Fe_{580}(mito),

Zn_{1760}(brain) ≈ Zn_{1500}(mito), Mn_{2710}(brain) ≈ Mn_{2000}(mito), and Mn_{1270}(brain) ≈ Mn_{1100}(mito). More work is needed to establish these associations.

The regulatory mechanisms used to sense the concentrations of these metals in the environment and to control the corresponding concentrations in the cytosol and mitochondria are not understood. The increased concentrations of particular LMM metal complexes when cells were grown on media that contained higher-than-normal concentrations of the same metal ion undoubtedly reflects such mechanisms. We suspect that (a) the rate of import of metal into the cytosol increases with the increase in nutrient metal concentration and (b) the increased cytosolic metal concentration increases the rate of import of metal from the cytosol into the mitochondria. Systematic studies are required to probe the specific nature of this regulation.

In summary, we have detected numerous labile LMM metal complexes in mitochondria using an LC-ICP-MS approach. The major advantage of this approach, relative to the more popular fluorescence-based metal binding probes, is that a portion of the detected metal complexes need not be destroyed. Keeping the complexes intact will allow for further downstream characterizations. The LC-ICP-MS method also allows individual metal complexes to be separated and cataloged such that the vague "pool" concept can eventually be discontinued. Also, the area under each chromatography peak can be quantified, thereby allowing estimates of the metal complex concentrations within cells and organelles.

The LC-ICP-MS approach does suffer some disadvantages, the most important being that cells must be disrupted during the preparation of extracts. Doing so could mix

cellular compartments, altering the pH and redox state of the environment in which the metal complexes exist. This might, in turn, induce ligand exchange or other reactions, resulting in artifacts that could easily be mistaken for bona fide endogenous metal complexes. Indeed, some metal complexes that we have detected here might be artifacts. Both the LC-ICP-MS approach and the fluorescence-based chelator approach will ultimately be required to detect, catalog, identify, and characterize the structure and function of these recalcitrant cellular components. Doing so will afford a far more sophisticated view of transition metal ion trafficking and regulation in cells, which should, in turn, provide significant new insights into metal-associated diseases.

CHAPTER IV

AN INTEGRATIVE ANALYSIS OF *MRS3*Δ*MRS4*Δ *SACCHAROMYCES CEREVISIAE* UNDER IRON-DEFICIENT AND IRON-SUFFICIENT CONDITIONS

Introduction

Mitochondria have a critical need for iron (Fe) since they are the major site of iron-sulfur cluster (ISC) biosynthesis in eukaryotic cells and the only site for the Fe-insertion step of heme biosynthesis.[187,188] Mrs3 and Mrs4 (Mrs3/4) in *Saccharomyces cerevisiae* are homologous mitochondrial inner membrane (IM) proteins that deliver cytosolic Fe (Fe_{cyt}) into the matrix, presumably for use in both processes.[99,132,133,135,189] Mammalian homologs of Mrs3/4 are called *mitoferrins*.[130,190,191] The cytosolic Fe species imported by these proteins is unknown, but the small, membrane-spanning channel through which the Fe must traverse suggests a low-molecular-mass (LMM) coordination complex.[132,139,170]

Mössbauer spectra of isolated mitochondria reveal a large pool of non-heme high-spin (NHHS) Fe^{II} complexes in the organelle.[144] The overall concentration of Fe in mitochondria typically ranges from 400 – 800 μM, while that of the Fe^{II} pool ranges from 60 – 200 μM.[143,174] The pool is selectively chelated when isolated mitochondria are treated with the membrane-permeable chelator 1,10-phenanthroline.[144] The same treatment inhibits ISC biosynthesis,[145,146,182] suggesting that the pool serves as feedstock for ISC assembly and perhaps heme biosynthesis.[192]

Size-exclusion chromatograms of LMM mitochondrial flow-through solutions (FTSs) from exponentially growing fermenting yeast cells exhibit a single Fe-containing

peak corresponding to a mass of ~580 Da.[48] The concentration of the so-called "Fe_{580}" species is the same order as that of the NHHS Fe^{II} pool, raising the possibility that Fe_{580} comprises the pool and that this complex is the Fe-containing substrate for ISC (and perhaps heme) biosynthesis. Mammalian mitochondrial FTSs also contain Fe_{580} as well as additional LMM Fe species.[48] Mitochondrial FTSs from fermenting yeast that were harvested under steady-state conditions exhibit a LMM Fe species with a mass of ~1100 Da. Inexplicably, anaerobic incubation of such a FTS resulted in the disappearance of Fe_{1100} and the appearance of Fe_{580} in the chromatogram.

Deleting either *MRS3* or *MRS4* affords no observable phenotype, indicating that the two proteins possess redundant functions.[132,189] However, simultaneous deletion of both genes, affording the ΔΔ strain, yields a slow-growth phenotype in Fe-deficient media. Mitochondria isolated from Fe-deficient ΔΔ cells contain low concentrations of hemes and exhibit low ISC-containing enzyme activities.[132,188] ΔΔ cells in Fe-sufficient medium grow at WT rates, and the activities of ISC-containing enzymes are ca. normal.[99,132,135,136,189]

Another phenotype of ΔΔ cells grown under both Fe-deficient and Fe-sufficient conditions is that they accumulate large amounts of iron relative to WT cells grown under the same conditions.[132,133,189] Fe accumulation reflects the activation of the iron regulon. The occurrence of this under Fe-sufficient conditions indicates Fe dysregulation. The iron regulon constitutes 20 – 30 genes, including *MRS3/4*, that are involved in Fe import, trafficking, and regulation. The regulon is activated when WT cells are Fe-starved (e.g., when grown in the presence of the Fe^{II} chelator BPS) or when ISC biosynthetic activity in mitochondria is low.[187,188] In WT cells, the Fe regulon is deactivated under Fe-sufficient

conditions. However, in ISC-mutant cells (e.g., Yfh1Δ), the iron regulon is activated regardless of the concentration of iron in the medium ([Fe_{med}]).[193] This results in a massive accumulation of Fe^{III} phosphate oxyhydroxide nanoparticles (NP) in mitochondria. Fe also accumulates in ΔΔ cells but not in mitochondria because the absence of Mrs3/4 impedes Fe import into this organelle.[132,189] The Fe concentration in ΔΔ mitochondria is ca. half of that in WT mitochondria.[132,189] The presence of Fe in the organelles from ΔΔ cells implies the existence of alternative Fe import pathways that do not involve Mrs3/4. Alternative pathways may involve Rim2, another IM Fe importer that also exchanges pyrimidine triphosphate.[70,136,194,195]

Vacuoles are acidic organelles in yeast that store and sequester iron and are another major organelle involved in Fe trafficking and regulation. Ccc1 is the only known vacuolar Fe importer of Fe_{cyt}.[196] In ΔΔ cells, the rate of vacuolar Fe import through Ccc1 is greater than in WT cells, despite lower-than-WT concentrations of the Ccc1 protein.[133] Li and Kaplan hypothesized that Ccc1 activity is higher in ΔΔ cells than in WT cells, and they proposed that there is a signaling pathway between mitochondria and vacuoles that regulates Ccc1 activity.[133,195]

In this study, we examined the ΔΔ yeast strain using biophysical and bioanalytical methods that allow their Fe content to be characterized more extensively than in previous studies. These methods included Mössbauer (MB), EPR, and UV-Vis spectroscopies, as well as liquid chromatography (LC) monitored by inductively coupled plasma mass spectrometry (LC-ICP-MS). In addition, offline ICP-MS was utilized to measure metal concentrations of ΔΔ cells and isolated mitochondria. Collectively, this study provides

new insights into iron trafficking and regulation in yeast. Our mechanism can explain how Fe-deficient Mrs3/4 ΔΔ cells recover in terms of growth and mitochondrial function when grown in Fe-sufficient medium, and how Fe homeostasis remains dysfunctional even under such conditions.

Results

ΔΔ and WT cells were grown in minimal medium containing 1, 10, or 40 μM Fe^{III} citrate. Some batches that contained 1 μM Fe^{III} citrate were pretreated with bathophenanthroline disulfonate (BPS) to chelate endogenous Fe and increase the degree of Fe deficiency. We will refer to the cells as *ΔΔ1* and *WT1*, *ΔΔ10* and *WT10*, *ΔΔ40* and *WT40*, and $\Delta\Delta1_{BPS}$ and $WT1_{BPS}$, respectively, where the number refers to the [$^{57}Fe_{med}$] in μM and the BPS subscript indicates the presence of the chelator. ^{57}Fe was added to BPS-treated media to enrich cells with the Mössbauer-active isotope. Glycerol and ethanol were exclusively used as nonfermentable carbon sources to force cells to respire. Cells and mitochondria were harvested during exponential growth phase. As expected, *MRS3* and *MRS4* were absent in ΔΔ cells (see Figure II-2).

The ΔΔ Slow-Growth Phenotype

Exponential growth rates (α) of respiring ΔΔ and WT cells grown under Fe-deficient and Fe-sufficient conditions were obtained from the slopes of $\ln(OD_{600})$ vs. time plots (Figure IV-1). Analysis of experimentally determined α values (Table IV-1) revealed an Fe-dependent growth defect in yeast cells lacking Mrs3/4. Under Fe-deficient

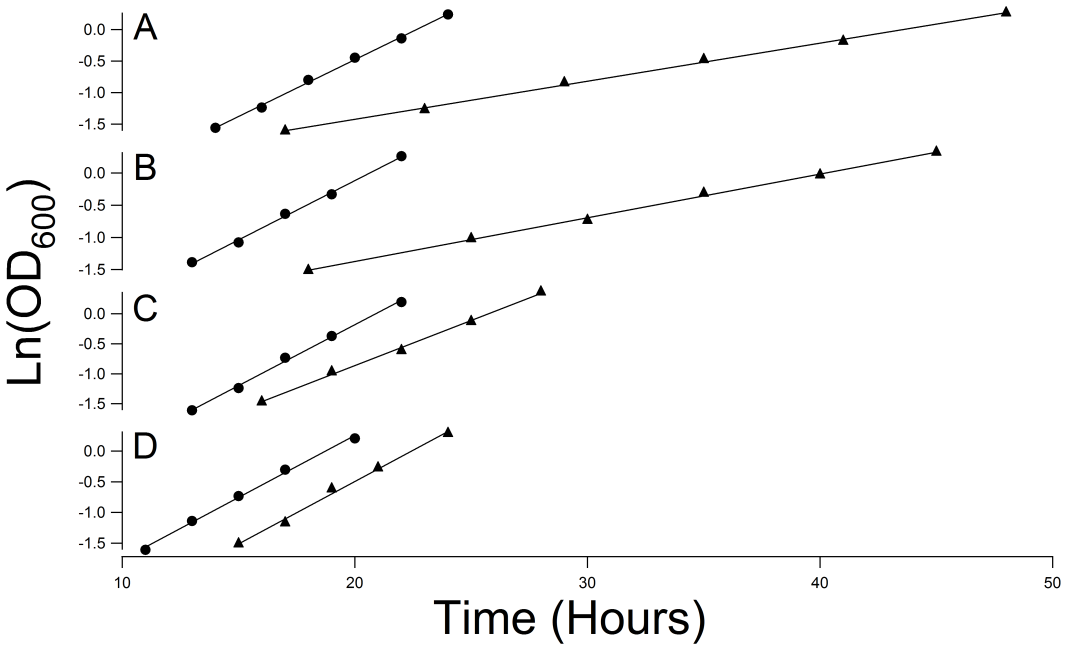

Figure IV-1. Growth rates of WT and ΔΔ cells. A, $WT1_{BPS}$ and $\Delta\Delta1_{BPS}$; B, WT1 and ΔΔ1; C, WT10 and ΔΔ10; D, WT40 and ΔΔ40. WT designated as circles and ΔΔ designated as triangles. Exponential growth rates (α) in units of hr^{-1} (Table IV-1) are the slopes of the plotted lines. Average R^2 for these fits was 0.997.

Table IV-1. Metal concentrations in whole cells and isolated mitochondria. All concentrations are expressed in units of μM. Whole cell concentrations and growth rates are averages from two independent experiments (n=2). Mitochondrial metal concentrations are from a single preparation for each strain and condition (n=1).

Sample	Growth Rate (α) (hr^{-1})	[Fe] (μM)	[Cu] (μM)	[Mn] (μM)	[Zn] (μM)
		Whole Cells			
$\Delta\Delta1_{BPS}$	0.060	360 ± 30	290 ± 10	32 ± 5	240 ± 45
ΔΔ1	0.068	680 ± 70	280 ± 30	25 ± 14	200 ± 50
ΔΔ10	0.150	2160 ± 60	320 ± 40	39 ± 8	190 ± 30
ΔΔ40	0.204	3920 ± 80	320 ± 10	29 ± 7	250 ± 25
		Ave: 1780 ± 1600	**Ave: 300 ± 30**	**Ave: 31 ± 6**	**Ave: 220 ± 30**
$WT1_{BPS}$	0.181	120 ± 20	120 ± 10	21 ± 4	310 ± 65
WT1	0.184	200 ± 20	140 ± 20	24 ± 6	300 ± 20
WT10	0.203	480 ± 30	130 ± 10	29 ± 3	315 ± 60
WT40	0.202	880 ± 70	140 ± 20	31 ± 11	330 ± 60
		Ave: 420 ± 340	**Ave: 130 ± 20**	**Ave: 29 ± 6**	**Ave: 310 ± 10**
		Isolated Mitochondria			
ΔΔ1		690	63	31	180
ΔΔ40		740	48	34	210
		Ave: 720 ± 20	**Ave: 60 ± 10**	**Ave: 32 ± 2**	**Ave: 200 ± 20**
WT1		430	110	22	250
WT40		690	89	27	320
		Ave: 560 ± 130	**Ave: 100 ± 20**	**Ave: 29 ± 5**	**Ave: 280 ± 50**

conditions, ΔΔ cells grew substantially slower than WT cells, whereas under Fe-sufficient conditions, they grew as fast as WT cells. Thus, the "slow-growth" phenotype of ΔΔ cells was ameliorated as the Fe concentration of the growth medium ([Fe_{med}]) increased.

Iron Concentrations in ΔΔ Cells and Mitochondria

To better characterize the Fe-dependent growth phenotype exhibited by ΔΔ cells, we examined the Fe concentration in ΔΔ cells ([Fe_{cell}]). [Fe_{cell}] in ΔΔ cells was substantially higher than in WT cells grown on the same medium (Table IV-1). This "iron overload" phenotype was observed for all nutrient conditions examined, including those for which the growth rates of ΔΔ cells were comparable to those of WT cells. Isolated ΔΔ mitochondria were not Fe-overloaded (Table IV-1), indicating that the excess Fe in ΔΔ cells had accumulated in non-mitochondrial locations. If mitochondria occupy 25% of the volume of respiring ΔΔ1 and ΔΔ40 cells, then non-mitochondrial regions would contain 680 and 5000 μM Fe, respectively. Similar calculations for WT1 and WT40 cells afford non-mitochondrial Fe concentrations of ca. 120 and 940 μM Fe, respectively. In both WT and ΔΔ cells, Fe accumulated in non-mitochondrial locations as [Fe_{med}] increased, but the extent of accumulation in ΔΔ cells was ~6 times greater.

The massive accumulation of Fe in ΔΔ cells indicates that the Fe regulon is activated under *both Fe-deficient and Fe-sufficient conditions*. Ironically, Fe-overloaded ΔΔ cells grown under Fe-sufficient conditions (for which ISC activity is normal) can be activated, we reasoned that the vast majority of the accumulated Fe must not be "sensed"

by the cell and is not part of Fe regulation. We also reasoned that the concentration of the sensed species in Fe-sufficient ΔΔ cells, whatever it is, must be *below* its set-point concentration. Thus, we sought to identify an Fe-containing species in the cell that was present in sub-WT concentrations in ΔΔ cells grown under all [Fe_{med}] conditions.

Mössbauer Spectra of Whole Cells and Isolated Mitochondria

To determine the forms of Fe that accumulate in ΔΔ cells and identify the sensed Fe species, we employed Mössbauer (MB) spectroscopy. All components and parameters used in MB simulations are given in Table IV-2. The low-temperature (5 K) low-field (0.05 T) MB spectrum of $WT1_{BPS}$ cells (Figure IV-2E) was dominated by a central quadrupole doublet (CD). A minor doublet with parameters typical of NHHS Fe^{II} was also evident. Both features were simulated above the spectrum (green and blue lines, respectively). The CD arises from $[Fe_4S_4]^{2+}$ clusters and LS Fe^{II} hemes (the two types of centers cannot be resolved by MB spectroscopy) (REF). MB spectra of respiring mitochondria are dominated by the CD. This situation arises because respiratory complexes contain large numbers of ISCs and heme centers, and these complexes are highly expressed in respiring cells (Holmes-Hampton 2012).

We previously assumed that *all* of the CD intensity in whole cell MB spectra arose from mitochondrial ISCs and LS Fe^{II} hemes (Holmes Hampton). However, non-mitochondrial $[Fe_4S_4]^{2+}$ clusters, assembled by the CIA (cytosolic iron-sulfur cluster assembly system) must contribute to the CD in whole cell MB—the only issue is how much it contributes. Our current MB spectra are most consistent assuming that roughly

Table IV-2. Summary of Fe percentages and concentrations determined by Mössbauer spectroscopy. Parameters for the NHHS Fe^{III} sextet in ΔΔ spectra: $\delta = 0.54 \pm 0.05$ mm/s; $\Delta E_Q = 0.62 \pm 0.08$ mm/s; $D = 0.3 \pm 0.1$ mm/s; $E/D = 0.29 \pm 0.02$; $\eta = 1.5 \pm 1$; $A_{iso} = -220 \pm 8$ kG; $\Gamma = 0.77 \pm 0.22$ mm/s. Parameters for the NHHS Fe^{III} sextet in WT spectra: $\delta = 0.56 \pm 0.03$ mm/s; $\Delta E_Q = 0.42 \pm 0.05$ mm/s; $D = 0.5$ mm/s; $E/D = 0.33 \pm 0.01$; $\eta = 1.8 \pm 0.5$; $A_{iso} = -228 \pm 3$ kG; $\Gamma = 0.4$ mm/s. Central doublet, [$\delta = 0.45 \pm 0.01$; $\Delta E_Q = 1.11 \pm 0.05$; $\Gamma = 0.50 \pm 0.15$]; NHHS Fe^{II} doublet, [$\delta = 1.23 \pm 0.06$; $\Delta E_Q = 3.07 \pm 0.17$; $\Gamma = 0.59 \pm 0.16$]; Heme Doublet, [$\delta = 0.87 \pm 0.11$; $\Delta E_Q = 2.22 \pm 0.04$; $\Gamma = 0.49 \pm 0.19$], $[Fe_2S_2]^{2+}$ Doublet [$\delta = 0.30 \pm 0.04$; $\Delta E_Q = 0.44 \pm 0.07$; $\Gamma = 0.48 \pm 0.19$], Fe^{III} nanoparticles [$\delta = 0.50 \pm 0.05$; $\Delta E_Q = 0.50 \pm 0.06$; $\Gamma = 0.4 \pm 0.04$] (all units in mm/s). The sum of all percentages of Mössbauer components was forced to 100% but 10% - 15% of spectral intensities were typically unaccounted for by these components.

Sample	Cells or Mitos	Fe^{III} Sextet	Central Doublet	NHHS Fe^{II} Doublet	Heme Doublet	$[Fe_2S_2]^{2+}$ Doublet	Fe^{III} Nanoparticles
		%; [μM]	%; [μM]	%; [μM]	%; [μM]	%; [μM]	%; [μM]
$\Delta\Delta1_{BPS}$	C	11; 40	25; 90	47; 170	6; 20	---	11; 40
ΔΔ1	C	50; 340	16; 110	20; 140	3; 20	---	11; 70
ΔΔ10	C	49; 1060	9; 190	6; 130	5; 110	---	31; 670
ΔΔ40	C	56; 2190	4; 160	4; 160	3; 120	---	33; 1290
$WT1_{BPS}$	C	0; 0	69; 84	12; 14	12; 14	7; 8	---
WT1	C	39; 78	39; 78	10; 20	4; 8	8; 16	---
WT10	C	39; 190	39; 190	11; 50	5; 20	6; 30	---
WT40	C	52; 460	25; 220	8; 70	6; 50	9; 80	---
ΔΔ1	M	9; 60	6; 40	8; 60	---	---	77; 530
ΔΔ40	M	0; 0	63; 475	15; 110	11; 80	---	10; 75
WT1	M	15; 60	42; 180	18; 80	4; 20	21; 90	---
WT40	M	0; 0	57; 390	30; 210	2;10	11;80	---

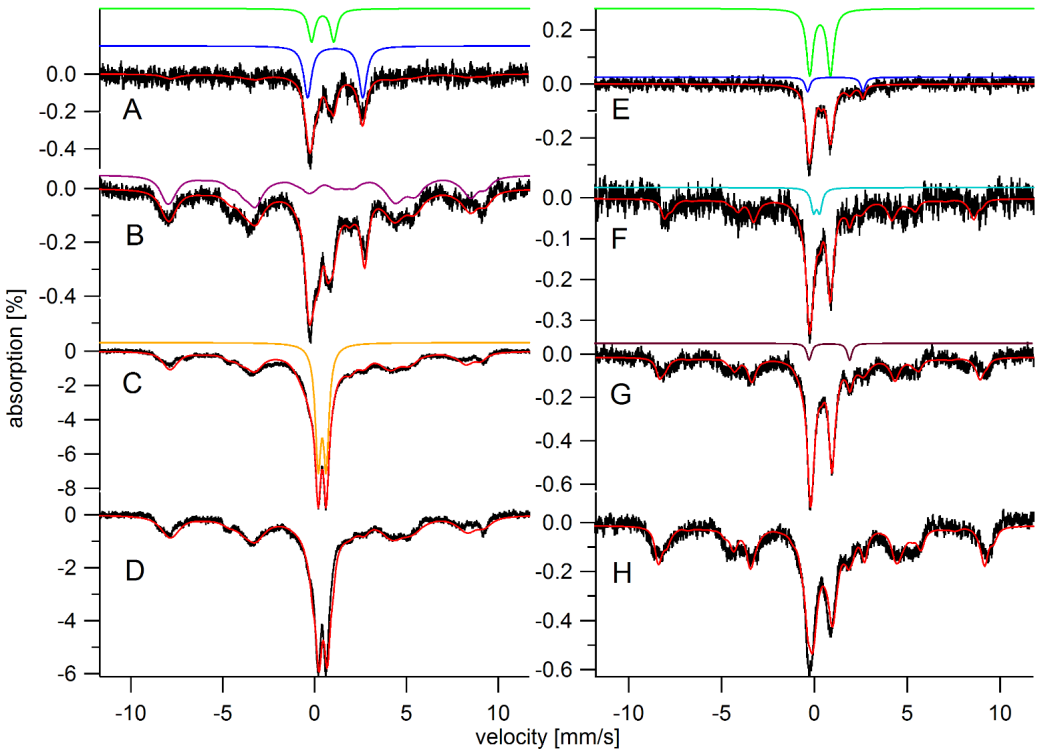

Figure IV-2. Mössbauer spectra of respiring whole cells. A, $\Delta\Delta1_{BPS}$; B, $\Delta\Delta1$; C, $\Delta\Delta10$; D, $\Delta\Delta40$; E, $WT1_{BPS}$; F, WT1; G, WT10; H, WT40. Solid lines are simulations for the Central Doublet (green), NHHS Fe^{II} doublet (blue), vacuolar HS Fe^{III} sextet (purple), Fe^{III} oxyhydroxide nanoparticles (gold), $[Fe_2S_2]^{2+}$ doublet (teal), and HS Fe^{II} heme doublet (brown). The temperature was 5 K and an applied field of 0.05 T was applied parallel to the gamma rays. The solid red lines are composite simulations assuming the area percentages for each component listed in Table IV-2.

half of the overall CD intensity in the $WT1_{BPS}$ spectrum is due to *non-mitochondrial* CIA-assembled $[Fe_4S_4]^{2+}$ clusters. Such a proportion is required to interpret the MB spectra of Fe-deficient ΔΔ cells (Figure IV-2, A and B).

The MB spectrum of $\Delta\Delta1_{BPS}$ cells (Figure IV-2A) was dominated by the same two doublets, albeit with different relative intensities. The CD was about *half* as intense as in the $WT1_{BPS}$ spectrum, whereas the NHHS Fe^{II} doublet was ~5 times more intense. A NHHS Fe^{III} sextet may be evident slightly above the $\Delta\Delta1_{BPS}$ spectral baseline. Since the MB spectrum of ΔΔ1 mitochondria (Figure IV-3A) was largely devoid of the CD, we conclude that most ISCs and NHHS Fe^{II} species exhibited in the $\Delta\Delta1_{BPS}$ spectrum are localized in non-mitochondrial regions of the cell. Conceivably, Fe^{II} in the cytosol of $\Delta\Delta1_{BPS}$ cells should be partially blocked from flowing into mitochondria because the high-affinity Mrs3/4 importers are absent and the alternative mitochondrial iron import pathway is slow under Fe-deficient conditions. Such a blockage should cause NHHS Fe^{II} to accumulate in the cytosol of $\Delta\Delta1_{BPS}$ cells as well as a deficiency of ISCs and hemes in mitochondria.

The MB spectrum of WT1 cells (Figure IV-2F) exhibited two major features, including the CD and a sextet assigned previously to vacuolar NHHS Fe^{III} (REF). More intense vacuolar-Fe sextets are evident in the MB spectrum of WT10 and WT40 cells (Figure IV-2, G and H, respectively). A simulation of this component (purple line) was shown above the spectrum of Figure IV-2B. Confirming earlier reports,[REF] the MB spectrum of mitochondria isolated from WT1 cells was dominated by the CD (Figure IV-

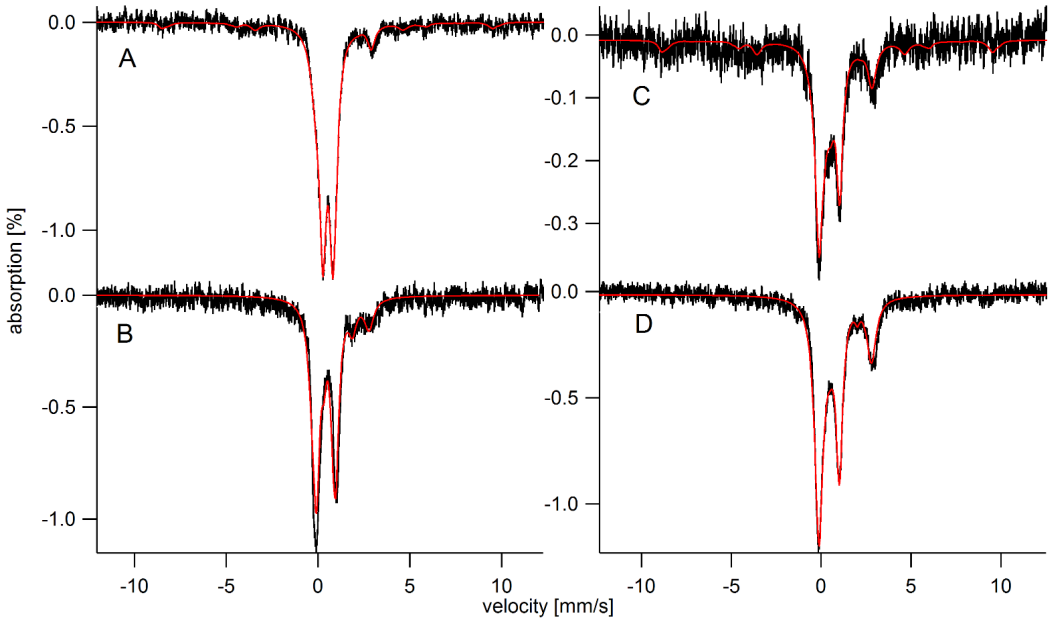

Figure IV-3. Mössbauer spectra of mitochondria isolated from ΔΔ and WT cells. A, ΔΔ1; B, ΔΔ40; C, WT1; D, WT40. The temperature was 5 K and an applied field of 0.05 T was applied parallel to the gamma rays. The solid red lines are composite simulations assuming the area percentages for each component listed in Table IV-2.

3C). We hypothesize that about half of the CD in the whole cell WT1 spectrum originates from mitochondria, with the other half from the CIA. The MB spectrum of WT1 mitochondria also exhibited a NHHS Fe^{II} doublet and a minor sextet suggesting a small amount of NHHS Fe^{III} in the organelle. Previous spectra of Fe-deficient WT mitochondria also included a semi-resolved doublet due to $[Fe_2S_2]^{2+}$ clusters (REF), and such a doublet (simulated by the solid teal line above Figure IV-2F) fits nicely into the whole cell WT1 spectrum.

The MB spectrum of ΔΔ1 cells (Figure IV-2B) was dominated by an intense NHHS Fe^{III} sextet, indicating that the vacuoles are essentially filled with Fe under these conditions. The intensity of the CD in the ΔΔ1 spectrum was lower than in the WT1 spectrum, while that of the NHHS Fe^{II} doublet was higher than in the WT spectrum. Again, the absence of Mrs3/4 in Fe-deficient ΔΔ cells likely results in the accumulation of Fe_{cyt} and reduction of mitochondrial ISCs. It is conceivable that elevated levels of Fe_{cyt} stimulates Ccc1-mediated Fe import into the vacuoles, consistent with this spectrum. The central region of the ΔΔ1 spectrum was poorly resolved, but the absorption that remained after removing known features was a doublet with parameters typical of Fe^{III} oxyhydroxide nanoparticles (NP).

The MB spectrum of mitochondria isolated from ΔΔ1 cells also exhibited a doublet due to nanoparticles (Figure IV-3A). A low-intensity NHHS Fe^{II} doublet was also present, *but no CD intensity was evident*. This indicates that few if any $[Fe_4S_4]^{2+}$ clusters and/or LS Fe^{II} hemes were present in ΔΔ1 mitochondria, and it suggests that most of the CD in the ΔΔ1 whole cell MB spectrum (Figure IV-2B) was due to non-mitochondrial ISCs

assembled by the CIA. Similarly, the strong intensity of NHHS Fe^{II} doublet in the ΔΔ1 whole cell spectrum is incompatible with NHHS Fe^{II} species being located in ΔΔ1 mitochondria (too little is present in the mitochondrial spectrum to make a significant contribution to the NHHS Fe^{II} doublet in the whole cell spectrum). These results reinforce our hypothesis that Fe^{II} accumulates in the cytosol of ΔΔ1 cells. This increase in Fe_{cyt} should induce Fe import into vacuoles, and indeed the concentration of vacuolar Fe^{III} in ΔΔ1 cells is 4 times that in WT1 cells. The majority of Fe in ΔΔ1 mitochondria is present as NP with few ISCs. The presence of some CD intensity in the whole cell ΔΔ1 MB spectrum suggests that cytosolic ISC assembly (CIA) is functioning in ΔΔ mutant cells grown under Fe-deficient conditions. Although ΔΔ1 cells were Fe-overloaded relative to WT1 cells, ΔΔ1 mitochondria contained about the same concentration of Fe as in WT1 mitochondria. Thus, the additional iron that flowed into ΔΔ1 cells did not localize to the mitochondria but rather accumulated in the cytosol and vacuoles.

The WT10 cell spectrum (Figure IV-2G) was dominated by the CD, due mainly to mitochondrial respiration-related proteins, and by the sextet due to vacuolar Fe^{III}. Minor doublets due to HS Fe^{II} hemes and NHHS Fe^{II} species were evident. A simulation of the HS Fe^{II} heme doublet (solid brown line) was displayed above this spectrum. The corresponding ΔΔ10 whole cell spectrum (Figure IV-2C) was far more intense, reflecting a higher Fe concentration in the cell (Table IV-1). It was dominated by intense sextet and NP doublets. The composite simulation of the ΔΔ10 spectrum included intensity due to the CD, but this doublet was not well resolved which made quantification difficult.

The MB spectrum of WT40 cells (Figure IV-2H) was similar to that of WT10, except that the sextet was more intense and the CD was less well resolved. The spectrum of mitochondria isolated from WT40 cells (Figure IV-3D) exhibited a strong CD and NHHS Fe^{II} doublet. The spectrum is generally consistent with previous reports (REF), but the intensity of the NHHS Fe^{II} doublet is more intense than in previous MB spectra of *respiring* mitochondria (REF). We previously reported that the size of the NHHS Fe^{II} pool was smaller in respiring mitochondria than in the organelle from fermenting cells; however, the NHHS Fe^{II} doublet in current respiring samples is about as intense as in fermenting cells.

The MB spectrum of ΔΔ40 cells (Figure IV-2D) was nearly identical to that of ΔΔ10 cells, again indicating the accumulation of NP and NHHS Fe^{III}. Surprisingly, the spectrum of ΔΔ40 mitochondria (Figure IV-3B) was devoid of nanoparticles but rather exhibited an intense CD. Thus, the nanoparticles and NHHS Fe^{III} in ΔΔ40 cells must be in a non-mitochondrial location. The spectrum of ΔΔ40 mitochondria also exhibited significant intensity due to the NHHS Fe^{II} pool (and perhaps some HS Fe^{II} hemes), but only about half as intense as in the WT40 mitochondria spectrum (Figure IV-3D). We conclude that *ΔΔ40 mitochondria have returned to a healthy state*. On the other hand, ΔΔ40 *cells* accumulated excessive amounts of Fe, implying that the Fe regulon was activated even though ΔΔ40 mitochondria exhibited a CD with about the same intensity as in WT mitochondria. This was puzzling because the Fe regulon is, by consensus, considered to be regulated by the ISC activity in mitochondria, with defective ISC activity activating the Fe regulon. Here, the ISC level is normal, yet the Fe regulon is activated.

We hypothesize that the slow-growth phenotype of ΔΔ1 cells is due to the absence of respiratory complexes (i.e., CD) in mitochondria, whereas the WT growth rate of ΔΔ40 cells is due to their presence. How this transformation occurred simply by increasing [Fe_{med}] is a puzzle, as is the reason why the cells continued to be Fe dysregulated even though the ISC levels were normal. We investigated these puzzles further using our subsidiary techniques, UV-Vis and EPR spectroscopies.

UV-Vis and EPR Investigations

UV-Vis spectra of mitochondria isolated from WT1 and WT40 cells (Figure IV-4, A and C, respectively) exhibited a Soret band at ~400 nm as well as α and β bands in the 500 – 620 nm region as is characteristic of Fe^{II} heme centers associated with mitochondrial cytochromes a, b, and c.[197] Both spectra exhibited distinct absorption peaks with similar intensities located at ~605, ~565, and ~550 nm that correspond to the α bands of heme a, b, and c, respectively. The UV-Vis spectrum of ΔΔ40 mitochondria (Figure IV-4D) showed similar heme features, albeit with about half of WT intensity. Mitochondria from ΔΔ1 cells (Figure IV-4B) was devoid of such features. This indicates that mitochondrial hemes were not synthesized in ΔΔ cells grown under Fe-deficient conditions but were synthesized by such cells under Fe-sufficient conditions.

Low temperature X-band EPR spectra of ΔΔ and WT whole cells are shown in Figure IV-5, A – H. All spectra in the g = 2 region were dominated by a hyperfine split signal due to mononuclear S = 5/2 Mn^{II} species. This signal has been observed previously in EPR spectra of yeast cells where it was shown to arise from most of the Mn in the cell.

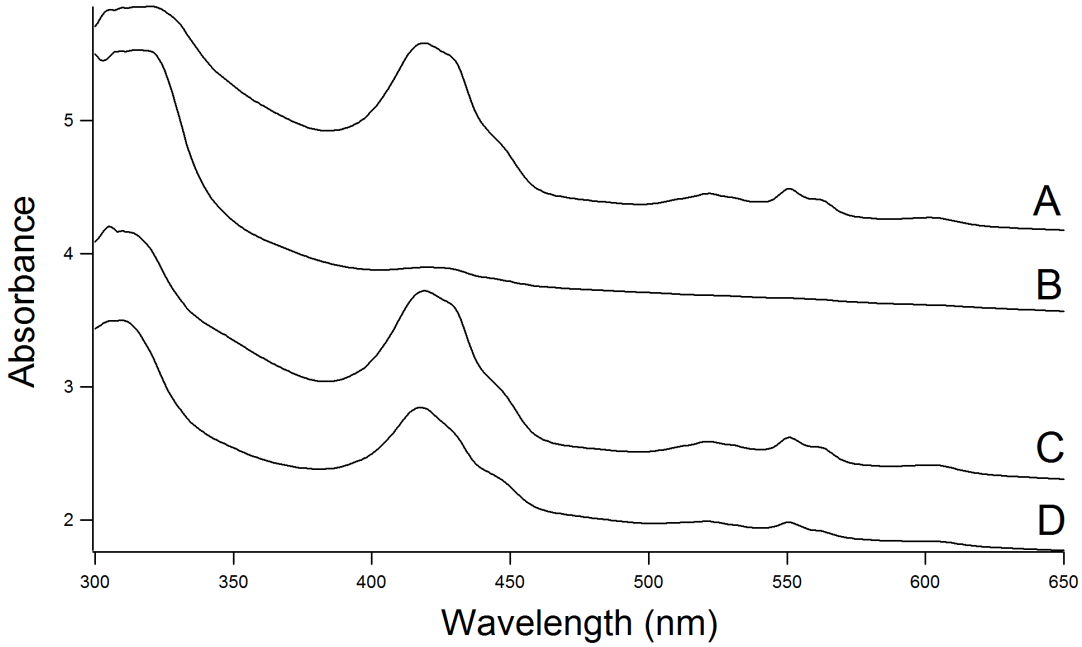

Figure IV-4. UV-Vis spectra of mitochondria isolated from respiring WT and ΔΔ cells. A, WT1; B, ΔΔ1; C, WT40; D, ΔΔ40. Solutions of isolated mitochondria were packed under anaerobic conditions into EPR tubes by centrifugation, and the volume of packed organelles in each sample was determined. Packed mitochondria were diluted 1:1 with 1xSH buffer (pH= 7.4) and transferred into 2 mm pathlength quartz cuvettes. Cuvettes were sealed with a rubber septum, removed from the glove box, and spectra were immediately collected at RT.

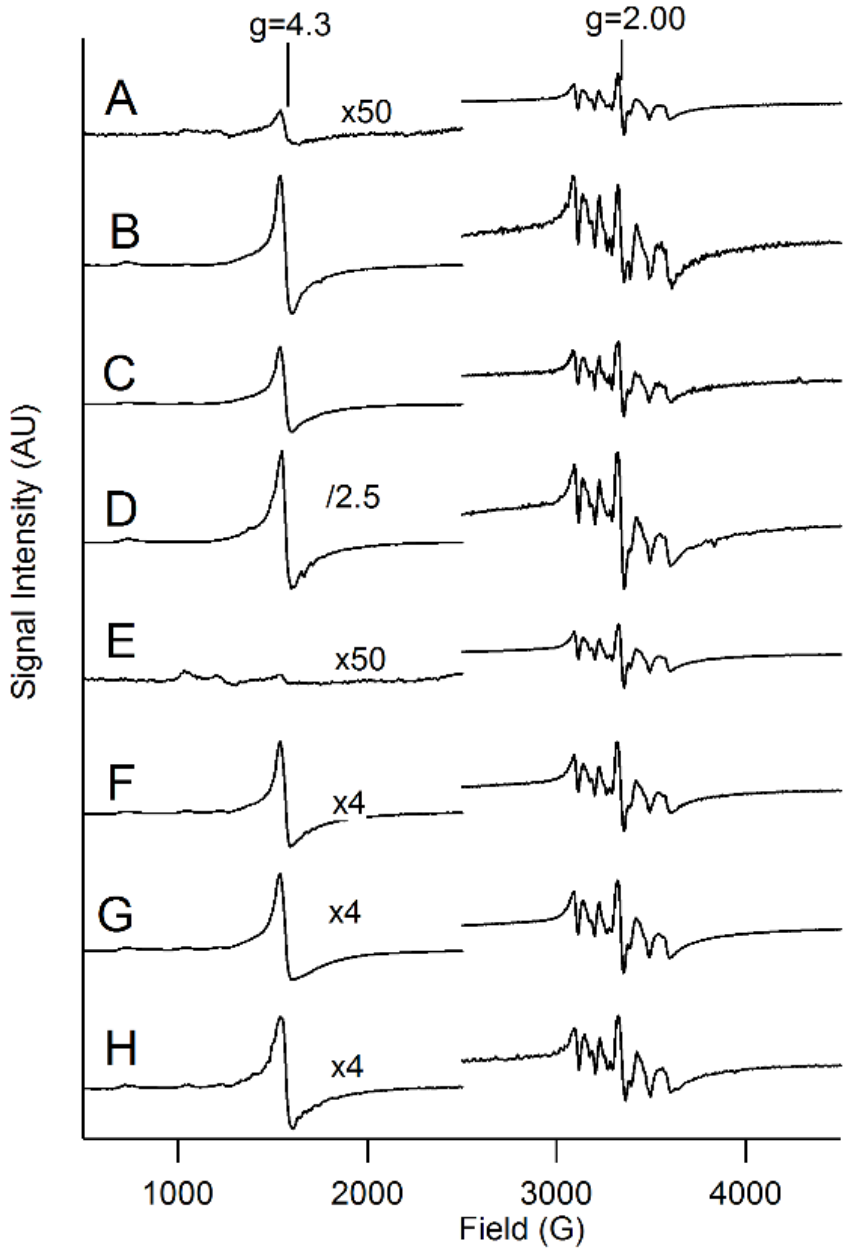

Figure IV-5. X-band EPR spectra of respiring ΔΔ and WT cells. A, $\Delta\Delta1_{BPS}$; B, ΔΔ1; C, ΔΔ10; D, ΔΔ40; E, $WT1_{BPS}$; F, WT1; G, WT10, and H, WT40. Temperatures in A, C, E, and G were 10 K while that in others was 4.2 K; intensities were temperature-adjusted to allow comparison. Other EPR parameters: average microwave frequency, 9.373 ± 0.003 GHz; microwave power, 0.2 mW; modulation amplitude, 10 G; Gain, 1000; conversion time, 0.3 sec. Displayed intensities on the left were adjusted as indicated for ease of viewing. None of the spectra on the right side was adjusted, allowing intensities to be directly compared.

The presence or absence of Mrs3/4 did not influence the shape or intensity of this signal.

Superimposed on the Mn-based signal was an isotropic signal at g = 2.00, present in all spectra and with similar intensities. We cannot assign this signal to a particular S = 1/2 species in the cell, as there are many candidates. There were no g = 1.94 type signals from S = 1/2 $[Fe_2S_2]^{1+}$ or $[Fe_4S_4]^{1+}$ clusters in the spectrum. Since such cluster types are present in these cells (as evidenced by the CD in MB spectra), the vast majority of such clusters (in exponentially growing cells) are in the oxidized S = 0 $[Fe_2S_2]^{2+}$ and $[Fe_4S_4]^{2+}$ states. Similarly, there were no EPR signals from LS Fe^{III} hemes, suggesting that the majority of such centers are in the reduced Fe^{II} state. Some WT EPR spectra exhibited low-intensity signals between g= 4 – 6 (minor features between 1000 – 1300 G), which have been previously assigned to the Heme a_3:Cu_B site of cytochrome oxidase with S = 5/2 $Fe^{III}a_3$ and S = 0 Cu^{I}_{B}. These signals were less obvious in spectra of ΔΔ cells because the g = 4.3 signal intensity dominated.

The most prominent signal in the low-field region (high g-value) is at g = 4.3 (and minor features at ca. g = 9.6) arising from high-spin S = 5/2 Fe^{III} species with rhombicity parameter E/D ~1/3. This signal arises from vacuolar Fe^{III} (REF). As expected, its intensity in WT cells increased as $[Fe_{med}]$ increased, consistent with increasing amounts of cellular Fe being stored in the vacuoles. The intensities of the g = 4.3 signal exhibited by ΔΔ cells were substantially higher than those exhibited by comparable WT cells, consistent with the differences observed in MB spectra. The most intense g = 4.3 signal was from the ΔΔ40 cells (n=1), which we defined as 100%. The average intensities of the ΔΔ10 (n = 3), ΔΔ1 (n = 4), $\Delta\Delta1_{BPS}$ (n = 4), WT40 (n = 1), WT10 (n = 2), WT1 (n = 2), and $WT1_{BPS}$ (n

= 4) was 53% ± 19%, 34% ± 16%, 2% ± 0.2%, 8%, 14% ± 5%, 9% ± 2, and 0%, respectively. These data confirm that ΔΔ cells contain substantially more vacuolar Fe^{III} than comparable WT cells, which is consistent with the MB spectra given above.

LC-ICP-MS of ΔΔ Mitochondrial FTSs

We initially hypothesized that Fe_{580} passes as an intact complex from the cytosol, through Mrs3/4, and into the mitochondrial matrix. Thus, we expected to observe Fe_{580} in FTSs of WT1 and WT40 mitochondria, but not in ΔΔ1 and ΔΔ40 samples. Fe_{580} was indeed observed in FTSs of WT1 and WT40 mitochondrial extracts (Figure IV-6, A and C, respectively), and it was not observed, as expected, in ΔΔ1 extracts (Figure IV-6B; two independent trials are shown). Unexpectedly, Fe_{580} was observed in the ΔΔ40 trace (Figure IV-6D), albeit with a weaker intensity than in the WT40 trace sample, indicating a lower concentration. Quantification of areas indicate an [Fe_{580}] concentration of 180 μM in WT40 mitochondria and 100 μM in ΔΔ40 mitochondria. The presence of Fe_{580} in ΔΔ40 mitochondria supports the idea that ΔΔ40 mitochondria have recovered to a healthy state under Fe-sufficient conditions. The trace of ΔΔ1 FTS exhibited two very weak LMM Fe peaks, at ~2700 and ~2100 Da. These species are characteristic of oxidized mitochondria and presumably have no physiological role.

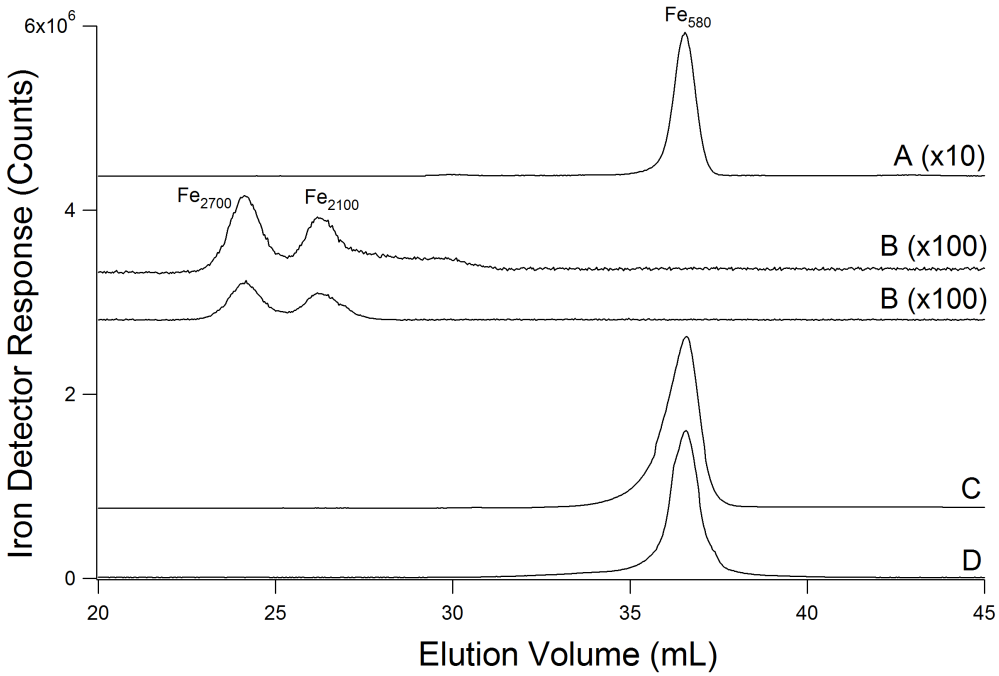

Figure IV-6. Iron chromatograms of LMM FTSs prepared from WT and ΔΔ mitochondrial extracts. A, WT1; B, ΔΔ1 (two independent trials); C, WT40; D, ΔΔ40. Trace intensities were adjusted as shown for ease of viewing. Chromatograms were obtained by using an online LC-ICP-MS system and detecting for ^{57}Fe.

Electrospray Ionization Mass Spectrometry (ESI-MS) of Fe_{580}

We have obtained preliminary ESI-MS spectra of the Fe_{580}-containing fraction collected from an LC-ICP-MS chromatogram (Figure IV-7, top panel). The FTS used for this experiment was from mitochondria isolated from WT40 cells grown on medium containing an approximate 1:1 molar ratio of ^{56}Fe:^{57}Fe. ICP-MS detector responses for ^{57}Fe (red) and ^{56}Fe (black) confirm that Fe_{580} was enriched in both isotopes. The ESI-MS spectrum of the Fe_{580}-containing fraction exhibited two peak pairs at {664.46 and 665.46 amu} and {685.39 and 686.39 amu} (Figure IV-7B, inset). We consider both pairs as Fe_{580} *candidates*, and they raise the possibility that Fe_{580} consists of two species that co-migrate on our LC column. None of these peak pairs was present in spectra of column fractions before (Figure IV-7A) or after (Figure IV-7C) the Fe_{580} peak. We regard this as progress in identifying Fe_{580} but realize that further work is required to establish its mass and chemical composition.

Relationship Between Fe_{1100} and Fe_{580}

Mitochondria harvested from fermenting yeast cells during postexponential (stationary-state) growth phase were shown to contain a LMM Fe species called Fe_{1100} rather than Fe_{580} in Chapter III of this dissertation. Curiously, allowing FTSs from mitochondrial extracts to incubate in a refrigerated anaerobic glove box for a few days resulted in the conversion of $Fe_{1100} \rightarrow Fe_{580}$. The same transformation occurred in our current studies involving respiring yeast cells. One batch of WT mitochondria was harvested at an OD_{600} ~1.2 (typically we harvest at OD_{600} = 0.8), which is typically the

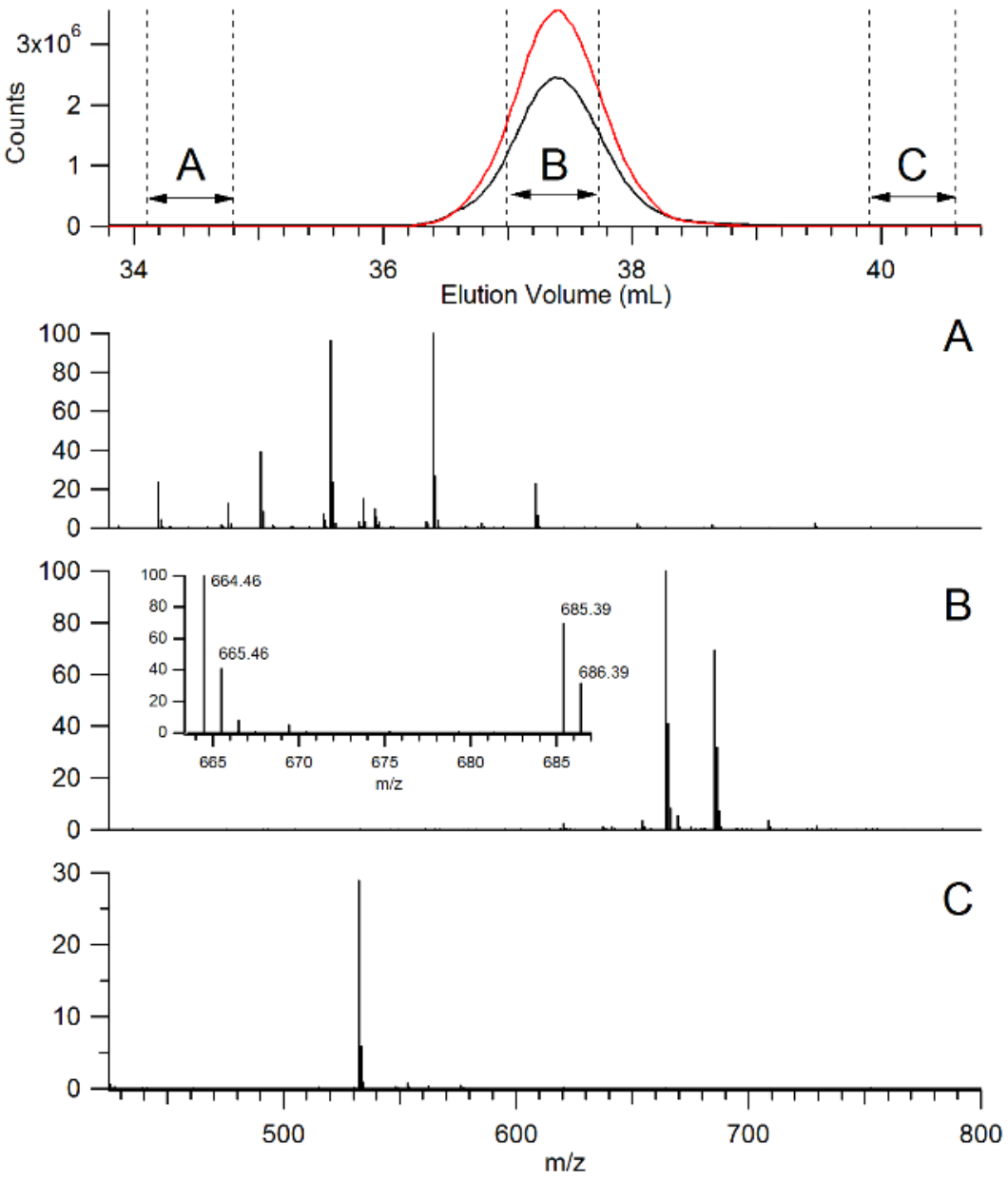

Figure IV-7. Electrospray ionization mass spectrometry of Fe_{580}-containing LC fractions. Top Panel: LC trace of FTS from isolated mitochondrial extract obtained from cells grown on medium with an approximate 1:1 molar ratio of ^{56}Fe:^{57}Fe. The dashed lines and double-arrow lines indicate where fractions were obtained. The buffer was 20 mM $(NH_4)_2CO_3$, pH 8.5. Bottom Panels: A, ESI-MS of the LC fraction before the Fe_{580}-containing fraction; B, the Fe_{580}-containing fraction; C, the LC fraction after the Fe_{580}-containing fraction. Inset in B shows a close-up of the peaks associated with the candidate Fe_{580} species.

OD at which cells are transitioning from exponential to stationary state. The resulting LC-ICP-MS trace of the FTS from mitochondria isolated from these cells was dominated by Fe_{1100} (Figure IV-8A); some Fe_{580} was evident. After incubation for 5 days, the same FTS exhibited a strong Fe_{580} peak but no Fe_{1100} peak (Figure IV-8B). Corresponding P and S traces are shown (Figure IV-8, B and C, respectively). This indicates that the two LMM Fe species are related—the simplest explanation being that Fe_{1100} is a dimer of Fe_{580}. The associated P and S traces show that neither P or S peaks comigrate with either Fe peak. We conclude that Fe_{1100} and Fe_{580} do not contain P or S atoms; this suggests that the donor atoms to the Fe ions are O and or N.

Effect of Mrs3/4 Deletion on Other Metals

Although the focus of this study was on iron, copper trafficking and regulation also seems to have been affected by deleting Mrs3/4. The average Cu concentration in ΔΔ cells was ca. double that in WT cells (Table IV-1), regardless of $[Fe_{med}]$. In contrast, the average Cu concentration in ΔΔ mitochondria was about half of that in WT mitochondria. This suggests that Cu is dysregulated in ΔΔ mitochondria, and that a deficiency of Cu in ΔΔ mitochondria either increases Cu import into the cell or decreases Cu export. Such effects were not observed for Zn or Mn (Table IV-1); the cellular and mitochondrial concentrations of these metals were unaffected by $[Fe_{med}]$ or deletion of Mrs3/4.

LMM Cu, Mn, and Zn chromatograms (Figure IV-9 – Figure IV-11) of FTSs from mitochondria isolated from *respiring* WT and ΔΔ cells exhibited the same LMM species as with fermenting cells (REF), including Cu_{5000}, Mn_{1100}, and Zn_{1200}. Cu_{5000} LC peaks were

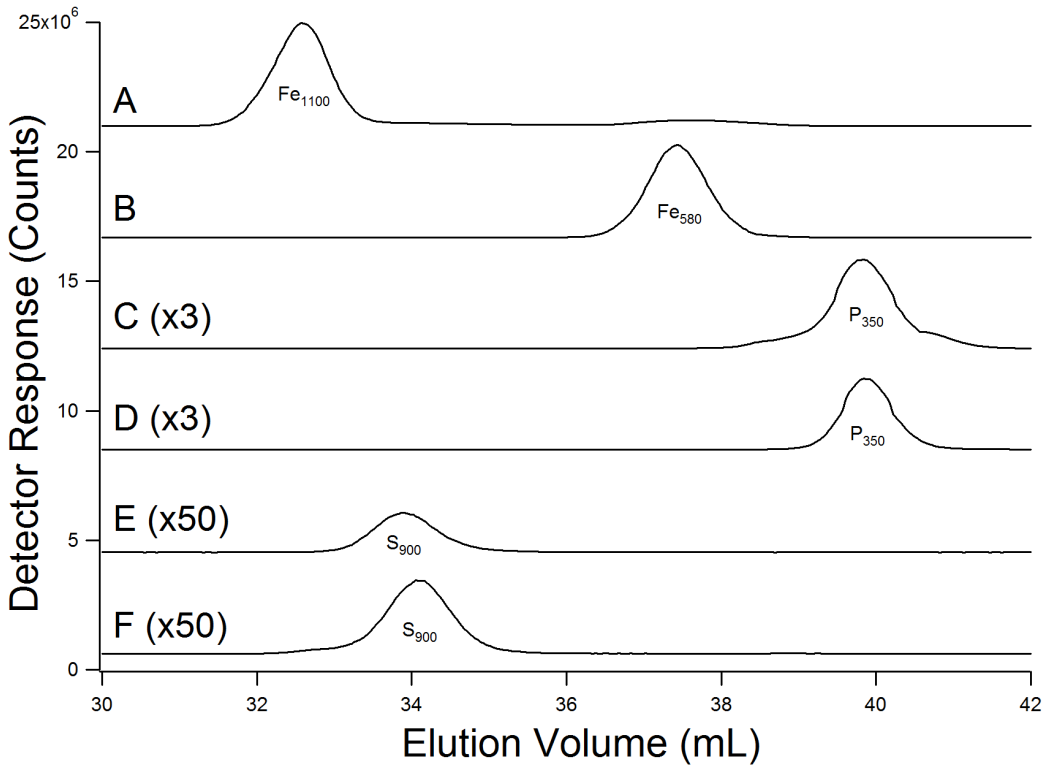

Figure IV-8. Relationship between Fe_{1100} and Fe_{580}. ^{56}Fe, ^{34}S, and ^{31}P detection of FTSs from mitochondria harvested from WT40 cells harvested as cells were transitioning to stationary state: Traces A, C, and E were of fresh FTSs detected by Fe, P, and S. Traces B, D, and F detected the same respective elements in the same FTS but after a 5-day incubation inside a refrigerated N_2-atmosphere glove box.

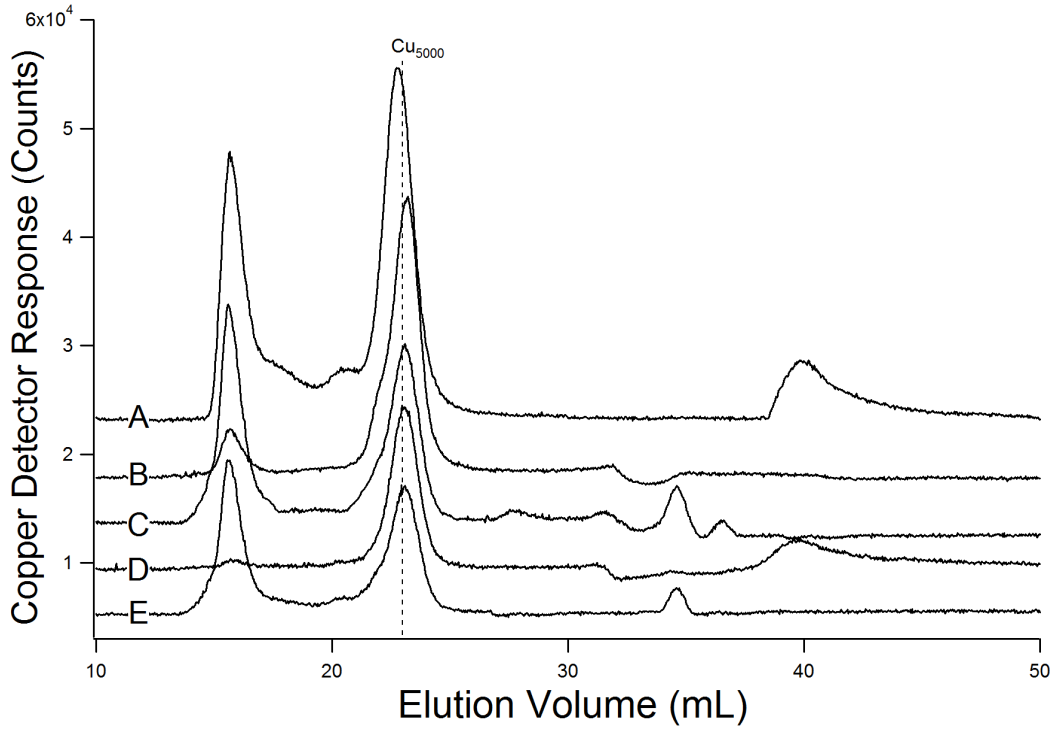

Figure IV-9. Copper chromatograms of LMM FTSs prepared from WT and ΔΔ mitochondrial extracts. A, WT1; B, WT40; C, ΔΔ1; D, ΔΔ1 (n=2); E, ΔΔ40. Chromatograms were collected simultaneously with the Fe traces shown in Figure IV-6.

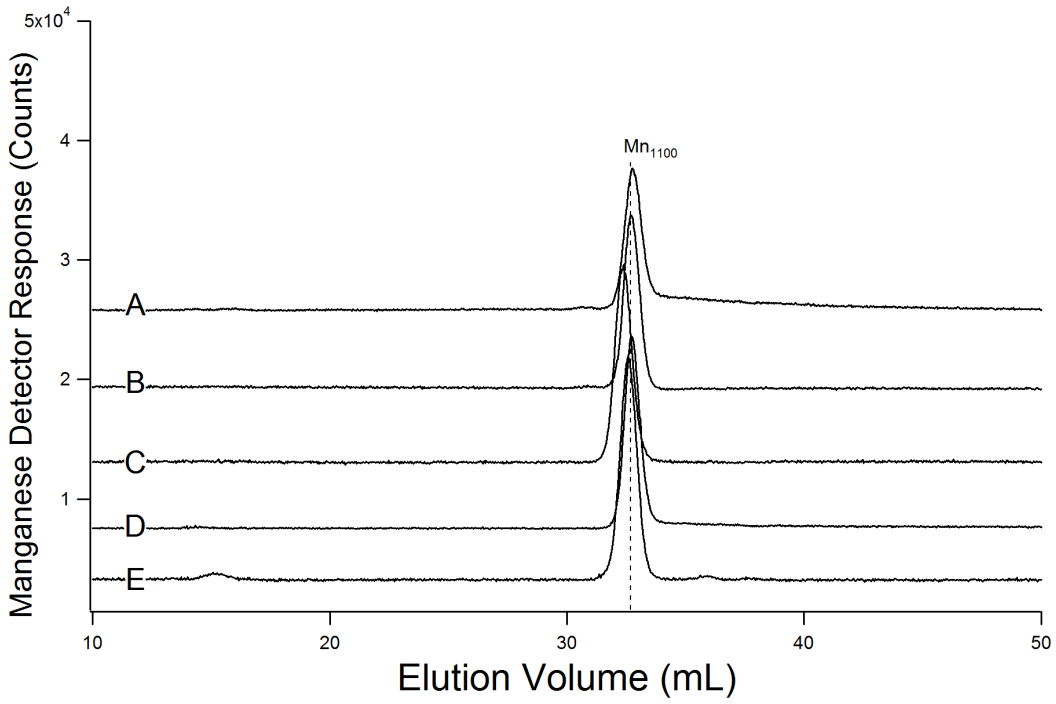

Figure IV-10. Manganese chromatograms of LMM FTSs prepared from WT and ΔΔ mitochondrial extracts. A, WT1; B, WT40; C, ΔΔ1; D, ΔΔ1 (n=2); E, ΔΔ40. Chromatograms were collected simultaneously with the Fe traces shown in Figure IV-6.

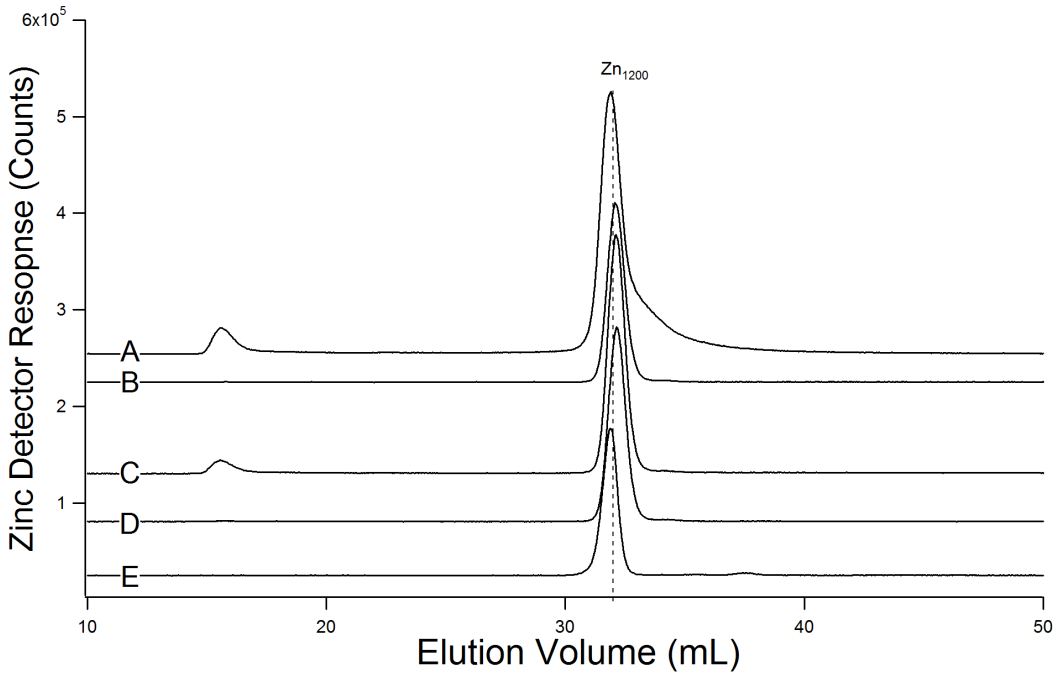

Figure IV-11. Zinc chromatograms of LMM FTSs prepared from WT and ΔΔ mitochondrial extracts. A, WT1; B, WT40; C, ΔΔ1; D, ΔΔ1 (n=2); E, ΔΔ40. Chromatograms were collected simultaneously with the Fe traces shown in Figure IV-6.

less intense in ΔΔ traces compared to those in WT, consistent with the lower Cu concentration in ΔΔ mitochondria. Low-intensity Cu species with masses between 200 – 3000 Da were present in some traces, but they were not reproducible and could be artifacts generated during sample preparation.

Discussion

In this study, we have used an integrative biophysical and bioanalytical approach to explain the phenotype of yeast cells in which Mrs3 and Mrs4, the high-affinity Fe importers on the mitochondrial IM, have both been deleted. Under Fe-deficient conditions, ΔΔ cells grew slowly relative to WT cells, whereas Fe-sufficient ΔΔ cells grew at WT rates. Our results suggested that under Fe-deficiency, Fe import into mitochondria was too slow to prevent O_2 from diffusing into the matrix. This was because the size of the NHHS Fe^{II} pool in the matrix was insufficient to generate normal WT levels of ISCs, hemes, and thus respiratory complexes. Under such conditions, much of the O_2 that diffused across the IM penetrated the matrix to react with the Fe^{II} pool to generate nanoparticles and ROS. This resulted in a vicious cycle in which decreasing mitochondrial Fe^{II} concentrations limited the assembly of ISC/hemes and thus respiratory complexes. Conceivably, the membrane potential was also affected. In the case of Fe-sufficiency, the process reversed. A higher concentration of cytosolic Fe stimulated Fe import into mitochondria, increasing the size of the NHHS Fe^{II} pool and the concentration of respiratory complexes. Normal respiratory activity returns, rendering the matrix anaerobic and reestablishing membrane potential.

To explain why the iron regulon was activated in ΔΔ cells under Fe-sufficient conditions, even though such cells grew at normal rates and their mitochondria were generally healthy, we sought to identify the intracellular Fe species that serves as a sensor for the iron regulon. The concentration of such a sensor in *both* Fe-deficient and Fe-sufficient ΔΔ cells should be *below* its normal WT concentration—such a situation is required to maintain the Fe regulon in the activated state. ISC assembly activity is thought to generate the sensor X-S for regulation.[187,188] However, the proxy previously used to estimate this activity, namely the intensity of the CD in MB spectra was normal in ΔΔ40 cells.[198] We considered Fe_{cyt} as a possible sensor, but its concentration was actually *higher* than normal in ΔΔ40 cells. Nanoparticles were excluded for the same reason. The only observed Fe species that fulfilled the requirement was the mitochondrial NHHS Fe^{II} pool, the concentration of which was lower-than-WT in both ΔΔ1 and ΔΔ40 mitochondria. Thus, we propose that *the size of this pool controls the Fe regulon activity*. This does not preclude the use of X-S as a sensor; e.g., both may be involved in assembling Fe_2S_2 clusters that are involved in downstream signaling. Our proposal is also consistent with previous interpretations of Fe dysregulation in ISC-mutant strains (e.g. Yfh1Δ) because in such mutants, both ISC and Fe^{II} pool levels are reduced.[187,188]

Our results provide strong evidence that the mitochondrial NHHS Fe^{II} pool in exponentially growing yeast mitochondria is composed *exclusively* of Fe_{580}. This species was also observed in mammalian mitochondria. The Fe concentration associated with the Fe^{II} pool in yeast ranges from 60 - 200 μM (Table IV-2), depending on strain and [Fe_{med}].

We previously estimated the concentration of Fe_{580} in mitochondria to be in the same ballpark, ca. 100 μM.[48]

We are pursuing the chemical composition of Fe_{580}, and report here preliminary ESI-MS data in which two candidate species have been detected, at m/z = 665 and 686 Da. Further studies are underway to connect these species unambiguously to Fe_{580} and to obtain and analyze MS/MS fragmentation patterns. Our current LC-ICP-MS results suggest that the irons of Fe_{580} and Fe_{1100} are coordinated mainly by O and/or N donor ligands, not by S. In support of this, the ΔE_Q and δ of the NHHS Fe^{II} doublet in MB spectra of isolated mitochondria (3.07 mm/s and 1.23 mm/s, respectively) are typical of Fe^{II} complexes with 4 – 6 O and 0 – 2 N donor ligands.

Fe_{580} may also be present in the cytosol and pass as an *intact* complex through the channels of Mrs3/4 into the matrix. Alternatively, the endogenous ligands of Fe_{cyt} might dissociate, Fe^{II} ions may flow through the Mrs3/4 channels (handed off from one protein-based ligand to the next), and then other ligands localized within the matrix may coordinate the entering Fe^{II} ions as they emerge from the channels into this space. Our results impact this discussion. If "intact-channeling" occurred and if Fe_{580} were exclusively imported via Mrs3/4 channels, then Fe_{580} should not have been present in the FTS of ΔΔ40 mitochondria (but it was). If Fe_{580} also channeled through the alternative import transporter intact, then Fe_{580} should have been present in the FTS of ΔΔ1 mitochondria (but it was not). One caveat is that the loss of membrane potential in ΔΔ1 mitochondria might prevent Fe_{580} import through the alternative importer; thus, the intact channeling mechanism could still be operative. However, we contend with this possibility

for a couple reasons. First, we find it unlikely that both Mrs3/4 and the alternative Fe import pathway mediate transport for the same LMM complex. Moreover, the requirement for a specific Fe complex is belied by the ability of simple (hexaaqua) Fe^{II} ions to successfully enter isolated mitochondria.[99] On the other hand, such a lack of specificity is expected for the unwrapping/rewrapping mechanism. Accordingly, whether Fe_{580} assembles in the matrix upon exiting the channel depends on the metabolic state of the organelle. Fe_{580} may not form if the matrix is devoid of the appropriate ligand(s), or if the matrix is not sufficiently anaerobic, or if the mitochondria lack sufficient membrane potential. Under stationary-state conditions, the ligand environment may be different than under exponential growth conditions (e.g., the concentrations of potential coordinating ligands might vary) such that Fe_{1100} (or Fe_{2700} or Fe_{2100}) forms instead. Overall, these considerations support the unwrapping/rewrapping mechanism.

In 2001, Lutz et al. discovered that ISC assembly in isolated mitochondria was inhibited following treatment with the IM-permeable chelator 1,10-phenanthroline (Phen).[145] A few years later, Amutha et al. and Pandey et al. concluded from similar studies that mitochondria must contain an endogenous pool of Fe that is used as feedstock for ISC (and heme) biosynthesis.[146,182] In 2010, Holmes-Hampton et al. discovered that the NHHS Fe^{II} pool observed in MB spectra of isolated mitochondria was selectively coordinated by Phen, suggesting that this is the pool proposed previously.[144] Here we confirm and extend our previous studies to show that Fe_{580} composes this pool and that this LMM Fe complex serves as feedstock for ISC and likely heme biosynthesis. Also of significance is that Fe does not accumulate in mitochondria in which *YFH1*, *MRS3*, and *MRS4* are all

deleted.[99,132,135,189] This strongly suggests that the Fe accumulating within mitochondria of Friedreich's ataxia patients passes through the human orthologs of Mrs3/4, namely mitoferrins 1/2. The Fe oxidation state in nanoparticles is Fe^{III}, whereas that for the mitochondrial Fe pool is Fe^{II}. This implies that Fe_{580} is an Fe^{II} complex that reacts with O_2 (in Friedreich's Ataxia) to generate the nanoparticle accumulation phenotype. NP are often described as "toxic" to the cell, since ROS is formed in association with the nanoparticles. However, from a chemical perspective, nanoparticles should be benign. It is more likely that the reaction of Fe^{II}_{580} with O_2 is deleterious. Thus, the reaction chemistry of Fe_{580} may be of critical importance for understanding the pathophysiology of Friedreich's ataxia.[199]

Our results confirm previous results that ΔΔ cells contain twice as much Cu as WT cells,[133] indicating Cu dysregulation. Since ΔΔ mitochondria contain substantially *less* Cu than WT mitochondria, we conclude that a mitochondrial Cu deficiency *stimulates* cellular Cu import. This can also explain the increased sensitivity of Cu in ΔΔ cells.[133] The non-mitochondrial location of the accumulated cellular Cu is unknown but cytosol and vacuoles are reasonable possibilities.

The majority of Cu in mitochondria is thought to be in the form of a labile nonproteinaceous Cu species called Cu_L.[44,68,69] Cu_L is thought to be imported from the cytosol through IM proteins Pic2 and Mrs3, stored in the matrix, and then trafficked back into the IMS through an unidentified Cu exporter on the IM. Cu_L is touted as being LMM, but it was reported to have a mass of ~13,000 Da, which is simply too large to pass through channels of an IM protein. Cu_{5000} is similarly too large to enter the matrix via channels in an IM protein, and so it cannot be Cu_L (also, it represents only ~20% of mitochondrial Cu,

whereas Cu_L reportedly represents ~90% of yeast mitochondrial Cu). FTSs of mitochondrial extracts from fermenting yeast contain no reproducibly observed LMM Cu species with a mass <3000 Da[48] and here we show the same, only for respiring yeast mitochondria. In brief, our evidence strongly suggests that Cu_L (defined as a LMM Cu complex that resides in the matrix and represents > 80% of mitochondrial Cu) does not exist. Our evidence indicates that Cu_{5000} does exist (at least in yeast mitochondria), but we have no further insight into its physiological role. We have hypothesized that Cu_{5000} is present in the IMS where so much mitochondrial Cu chemistry occurs,[48,192] but further studies are needed to establish this. We agree that the decline in the concentration of mitochondrial Cu (and Cu_{5000}) in ΔΔ cells along with the increase of cellular Cu in these cells is *consistent* with Mrs3 functioning as an IM Cu importer, as concluded,[68] but this decline may also arise from secondary effects.

CHAPTER V

CONCLUSIONS AND FUTURE WORK

Conclusions

The principal objective of this dissertation was to investigate chemical-level details of the mitochondrial labile iron pool (LIP) by integrating knowledge obtained from several different analyses, including Mössbauer, EPR, and UV-Vis spectroscopies, as well as LC-ICP-MS. Within the past few decades, there has been a major push in the field to characterize mitochondrial labile metal pools (LMPs) using fluorescence-based sensors. A key advantage of these sensors is that they can traverse into cells and organelles without destroying them, which makes them particularly useful for detecting and monitoring endogenous metal pools within their biological milieu. However, this chelator-based strategy is fundamentally limited in its ability to chemically characterize LMPs since the endogenous metal complexes of interest are destroyed during their detection. Thus, the LMPs have largely remained uncharacterized. To solve this problem, we applied an integrative biophysical and bioanalytical approach relying on various spectroscopic methods in conjunction with a novel LC-ICP-MS system to characterize the mitochondrial LIP.

The LIP is defined as a pool of LMM iron complexes that are weakly coordinated by unknown ligands. The study described in Chapter III established that mitochondria contain a diverse array of LMM metal complexes (< 10 kDa). This was determined via the application of an LC-ICP-MS system, consisting of size-exclusion chromatography

(SEC) columns interfaced online to an ICP-MS. In collaboration with Dr. Sean McCormick (Ferris State University), isolated mitochondria from WT fermenting yeast cells, human Jurkat cells, and mouse brain and liver were evaluated for the presence of LMM metal species. To prevent the degradation of such species via redox and ligand-exchange reactions during chromatographic workup, the entire LC component of the system was contained in a refrigerated N_2-atmosphere glove box. Another useful feature of this setup is that it includes a flow splitter at the bottom of the SEC columns that directs a portion of eluate to a fraction collector (located inside the glove box) for further analysis. This separations-based approach was utilized previously to detect and identify several LMM metal complexes in biological systems.[ref]

Using the LC-ICP-MS system described above, we detected numerous unidentified LMM P, S, Mn, Fe, Co, Cu, Zn, and Mo species (< 10 kDa) in yeast and mammalian mitochondrial extracts. While most of these LMM species were reproducibly observed in both yeast and mammalian mitochondria, the latter typically contained a few additional species. In this study, concentrations and approximate molecular masses of all LMM species were estimated. Treatment with chelators revealed that dominant LMM metal complexes were labile.

Fermenting wild-type (WT) mitochondria contained either of two major LMM iron complexes with approximate masses of 1100 and 580 Da (referred to as Fe_{1100} and Fe_{580}, respectively). Mitochondria harvested in exponential growth phase (OD_{600} ~0.8) contained Fe_{580}, whereas mitochondria harvested during postexponential growth, or stationary-state (OD_{600} ~1.2 – 1.6), exhibited Fe_{1100}. After 5 days of anaerobic incubation

in a refrigerated glove box, Fe_{1100} converted into Fe_{580}, suggesting a relationship between these two LMM Fe species.

The concentration of Fe_{580} in yeast mitochondria was ~100 μM, which is consistent with previous concentration estimates of the mitochondrial labile iron pool.[ref] Moreover, increasing the [Fe_{med}] yielded an increase in the mitochondrial concentration of Fe_{580} (other metals were unaffected). Mammalian mitochondria also contained Fe_{1100} and Fe_{580} along with a 1500 Da species (Fe_{1500}). Taken together, this strongly suggests that Fe_{580} is one of the predominant LMM complexes composing the mitochondrial LIP. Thus, we hypothesized that Fe_{580} is imported into the matrix (via Mrs3/4), where it serves as feedstock for iron-sulfur cluster (ISC) assembly, heme biosynthesis, or the metalation of mitochondrial Fe-containing proteins and enzymes.

In Chapter IV we characterized a yeast strain lacking the mitochondrial Fe importers Mrs3/4 with Mössbauer, EPR, and UV-Vis spectroscopies, as well as the LC-ICP-MS system. This work was done in collaboration with a fellow graduate student in the Lindahl Lab, Mr. Joshua Wofford (Texas A&M University), who analyzed the Mössbauer and EPR spectra. We hypothesized that the LIP is markedly reduced in mitochondria isolated from Mrs3/4-deficient (ΔΔ) cells. Based on the findings in Chapter III, we expected that Fe_{580} would be diminished or absent in ΔΔ cells. Since Mrs3/4 constitute the high-affinity Fe import pathway (i.e., they mediate mitochondrial Fe uptake when Fe_{cyt} levels are low), we grew ΔΔ cells on Fe-deficient and Fe-sufficient conditions. Thus, we expected to observe a substantial decrease in mitochondrial Fe species (e.g., ISCs, hemes, and the LIP) in the ΔΔ strain under Fe-deficient conditions. Conversely, such

mitochondrial Fe species should be comparable in Fe-sufficient ΔΔ cells due to alternative low-affinity Fe import pathways.

Respiring ΔΔ cells exhibited an Fe-dependent "slow-growth" phenotype under Fe-deficient conditions. To elucidate this ΔΔ slow-growth phenotype, we examined intracellular Fe concentrations, the results of which revealed that ΔΔ cells accumulated excessive amounts of Fe regardless of [Fe_{med}] and that the excess Fe accumulated in non-mitochondrial locations. Additionally, iron overload in ΔΔ cells under Fe-sufficient conditions reflected Fe dysregulation. We hypothesized that this dysregulation was due to reduced levels of some Fe species that is "sensed" by cellular regulatory systems.

We searched for this intracellular "sensed" Fe species via Mössbauer (MB) spectroscopy. Fe-deficient ΔΔ cells accumulated NHHS Fe^{II} (presumably in the cytosol) and contained decreased levels of central doublet ($[Fe_4S_4]^{2+}$ clusters and LS Fe^{II} hemes), which is mostly associated with the respiratory complexes in mitochondria and serve as an indicator of the health status of mitochondria. Fe-sufficient ΔΔ cells accumulated Fe^{III} oxyhydroxide nanoparticles (NP) and NHHS Fe^{III} in non-mitochondrial locations, most likely in the vacuoles and possibly in the cytosol. The accumulation of vacuolar HS Fe^{III} in ΔΔ cells was further corroborated via EPR analysis.

While Fe-deficient ΔΔ mitochondria accumulated NP and were devoid of CD, Fe-sufficient ΔΔ mitochondria exhibited WT levels of CD, indicating that they have recovered to a healthy state under such conditions. This observation was reinforced in UV-Vis spectra, which revealed that mitochondrial Fe^{II} heme levels were drastically reduced

in Fe-deficient ΔΔ mitochondria but roughly normal under Fe-sufficient conditions, again supporting the idea that Fe-sufficient ΔΔ mitochondria have recovered to a healthy status. Interestingly, the NHHS Fe^{II} pool was substantially reduced in Fe-sufficient ΔΔ mitochondria relative to its levels in WT. Integrating the results obtained from MB, EPR, and UV-Vis analyses, we proposed that (a) the "slow-growth" phenotype exhibited by respiring Fe-deficient ΔΔ mitochondria was due to diminished levels of mitochondrial respiratory complexes and (b) the Fe dysregulation (i.e., "iron overload phenotype") in Fe-sufficient ΔΔ cells resulted from reduced levels of the NHHS Fe^{II} pool in mitochondria.

As expected, Fe_{580} was present in Fe-deficient WT mitochondria but not in Fe-deficient ΔΔ mitochondria. Surprisingly, Fe_{580} was present in both Fe-sufficient WT and ΔΔ mitochondria as well as Fe-deficient WT mitochondria. Moreover, the mitochondrial concentration of Fe_{580} was markedly reduced in Fe-sufficient ΔΔ mitochondria, in agreement with the decrease in the NHHS Fe^{II} pool observed in MB spectra. Therefore, we propose that the NHHS Fe^{II} pool is composed predominantly of the LMM Fe complex, Fe_{580}, which is also found in fermenting yeast as well as mammalian mitochondria (Chapter III). Furthermore, we propose that Fe_{580} is a key component of cellular Fe regulation and homeostasis. Preliminary ESI-MS data yielded two candidate species with determined masses of 664.46 and 685.39 Da, suggesting the intriguing possibility that perhaps Fe_{580} consists of two distinct Fe complexes.

Future Work

Characterizing the chemical composition and biological function of the mitochondrial LIP has significant pathophysiological implications, given the multitude of diseases linked to defective iron homeostasis. Such diseases are often characterized by either iron overload or iron deficiency phenotypes. For example, Friedreich's ataxia and X-linked sideroblastic anemia are both marked by mitochondrial iron overload.[200,201] To elucidate the role of the LIP in health and disease states, future studies will be required to fully characterize its chemical nature.

One of the major conclusions presented in this dissertation is that the mitochondrial LIP is predominantly composed of Fe_{580}. Therefore, chemical characterization of Fe_{580} is of utmost importance. The first major step in structurally characterizing the Fe_{580} complex will be to determine its accurate molecular mass. We obtained preliminary ESI-MS results that revealed two *candidate* masses of Fe_{580} (664.46 and 685.39 Da) in the study described in Chapter IV, but further work is required before these masses can be accepted. This experiment should be repeated and will involve enriching Fe_{580} with an equimolar ratio of ^{56}Fe:^{57}Fe and observing this ratio in the ESI-MS peak intensities of Fe_{580}-containing fractions. The mass of Fe_{580} will be established by the presence of peak pairs separated by 1 amu with equal intensities (corresponding with a 1:1 enrichment ratio) in Fe_{580}-containing fractions and the absence of such features in negative controls.

More detailed ESI-MS studies along with MS/MS fragmentation analysis could provide chemical insights into the endogenous ligands bound to the iron. An example of the former would be to treat Fe_{580} with a chelator and observe how this affects the resulting

ESI-MS spectrum. Treatment of isolated Fe_{580} with 1,10-phenanthroline (phen) should show the disappearance of ESI-MS peaks with m/z = 664.46 and 685.39 and the emergence of a peak corresponding to the Fe-phenanthroline complex, $[Fe(phen)_3]^{2+}$. Comparison with a background spectrum of Fe_{580} (no phen treatment), would allow common features to be subtracted, which could reveal peaks corresponding to the dissociated endogenous ligands of Fe_{580}.

Once the mass of Fe_{580} has been established, studies will be aimed at determining its chemical structure. This will likely require the application of multiple techniques such as NMR, EPR, XAS, and perhaps even Mössbauer spectroscopy. One issue is that these methods likely require increased amounts and purer samples of Fe_{580}. One way to increase the amount of Fe_{580} for downstream structural analysis might require simply combining several Fe_{580}-containing fractions from multiple mitochondrial isolations. In Chapter III, it was observed that increasing the $[Fe_{med}]$ increases the mitochondrial concentration of Fe_{580}. Thus, growing cells on higher $[Fe_{med}]$ would yield a larger quantity of Fe_{580}. Increasing the purity of Fe_{580} could be achieved by adding another dimension of LC separation following gel filtration. Injecting Fe_{580}-containing fractions onto a hydrophobic interaction liquid chromatography (HILIC) column or an ion-exchange column could remove additional contaminants that might hinder structural analysis.

With sufficient amounts of purified Fe_{580}, analysis by NMR spectroscopy could potentially identify the structures of endogenous Fe_{580} ligands. One problem, however, is that because iron is paramagnetic it leads to extreme line broadening in spectra, making them difficult to interpret. One way to possibly overcome this, would be to collect spectra

of Fe_{580}-containing samples before and after treatment with a chelator. This type of analysis could potentially reveal signatures corresponding to the ligands associated with Fe_{580}.

Another important research endeavor involves elucidating the biological functions of Fe_{580}. Based on our integrative analysis, we proposed that the mitochondrial concentration of Fe_{580} can modulate cellular Fe homeostasis and regulation. Additionally, we proposed that Fe_{580} is utilized as a substrate in ISC assembly and perhaps heme biosynthesis. Future studies will be needed to substantiate both of these functions, which can be accomplished using the strategy employed in Chapter IV. Here, we investigated the mitochondrial LIP using biophysical spectroscopic methods, LC-ICP-MS, and a genetic mutant yeast strain lacking mitochondrial Fe importers Mrs3/4. This approach can be used to evaluate if there is, in fact, Fe dysregulation in mutant yeast strains that are expected to have diminished levels of Fe_{580} in mitochondria. For example, Rim2 is thought to serve as a low-affinity mitochondrial Fe importer. It would be interesting to examine a triple deletion mutant yeast strain lacking Rim2 and Mrs3/4. In this case, triple deletion mitochondria should be largely devoid of Fe_{580}, leading to cellular Fe dysregulation and an Fe overload phenotype. The role of Fe_{580} in ISC and heme biosynthesis could be investigated with an Mrs3/4-overexpression strain. In this case, mitochondria would be expected to contain elevated amounts of Fe_{580}, which would yield increased levels of ISCs and hemes.

REFERENCES

1. Lill, R., Hoffmann, B., Molik, S., Pierik, A. J., Rietzschel, N., Stehling, O., Uzarska, M. A., Webert, H., Wilbrecht, C., and Muhlenhoff, U. (2012) The role of mitochondria in cellular iron-sulfur protein biogenesis and iron metabolism, *Biochim Biophys Acta 1823*, 1491-1508.
2. Robinson, N. J., and Winge, D. R. (2010) Copper metallochaperones, *Annu Rev Biochem 79*, 537-562.
3. Atkinson, A., and Winge, D. R. (2009) Metal acquisition and availability in the mitochondria, *Chem Rev 109*, 4708-4721.
4. Culotta, V. C., Yang, M., and O'Halloran, T. V. (2006) Activation of superoxide dismutases: putting the metal to the pedal, *Biochim Biophys Acta 1763*, 747-758.
5. Colleluori, D. M., Morris, S. M., Jr., and Ash, D. E. (2001) Expression, purification, and characterization of human type II arginase, *Arch Biochem Biophys 389*, 135-143.
6. Touyz, R. M. (2014) Linking LOX-1 and arginase II through mitochondria: a novel paradigm in endothelial dysfunction, *Circ Res 115*, 412-414.
7. Zhao, H., Ruberu, K., Li, H., and Garner, B. (2013) Analysis of subcellular [57Co] cobalamin distribution in SH-SY5Y neurons and brain tissue, *J Neurosci Methods 217*, 67-74.
8. Ott, G., Havemeyer, A., and Clement, B. (2015) The mammalian molybdenum enzymes of mARC, *J Biol Inorg Chem 20*, 265-275.

9. Eide, D. J. (2006) Zinc transporters and the cellular trafficking of zinc, *Biochim Biophys Acta 1763*, 711-722.

10. Sturtz, L. A., Diekert, K., Jensen, L. T., Lill, R., and Culotta, V. C. (2001) A fraction of yeast Cu,Zn-superoxide dismutase and its metallochaperone, CCS, localize to the intermembrane space of mitochondria. A physiological role for SOD1 in guarding against mitochondrial oxidative damage, *J Biol Chem 276*, 38084-38089.

11. Pilgrim, D., and Young, E. T. (1987) Primary structure requirements for correct sorting of the yeast mitochondrial protein ADH III to the yeast mitochondrial matrix space, *Mol Cell Biol 7*, 294-304.

12. Bakker, B. M., Bro, C., Kotter, P., Luttik, M. A., van Dijken, J. P., and Pronk, J. T. (2000) The mitochondrial alcohol dehydrogenase Adh3p is involved in a redox shuttle in Saccharomyces cerevisiae, *J Bacteriol 182*, 4730-4737.

13. Mourier, A., Vallortigara, J., Yoboue, E. D., Rigoulet, M., and Devin, A. (2008) Kinetic activation of yeast mitochondrial D-lactate dehydrogenase by carboxylic acids, *Biochim Biophys Acta 1777*, 1283-1288.

14. Bito, A., Haider, M., Hadler, I., and Breitenbach, M. (1997) Identification and phenotypic analysis of two glyoxalase II encoding genes from Saccharomyces cerevisiae, GLO2 and GLO4, and intracellular localization of the corresponding proteins, *J Biol Chem 272*, 21509-21519.

15. Kohlhaw, G. B. (2003) Leucine biosynthesis in fungi: entering metabolism through the back door, *Microbiol Mol Biol Rev 67*, 1-15, table of contents.

16. Roeder, P. R., and Kohlhaw, G. B. (1980) alpha-Isopropylmalate synthase from yeast. A zinc metalloenzyme, *Biochim Biophys Acta 613*, 482-487.

17. Sankaranarayanan, R., Dock-Bregeon, A. C., Rees, B., Bovee, M., Caillet, J., Romby, P., Francklyn, C. S., and Moras, D. (2000) Zinc ion mediated amino acid discrimination by threonyl-tRNA synthetase, *Nat Struct Biol 7*, 461-465.

18. Ellenrieder, L., Martensson, C. U., and Becker, T. (2015) Biogenesis of mitochondrial outer membrane proteins, problems and diseases, *Biol Chem 396*, 1199-1213.

19. MacKenzie, J. A., and Payne, R. M. (2007) Mitochondrial protein import and human health and disease, *Biochim Biophys Acta 1772*, 509-523.

20. Mordas, A., and Tokatlidis, K. (2015) The MIA pathway: a key regulator of mitochondrial oxidative protein folding and biogenesis, *Acc Chem Res 48*, 2191-2199.

21. Pearce, D. A. (1999) Hereditary spastic paraplegia: mitochondrial metalloproteases of yeast, *Hum Genet 104*, 443-448.

22. Mossmann, D., Meisinger, C., and Vogtle, F. N. (2012) Processing of mitochondrial presequences, *Biochim Biophys Acta 1819*, 1098-1106.

23. Francis, B. R., and Thorsness, P. E. (2011) Hsp90 and mitochondrial proteases Yme1 and Yta10/12 participate in ATP synthase assembly in Saccharomyces cerevisiae, *Mitochondrion 11*, 587-600.

24. Fraga, H., Papaleo, E., Vega, S., Velazquez-Campoy, A., and Ventura, S. (2013) Zinc induced folding is essential for TIM15 activity as an mtHsp70 chaperone, *Biochim Biophys Acta 1830*, 2139-2149.

25. Ciesielski, G. L., Plotka, M., Manicki, M., Schilke, B. A., Dutkiewicz, R., Sahi, C., Marszalek, J., and Craig, E. A. (2013) Nucleoid localization of Hsp40 Mdj1 is important for its function in maintenance of mitochondrial DNA, *Biochim Biophys Acta 1833*, 2233-2243.

26. Ceh-Pavia, E., Spiller, M. P., and Lu, H. (2013) Folding and biogenesis of mitochondrial small Tim proteins, *Int J Mol Sci 14*, 16685-16705.

27. Sirrenberg, C., Endres, M., Folsch, H., Stuart, R. A., Neupert, W., and Brunner, M. (1998) Carrier protein import into mitochondria mediated by the intermembrane proteins Tim10/Mrs11 and Tim12/Mrs5, *Nature 391*, 912-915.

28. Terziyska, N., Lutz, T., Kozany, C., Mokranjac, D., Mesecke, N., Neupert, W., Herrmann, J. M., and Hell, K. (2005) Mia40, a novel factor for protein import into the intermembrane space of mitochondria is able to bind metal ions, *FEBS Lett 579*, 179-184.

29. Mesecke, N., Bihlmaier, K., Grumbt, B., Longen, S., Terziyska, N., Hell, K., and Herrmann, J. M. (2008) The zinc-binding protein Hot13 promotes oxidation of the mitochondrial import receptor Mia40, *EMBO Rep 9*, 1107-1113.

30. Morgan, B., Ang, S. K., Yan, G., and Lu, H. (2009) Zinc can play chaperone-like and inhibitor roles during import of mitochondrial small Tim proteins, *J Biol Chem 284*, 6818-6825.

31. Zeth, K., and Thein, M. (2010) Porins in prokaryotes and eukaryotes: common themes and variations, *Biochem J 431*, 13-22.

32. Mertins, B., Psakis, G., and Essen, L. O. (2014) Voltage-dependent anion channels: the wizard of the mitochondrial outer membrane, *Biol Chem 395*, 1435-1442.

33. Cobine, P. A., Pierrel, F., and Winge, D. R. (2006) Copper trafficking to the mitochondrion and assembly of copper metalloenzymes, *Biochim Biophys Acta 1763*, 759-772.

34. Palacios, O., Atrian, S., and Capdevila, M. (2011) Zn- and Cu-thioneins: a functional classification for metallothioneins?, *J Biol Inorg Chem 16*, 991-1009.

35. Giedroc, D. P., and Arunkumar, A. I. (2007) Metal sensor proteins: nature's metalloregulated allosteric switches, *Dalton Trans*, 3107-3120.

36. Ba, L. A., Doering, M., Burkholz, T., and Jacob, C. (2009) Metal trafficking: from maintaining the metal homeostasis to future drug design, *Metallomics 1*, 292-311.

37. Outten, C. E., and O'Halloran, T. V. (2001) Femtomolar sensitivity of metalloregulatory proteins controlling zinc homeostasis, *Science 292*, 2488-2492.

38. Rae, T. D., Schmidt, P. J., Pufahl, R. A., Culotta, V. C., and O'Halloran, T. V. (1999) Undetectable intracellular free copper: the requirement of a copper chaperone for superoxide dismutase, *Science 284*, 805-808.

39. Harrison, M. D., Jones, C. E., Solioz, M., and Dameron, C. T. (2000) Intracellular copper routing: the role of copper chaperones, *Trends Biochem Sci 25*, 29-32.

40. Greenberg, G. R., and Wintrobe, M. M. (1946) A labile iron pool, *J Biol Chem 165*, 397.

41. Jacobs, A. (1977) Low molecular weight intracellular iron transport compounds, *Blood 50*, 433-439.

42. Rauen, U., Springer, A., Weisheit, D., Petrat, F., Korth, H. G., de Groot, H., and Sustmann, R. (2007) Assessment of chelatable mitochondrial iron by using mitochondrion-selective fluorescent iron indicators with different iron-binding affinities, *Chembiochem 8*, 341-352.

43. Sensi, S. L., Ton-That, D., Sullivan, P. G., Jonas, E. A., Gee, K. R., Kaczmarek, L. K., and Weiss, J. H. (2003) Modulation of mitochondrial function by endogenous Zn2+ pools, *Proc Natl Acad Sci U S A 100*, 6157-6162.

44. Cobine, P. A., Ojeda, L. D., Rigby, K. M., and Winge, D. R. (2004) Yeast contain a non-proteinaceous pool of copper in the mitochondrial matrix, *J Biol Chem 279*, 14447-14455.

45. Maret, W. (2015) Analyzing free zinc(II) ion concentrations in cell biology with fluorescent chelating molecules, *Metallomics 7*, 202-211.

46. Aron, A. T., Ramos-Torres, K. M., Cotruvo, J. A., Jr., and Chang, C. J. (2015) Recognition- and reactivity-based fluorescent probes for studying transition metal signaling in living systems, *Acc Chem Res 48*, 2434-2442.

47. Figueroa, J. A., Vignesh, K. S., Deepe, G. S., Jr., and Caruso, J. (2014) Selectivity and specificity of small molecule fluorescent dyes/probes used for the detection of Zn2+ and Ca2+ in cells, *Metallomics 6*, 301-315.

48. McCormick, S. P., Moore, M. J., and Lindahl, P. A. (2015) Detection of labile low-molecular-mass transition metal complexes in mitochondria, *Biochemistry 54*, 3442-3453.

49. Greenawalt, J. W. (1979) Survey and update of outer and inner mitochondrial membrane separation, *Methods Enzymol 55*, 88-98.

50. Irazusta, V., Moreno-Cermeno, A., Cabiscol, E., Ros, J., and Tamarit, J. (2008) Major targets of iron-induced protein oxidative damage in frataxin-deficient yeasts are magnesium-binding proteins, *Free Radic Biol Med 44*, 1712-1723.

51. Wiseman, H., and Halliwell, B. (1996) Damage to DNA by reactive oxygen and nitrogen species: role in inflammatory disease and progression to cancer, *Biochem J 313 (Pt 1)*, 17-29.

52. Drake, I. M., Mapstone, N. P., Schorah, C. J., White, K. L., Chalmers, D. M., Dixon, M. F., and Axon, A. T. (1998) Reactive oxygen species activity and lipid peroxidation in Helicobacter pylori associated gastritis: relation to gastric mucosal ascorbic acid concentrations and effect of H pylori eradication, *Gut 42*, 768-771.

53. Frederickson, C. J., Koh, J. Y., and Bush, A. I. (2005) The neurobiology of zinc in health and disease, *Nat Rev Neurosci 6*, 449-462.

54. Madsen, E., and Gitlin, J. D. (2007) Copper and iron disorders of the brain, *Annu Rev Neurosci 30*, 317-337.

55. Donnelly, P. S., Xiao, Z., and Wedd, A. G. (2007) Copper and Alzheimer's disease, *Curr Opin Chem Biol 11*, 128-133.

56. Gaggelli, E., Kozlowski, H., Valensin, D., and Valensin, G. (2006) Copper homeostasis and neurodegenerative disorders (Alzheimer's, prion, and Parkinson's diseases and amyotrophic lateral sclerosis), *Chem Rev 106*, 1995-2044.

57. Miller, Y., Ma, B., and Nussinov, R. (2010) Zinc ions promote Alzheimer Abeta aggregation via population shift of polymorphic states, *Proc Natl Acad Sci U S A 107*, 9490-9495.

58. Lovell, M. A., Robertson, J. D., Teesdale, W. J., Campbell, J. L., and Markesbery, W. R. (1998) Copper, iron and zinc in Alzheimer's disease senile plaques, *J Neurol Sci 158*, 47-52.

59. Hashimoto, M., Hsu, L. J., Xia, Y., Takeda, A., Sisk, A., Sundsmo, M., and Masliah, E. (1999) Oxidative stress induces amyloid-like aggregate formation of NACP/alpha-synuclein in vitro, *Neuroreport 10*, 717-721.

60. Kim, Y. S., Lee, D., Lee, E. K., Sung, J. Y., Chung, K. C., Kim, J., and Paik, S. R. (2001) Multiple ligand interaction of alpha-synuclein produced various forms of protein aggregates in the presence of Abeta25-35, copper, and eosin, *Brain Res 908*, 93-98.

61. Galaris, D., Skiada, V., and Barbouti, A. (2008) Redox signaling and cancer: the role of "labile" iron, *Cancer Lett 266*, 21-29.

62. Steinbrecher, U. P., Parthasarathy, S., Leake, D. S., Witztum, J. L., and Steinberg, D. (1984) Modification of low density lipoprotein by endothelial cells involves lipid peroxidation and degradation of low density lipoprotein phospholipids, *Proc Natl Acad Sci U S A 81*, 3883-3887.

63. Wilkins, R. G. (1991) *Kinetics and mechanism of reactions of transition metal complexes*, Wiley.

64. Shin, W., and Lindahl, P. A. (1992) Discovery of a labile nickel ion required for CO/acetyl-CoA exchange activity in the NiFe complex of carbon monoxide dehydrogenase from Clostridium thermoaceticum, *Journal of the American Chemical Society 114*, 9718-9719.

65. Saha, R., Saha, N., Donofrio, R. S., and Bestervelt, L. L. (2013) Microbial siderophores: a mini review, *J Basic Microbiol 53*, 303-317.

66. Cobine, P. A., Pierrel, F., Bestwick, M. L., and Winge, D. R. (2006) Mitochondrial matrix copper complex used in metallation of cytochrome oxidase and superoxide dismutase, *J Biol Chem 281*, 36552-36559.

67. Vest, K. E., Leary, S. C., Winge, D. R., and Cobine, P. A. (2013) Copper import into the mitochondrial matrix in Saccharomyces cerevisiae is mediated by Pic2, a mitochondrial carrier family protein, *J Biol Chem 288*, 23884-23892.

68. Vest, K. E., Wang, J., Gammon, M. G., Maynard, M. K., White, O. L., Cobine, J. A., Mahone, W. K., and Cobine, P. A. (2016) Overlap of copper and iron uptake systems in mitochondria in Saccharomyces cerevisiae, *Open Biol 6*, 150223.

69. Leary, S. C., Winge, D. R., and Cobine, P. A. (2009) "Pulling the plug" on cellular copper: the role of mitochondria in copper export, *Biochim Biophys Acta 1793*, 146-153.

70. Palmieri, F. (2013) The mitochondrial transporter family SLC25: identification, properties and physiopathology, *Mol Aspects Med 34*, 465-484.

71. Heaton, D., Nittis, T., Srinivasan, C., and Winge, D. R. (2000) Mutational analysis of the mitochondrial copper metallochaperone Cox17, *J Biol Chem 275*, 37582-37587.

72. Horng, Y. C., Cobine, P. A., Maxfield, A. B., Carr, H. S., and Winge, D. R. (2004) Specific copper transfer from the Cox17 metallochaperone to both Sco1 and Cox11 in the assembly of yeast cytochrome C oxidase, *J Biol Chem 279*, 35334-35340.

73. Beers, J., Glerum, D. M., and Tzagoloff, A. (1997) Purification, characterization, and localization of yeast Cox17p, a mitochondrial copper shuttle, *J Biol Chem 272*, 33191-33196.

74. Glerum, D. M., Shtanko, A., and Tzagoloff, A. (1996) Characterization of COX17, a yeast gene involved in copper metabolism and assembly of cytochrome oxidase, *J Biol Chem 271*, 14504-14509.

75. Nobrega, M. P., Bandeira, S. C., Beers, J., and Tzagoloff, A. (2002) Characterization of COX19, a widely distributed gene required for expression of mitochondrial cytochrome oxidase, *J Biol Chem 277*, 40206-40211.

76. Bode, M., Woellhaf, M. W., Bohnert, M., van der Laan, M., Sommer, F., Jung, M., Zimmermann, R., Schroda, M., and Herrmann, J. M. (2015) Redox-regulated dynamic interplay between Cox19 and the copper-binding protein Cox11 in the intermembrane space of mitochondria facilitates biogenesis of cytochrome c oxidase, *Mol Biol Cell 26*, 2385-2401.

77. Chacinska, A., Pfannschmidt, S., Wiedemann, N., Kozjak, V., Sanjuan Szklarz, L. K., Schulze-Specking, A., Truscott, K. N., Guiard, B., Meisinger, C., and Pfanner, N. (2004) Essential role of Mia40 in import and assembly of mitochondrial intermembrane space proteins, *EMBO J 23*, 3735-3746.

78. Maxfield, A. B., Heaton, D. N., and Winge, D. R. (2004) Cox17 is functional when tethered to the mitochondrial inner membrane, *J Biol Chem 279*, 5072-5080.

79. Leary, S. C. (2010) Redox regulation of SCO protein function: controlling copper at a mitochondrial crossroad, *Antioxid Redox Signal 13*, 1403-1416.

80. Ghosh, A., Trivedi, P. P., Timbalia, S. A., Griffin, A. T., Rahn, J. J., Chan, S. S., and Gohil, V. M. (2014) Copper supplementation restores cytochrome c oxidase assembly defect in a mitochondrial disease model of COA6 deficiency, *Hum Mol Genet 23*, 3596-3606.

81. Yang, L., McRae, R., Henary, M. M., Patel, R., Lai, B., Vogt, S., and Fahrni, C. J. (2005) Imaging of the intracellular topography of copper with a fluorescent sensor and by synchrotron x-ray fluorescence microscopy, *Proc Natl Acad Sci U S A 102*, 11179-11184.

82. Dodani, S. C., Leary, S. C., Cobine, P. A., Winge, D. R., and Chang, C. J. (2011) A targetable fluorescent sensor reveals that copper-deficient SCO1 and SCO2 patient cells prioritize mitochondrial copper homeostasis, *J Am Chem Soc 133*, 8606-8616.

83. Giuffrida, M. L., Rizzarelli, E., Tomaselli, G. A., Satriano, C., and Trusso Sfrazzetto, G. (2014) A novel fully water-soluble Cu(I) probe for fluorescence live cell imaging, *Chem Commun (Camb) 50*, 9835-9838.

84. Atkinson, A., Khalimonchuk, O., Smith, P., Sabic, H., Eide, D., and Winge, D. R. (2010) Mzm1 influences a labile pool of mitochondrial zinc important for respiratory function, *J Biol Chem 285*, 19450-19459.

85. Tomat, E., Nolan, E. M., Jaworski, J., and Lippard, S. J. (2008) Organelle-specific zinc detection using zinpyr-labeled fusion proteins in live cells, *J Am Chem Soc 130*, 15776-15777.

86. Sensi, S. L., Ton-That, D., and Weiss, J. H. (2002) Mitochondrial sequestration and Ca(2+)-dependent release of cytosolic Zn(2+) loads in cortical neurons, *Neurobiol Dis 10*, 100-108.

87. Malaiyandi, L. M., Vergun, O., Dineley, K. E., and Reynolds, I. J. (2005) Direct visualization of mitochondrial zinc accumulation reveals uniporter-dependent and -independent transport mechanisms, *J Neurochem 93*, 1242-1250.

88. Pierrel, F., Cobine, P. A., and Winge, D. R. (2007) Metal Ion availability in mitochondria, *Biometals 20*, 675-682.

89. Lee, S., Hennigar, S. R., Alam, S., Nishida, K., and Kelleher, S. L. (2015) Essential role for zinc transporter 2 (ZnT2)-mediated zinc transport in mammary gland development and function during lactation, *J Biol Chem 290*, 13064-13078.

90. Jiang, D., Sullivan, P. G., Sensi, S. L., Steward, O., and Weiss, J. H. (2001) Zn(2+) induces permeability transition pore opening and release of pro-apoptotic peptides from neuronal mitochondria, *J Biol Chem 276*, 47524-47529.

91. Sun, Q., Zhong, W., Zhang, W., Li, Q., Sun, X., Tan, X., Sun, X., Dong, D., and Zhou, Z. (2015) Zinc deficiency mediates alcohol-induced apoptotic cell death in the liver of rats through activating ER and mitochondrial cell death pathways, *Am J Physiol Gastrointest Liver Physiol 308*, G757-766.

92. Dineley, K. E., Richards, L. L., Votyakova, T. V., and Reynolds, I. J. (2005) Zinc causes loss of membrane potential and elevates reactive oxygen species in rat brain mitochondria, *Mitochondrion 5*, 55-65.

93. Devinney, M. J., Malaiyandi, L. M., Vergun, O., DeFranco, D. B., Hastings, T. G., and Dineley, K. E. (2009) A comparison of Zn2+- and Ca2+-triggered depolarization of liver mitochondria reveals no evidence of Zn2+-induced permeability transition, *Cell Calcium 45*, 447-455.

94. Gazaryan, I. G., Krasinskaya, I. P., Kristal, B. S., and Brown, A. M. (2007) Zinc irreversibly damages major enzymes of energy production and antioxidant defense prior to mitochondrial permeability transition, *J Biol Chem 282*, 24373-24380.

95. Lesuisse, E., Santos, R., Matzanke, B. F., Knight, S. A., Camadro, J. M., and Dancis, A. (2003) Iron use for haeme synthesis is under control of the yeast frataxin homologue (Yfh1), *Hum Mol Genet 12*, 879-889.

96. Camadro, J. M., and Labbe, P. (1982) Kinetic studies of ferrochelatase in yeast. Zinc or iron as competing substrates, *Biochim Biophys Acta 707*, 280-288.

97. Camadro, J. M., Matringe, M., Scalla, R., and Labbe, P. (1991) Kinetic studies on protoporphyrinogen oxidase inhibition by diphenyl ether herbicides, *Biochem J 277 (Pt 1)*, 17-21.

98. Santos, R., Dancis, A., Eide, D., Camadro, J. M., and Lesuisse, E. (2003) Zinc suppresses the iron-accumulation phenotype of Saccharomyces cerevisiae lacking the yeast frataxin homologue (Yfh1), *Biochem J 375*, 247-254.

99. Zhang, Y., Lyver, E. R., Knight, S. A., Lesuisse, E., and Dancis, A. (2005) Frataxin and mitochondrial carrier proteins, Mrs3p and Mrs4p, cooperate in providing iron for heme synthesis, *J Biol Chem 280*, 19794-19807.

100. Outten, C. E., and Albetel, A. N. (2013) Iron sensing and regulation in Saccharomyces cerevisiae: Ironing out the mechanistic details, *Curr Opin Microbiol 16*, 662-668.

101. Lorusso, M., Cocco, T., Sardanelli, A. M., Minuto, M., Bonomi, F., and Papa, S. (1991) Interaction of Zn2+ with the bovine-heart mitochondrial bc1 complex, *Eur J Biochem 197*, 555-561.

102. Gazaryan, I. G., Krasnikov, B. F., Ashby, G. A., Thorneley, R. N., Kristal, B. S., and Brown, A. M. (2002) Zinc is a potent inhibitor of thiol oxidoreductase activity and stimulates reactive oxygen species production by lipoamide dehydrogenase, *J Biol Chem 277*, 10064-10072.

103. Atkinson, A., Smith, P., Fox, J. L., Cui, T. Z., Khalimonchuk, O., and Winge, D. R. (2011) The LYR protein Mzm1 functions in the insertion of the Rieske Fe/S protein in yeast mitochondria, *Mol Cell Biol 31*, 3988-3996.

104. Liuzzi, J. P., Guo, L., Yoo, C., and Stewart, T. S. (2014) Zinc and autophagy, *Biometals 27*, 1087-1096.

105. McCranor, B. J., Bozym, R. A., Vitolo, M. I., Fierke, C. A., Bambrick, L., Polster, B. M., Fiskum, G., and Thompson, R. B. (2012) Quantitative imaging of mitochondrial and cytosolic free zinc levels in an in vitro model of ischemia/reperfusion, *J Bioenerg Biomembr 44*, 253-263.

106. Park, J. G., Qin, Y., Galati, D. F., and Palmer, A. E. (2012) New sensors for quantitative measurement of mitochondrial Zn(2+), *ACS Chem Biol 7*, 1636-1640.

107. Wispe, J. R., Clark, J. C., Burhans, M. S., Kropp, K. E., Korfhagen, T. R., and Whitsett, J. A. (1989) Synthesis and processing of the precursor for human mangano-superoxide dismutase, *Biochim Biophys Acta 994*, 30-36.

108. Magnoni, R., Palmfeldt, J., Hansen, J., Christensen, J. H., Corydon, T. J., and Bross, P. (2014) The Hsp60 folding machinery is crucial for manganese superoxide dismutase folding and function, *Free Radic Res 48*, 168-179.

109. Luk, E., Yang, M., Jensen, L. T., Bourbonnais, Y., and Culotta, V. C. (2005) Manganese activation of superoxide dismutase 2 in the mitochondria of Saccharomyces cerevisiae, *J Biol Chem 280*, 22715-22720.

110. Luk, E., Carroll, M., Baker, M., and Culotta, V. C. (2003) Manganese activation of superoxide dismutase 2 in Saccharomyces cerevisiae requires MTM1, a member of the mitochondrial carrier family, *Proc Natl Acad Sci U S A 100*, 10353-10357.

111. Yang, M., Cobine, P. A., Molik, S., Naranuntarat, A., Lill, R., Winge, D. R., and Culotta, V. C. (2006) The effects of mitochondrial iron homeostasis on cofactor specificity of superoxide dismutase 2, *EMBO J 25*, 1775-1783.

112. Naranuntarat, A., Jensen, L. T., Pazicni, S., Penner-Hahn, J. E., and Culotta, V. C. (2009) The interaction of mitochondrial iron with manganese superoxide dismutase, *J Biol Chem 284*, 22633-22640.

113. Park, J., McCormick, S. P., Chakrabarti, M., and Lindahl, P. A. (2013) Insights into the iron-ome and manganese-ome of Deltamtm1 Saccharomyces cerevisiae mitochondria, *Metallomics 5*, 656-672.

114. Miao, R., Kim, H., Koppolu, U. M., Ellis, E. A., Scott, R. A., and Lindahl, P. A. (2009) Biophysical characterization of the iron in mitochondria from Atm1p-depleted Saccharomyces cerevisiae, *Biochemistry 48*, 9556-9568.

115. Miao, R., Martinho, M., Morales, J. G., Kim, H., Ellis, E. A., Lill, R., Hendrich, M. P., Munck, E., and Lindahl, P. A. (2008) EPR and Mossbauer spectroscopy of intact mitochondria isolated from Yah1p-depleted Saccharomyces cerevisiae, *Biochemistry 47*, 9888-9899.

116. Whittaker, M. M., Penmatsa, A., and Whittaker, J. W. (2015) The Mtm1p carrier and pyridoxal 5'-phosphate cofactor trafficking in yeast mitochondria, *Arch Biochem Biophys 568*, 64-70.

117. Gherasim, C., Lofgren, M., and Banerjee, R. (2013) Navigating the B(12) road: assimilation, delivery, and disorders of cobalamin, *J Biol Chem 288*, 13186-13193.

118. Dobson, C. M., Wai, T., Leclerc, D., Kadir, H., Narang, M., Lerner-Ellis, J. P., Hudson, T. J., Rosenblatt, D. S., and Gravel, R. A. (2002) Identification of the gene responsible for the cblB complementation group of vitamin B12-dependent methylmalonic aciduria, *Hum Mol Genet 11*, 3361-3369.

119. Banerjee, R., Gherasim, C., and Padovani, D. (2009) The tinker, tailor, soldier in intracellular B12 trafficking, *Curr Opin Chem Biol 13*, 484-491.

120. Froese, D. S., Kochan, G., Muniz, J. R., Wu, X., Gileadi, C., Ugochukwu, E., Krysztofinska, E., Gravel, R. A., Oppermann, U., and Yue, W. W. (2010) Structures of the human GTPase MMAA and vitamin B12-dependent methylmalonyl-CoA mutase and insight into their complex formation, *J Biol Chem 285*, 38204-38213.

121. Klein, J. M., and Schwarz, G. (2012) Cofactor-dependent maturation of mammalian sulfite oxidase links two mitochondrial import pathways, *J Cell Sci 125*, 4876-4885.

122. Schwarz, G., and Mendel, R. R. (2006) Molybdenum cofactor biosynthesis and molybdenum enzymes, *Annu Rev Plant Biol 57*, 623-647.

123. Deistung, J., and Bray, R. C. (1989) Isolation, in the intact state, of the pterin molybdenum cofactor from xanthine oxidase, *Biochem J 263*, 477-483.

124. Neve, E. P., Kofeler, H., Hendriks, D. F., Nordling, A., Gogvadze, V., Mkrtchian, S., Naslund, E., and Ingelman-Sundberg, M. (2015) Expression and function of mARC: roles in lipogenesis and metabolic activation of ximelagatran, *PLoS One 10*, e0138487.

125. Gruenewald, S., Wahl, B., Bittner, F., Hungeling, H., Kanzow, S., Kotthaus, J., Schwering, U., Mendel, R. R., and Clement, B. (2008) The fourth molybdenum containing enzyme mARC: cloning and involvement in the activation of N-hydroxylated prodrugs, *J Med Chem 51*, 8173-8177.

126. Havemeyer, A., Grunewald, S., Wahl, B., Bittner, F., Mendel, R., Erdelyi, P., Fischer, J., and Clement, B. (2010) Reduction of N-hydroxy-sulfonamides, including N-hydroxy-valdecoxib, by the molybdenum-containing enzyme mARC, *Drug Metab Dispos 38*, 1917-1921.

127. Jakobs, H. H., Froriep, D., Havemeyer, A., Mendel, R. R., Bittner, F., and Clement, B. (2014) The mitochondrial amidoxime reducing component (mARC): involvement in metabolic reduction of N-oxides, oximes and N-hydroxyamidinohydrazones, *ChemMedChem 9*, 2381-2387.

128. Wahl, B., Reichmann, D., Niks, D., Krompholz, N., Havemeyer, A., Clement, B., Messerschmidt, T., Rothkegel, M., Biester, H., Hille, R., Mendel, R. R., and Bittner, F. (2010) Biochemical and spectroscopic characterization of the human mitochondrial amidoxime reducing components hmARC-1 and hmARC-2 suggests the existence of a new molybdenum enzyme family in eukaryotes, *J Biol Chem 285*, 37847-37859.

129. Mendel, R. R., and Leimkuhler, S. (2015) The biosynthesis of the molybdenum cofactors, *J Biol Inorg Chem 20*, 337-347.

130. Shaw, G. C., Cope, J. J., Li, L., Corson, K., Hersey, C., Ackermann, G. E., Gwynn, B., Lambert, A. J., Wingert, R. A., Traver, D., Trede, N. S., Barut, B. A., Zhou,

Y., Minet, E., Donovan, A., Brownlie, A., Balzan, R., Weiss, M. J., Peters, L. L., Kaplan, J., Zon, L. I., and Paw, B. H. (2006) Mitoferrin is essential for erythroid iron assimilation, *Nature 440*, 96-100.

131. Froschauer, E. M., Schweyen, R. J., and Wiesenberger, G. (2009) The yeast mitochondrial carrier proteins Mrs3p/Mrs4p mediate iron transport across the inner mitochondrial membrane, *Biochim Biophys Acta 1788*, 1044-1050.

132. Muhlenhoff, U., Stadler, J. A., Richhardt, N., Seubert, A., Eickhorst, T., Schweyen, R. J., Lill, R., and Wiesenberger, G. (2003) A specific role of the yeast mitochondrial carriers MRS3/4p in mitochondrial iron acquisition under iron-limiting conditions, *J Biol Chem 278*, 40612-40620.

133. Li, L., and Kaplan, J. (2004) A mitochondrial-vacuolar signaling pathway in yeast that affects iron and copper metabolism, *J Biol Chem 279*, 33653-33661.

134. Monne, M., and Palmieri, F. (2014) Antiporters of the mitochondrial carrier family, *Curr Top Membr 73*, 289-320.

135. Zhang, Y., Lyver, E. R., Knight, S. A., Pain, D., Lesuisse, E., and Dancis, A. (2006) Mrs3p, Mrs4p, and frataxin provide iron for Fe-S cluster synthesis in mitochondria, *J Biol Chem 281*, 22493-22502.

136. Yoon, H., Zhang, Y., Pain, J., Lyver, E. R., Lesuisse, E., Pain, D., and Dancis, A. (2011) Rim2, a pyrimidine nucleotide exchanger, is needed for iron utilization in mitochondria, *Biochem J 440*, 137-146.

137. Froschauer, E. M., Rietzschel, N., Hassler, M. R., Binder, M., Schweyen, R. J., Lill, R., Muhlenhoff, U., and Wiesenberger, G. (2013) The mitochondrial carrier Rim2 co-imports pyrimidine nucleotides and iron, *Biochem J 455*, 57-65.

138. Robinson, A. J., and Kunji, E. R. (2006) Mitochondrial carriers in the cytoplasmic state have a common substrate binding site, *Proc Natl Acad Sci U S A 103*, 2617-2622.

139. Brazzolotto, X., Pierrel, F., and Pelosi, L. (2014) Three conserved histidine residues contribute to mitochondrial iron transport through mitoferrins, *Biochem J 460*, 79-89.

140. Tangeras, A., Flatmark, T., Backstrom, D., and Ehrenberg, A. (1980) Mitochondrial iron not bound in heme and iron-sulfur centers. Estimation, compartmentation and redox state, *Biochim Biophys Acta 589*, 162-175.

141. Petrat, F., de Groot, H., and Rauen, U. (2001) Subcellular distribution of chelatable iron: a laser scanning microscopic study in isolated hepatocytes and liver endothelial cells, *Biochem J 356*, 61-69.

142. Petrat, F., Weisheit, D., Lensen, M., de Groot, H., Sustmann, R., and Rauen, U. (2002) Selective determination of mitochondrial chelatable iron in viable cells with a new fluorescent sensor, *Biochem J 362*, 137-147.

143. Garber Morales, J., Holmes-Hampton, G. P., Miao, R., Guo, Y., Munck, E., and Lindahl, P. A. (2010) Biophysical characterization of iron in mitochondria isolated from respiring and fermenting yeast, *Biochemistry 49*, 5436-5444.

144. Holmes-Hampton, G. P., Miao, R., Garber Morales, J., Guo, Y., Munck, E., and Lindahl, P. A. (2010) A nonheme high-spin ferrous pool in mitochondria isolated from fermenting Saccharomyces cerevisiae, *Biochemistry 49*, 4227-4234.

145. Lutz, T., Westermann, B., Neupert, W., and Herrmann, J. M. (2001) The mitochondrial proteins Ssq1 and Jac1 are required for the assembly of iron sulfur clusters in mitochondria, *J Mol Biol 307*, 815-825.

146. Pandey, A., Pain, J., Ghosh, A. K., Dancis, A., and Pain, D. (2015) Fe-S cluster biogenesis in isolated mammalian mitochondria: coordinated use of persulfide sulfur and iron and requirements for GTP, NADH, and ATP, *J Biol Chem 290*, 640-657.

147. Lange, H., Kispal, G., and Lill, R. (1999) Mechanism of iron transport to the site of heme synthesis inside yeast mitochondria, *J Biol Chem 274*, 18989-18996.

148. Wu, C. K., Dailey, H. A., Rose, J. P., Burden, A., Sellers, V. M., and Wang, B. C. (2001) The 2.0 A structure of human ferrochelatase, the terminal enzyme of heme biosynthesis, *Nat Struct Biol 8*, 156-160.

149. Cotgreave, I. A., and Gerdes, R. G. (1998) Recent trends in glutathione biochemistry--glutathione-protein interactions: a molecular link between oxidative stress and cell proliferation?, *Biochem Biophys Res Commun 242*, 1-9.

150. Aliaga, M. E., Lopez-Alarcon, C., Bridi, R., and Speisky, H. (2016) Redox-implications associated with the formation of complexes between copper ions and reduced or oxidized glutathione, *J Inorg Biochem 154*, 78-88.

151. Mari, M., Morales, A., Colell, A., Garcia-Ruiz, C., and Fernandez-Checa, J. C. (2009) Mitochondrial glutathione, a key survival antioxidant, *Antioxid Redox Signal 11*, 2685-2700.

152. Qi, W., and Cowan, J. A. (2011) Mechanism of glutaredoxin-ISU [2Fe-2S] cluster exchange, *Chem Commun (Camb) 47*, 4989-4991.

153. Hider, R. C., and Kong, X. (2013) Iron speciation in the cytosol: an overview, *Dalton Trans 42*, 3220-3229.

154. Silva, A. M., Kong, X., Parkin, M. C., Cammack, R., and Hider, R. C. (2009) Iron(III) citrate speciation in aqueous solution, *Dalton Trans*, 8616-8625.

155. Srinivasan, V., Pierik, A. J., and Lill, R. (2014) Crystal structures of nucleotide-free and glutathione-bound mitochondrial ABC transporter Atm1, *Science 343*, 1137-1140.

156. Schaedler, T. A., Thornton, J. D., Kruse, I., Schwarzlander, M., Meyer, A. J., van Veen, H. W., and Balk, J. (2014) A conserved mitochondrial ATP-binding cassette transporter exports glutathione polysulfide for cytosolic metal cofactor assembly, *J Biol Chem 289*, 23264-23274.

157. Li, J., and Cowan, J. A. (2015) Glutathione-coordinated [2Fe-2S] cluster: a viable physiological substrate for mitochondrial ABCB7 transport, *Chem Commun (Camb) 51*, 2253-2255.

158. McCormick, S. P., Chakrabarti, M., Cockrell, A. L., Park, J., Lindahl, L. S., and Lindahl, P. A. (2013) Low-molecular-mass metal complexes in the mouse brain, *Metallomics 5*, 232-241.

159. Mossbauer, R. L. (1962) Recoilless Nuclear Resonance Absorption of Gamma Radiation: A new principle yields gamma lines of extreme narrowness for measurements of unprecedented accuracy, *Science 137*, 731-738.

160. Que, L. (2000) *Physical methods in bioinorganic chemistry: spectroscopy and magnetism*, University Science Books.

161. Keilin, D. (1925) On cytochrome, a respiratory pigment, common to animals, yeast, and higher plants, *Proceedings of the Royal Society of London. Series B, Containing Papers of a Biological Character 98*, 312-339.

162. Albrecht, A. G., Netz, D. J., Miethke, M., Pierik, A. J., Burghaus, O., Peuckert, F., Lill, R., and Marahiel, M. A. (2010) SufU is an essential iron-sulfur cluster scaffold protein in Bacillus subtilis, *J Bacteriol 192*, 1643-1651.

163. Cardenas, J., Mortenson, L. E., and Yoch, D. C. (1976) Purification and properties of paramagnetic protein from Clostridium pasteurianum W5, *Biochim Biophys Acta 434*, 244-257.

164. Berry, E. A., and Trumpower, B. L. (1987) Simultaneous determination of hemes a, b, and c from pyridine hemochrome spectra, *Anal Biochem 161*, 1-15.

165. Lindahl, P. A., Morales, J. G., Miao, R., and Holmes-Hampton, G. (2009) Chapter 15 Isolation of Saccharomyces cerevisiae mitochondria for Mossbauer, EPR, and electronic absorption spectroscopic analyses, *Methods Enzymol 456*, 267-285.

166. Jhurry, N. D., Chakrabarti, M., McCormick, S. P., Gohil, V. M., and Lindahl, P. A. (2013) Mossbauer study and modeling of iron import and trafficking in human jurkat cells, *Biochemistry 52*, 7926-7942.

167. Holmes-Hampton, G. P., Chakrabarti, M., Cockrell, A. L., McCormick, S. P., Abbott, L. C., Lindahl, L. S., and Lindahl, P. A. (2012) Changing iron content of the mouse brain during development, *Metallomics 4*, 761-770.

168. Chakrabarti, M., Cockrell, A. L., Park, J., McCormick, S. P., Lindahl, L. S., and Lindahl, P. A. (2015) Speciation of iron in mouse liver during development, iron deficiency, IRP2 deletion and inflammatory hepatitis, *Metallomics 7*, 93-101.

169. Jhurry, N. D., Chakrabarti, M., McCormick, S. P., Holmes-Hampton, G. P., and Lindahl, P. A. (2012) Biophysical investigation of the ironome of human jurkat cells and mitochondria, *Biochemistry 51*, 5276-5284.

170. Breuer, W., Shvartsman, M., and Cabantchik, Z. I. (2008) Intracellular labile iron, *Int J Biochem Cell Biol 40*, 350-354.

171. New, E. J. (2013) Tools to study distinct metal pools in biology, *Dalton Trans 42*, 3210-3219.

172. Dudek, J., Rehling, P., and van der Laan, M. (2013) Mitochondrial protein import: common principles and physiological networks, *Biochim Biophys Acta 1833*, 274-285.

173. Benz, R. (1990) Biophysical properties of porin pores from mitochondrial outer membrane of eukaryotic cells, *Experientia 46*, 131-137.

174. Holmes-Hampton, G. P., Jhurry, N. D., McCormick, S. P., and Lindahl, P. A. (2013) Iron content of Saccharomyces cerevisiae cells grown under iron-deficient and iron-overload conditions, *Biochemistry 52*, 105-114.

175. Hudder, B. N., Morales, J. G., Stubna, A., Munck, E., Hendrich, M. P., and Lindahl, P. A. (2007) Electron paramagnetic resonance and Mossbauer spectroscopy of intact mitochondria from respiring Saccharomyces cerevisiae, *J Biol Inorg Chem 12*, 1029-1053.

176. Theobald, U., Mailinger, W., Baltes, M., Rizzi, M., and Reuss, M. (1997) In vivo analysis of metabolic dynamics in Saccharomyces cerevisiae .1. Experimental observations, *Biotechnol. Bioeng. 55*, 305-316.

177. Albe, K. R., Butler, M. H., and Wright, B. E. (1990) Cellular concentrations of enzymes and their substrates, *J Theor Biol 143*, 163-195.

178. Ash, D. E. (2004) Structure and function of arginases, *J Nutr 134*, 2760S-2764S; discussion 2765S-2767S.

179. Colleluori, D. M., and Ash, D. E. (2001) Classical and slow-binding inhibitors of human type II arginase, *Biochemistry 40*, 9356-9362.

180. Costello, L. C., Guan, Z., Franklin, R. B., and Feng, P. (2004) Metallothionein can function as a chaperone for zinc uptake transport into prostate and liver mitochondria, *J Inorg Biochem 98*, 664-666.

181. Chyan, W., Zhang, D. Y., Lippard, S. J., and Radford, R. J. (2014) Reaction-based fluorescent sensor for investigating mobile Zn2+ in mitochondria of healthy versus cancerous prostate cells, *Proc Natl Acad Sci U S A 111*, 143-148.

182. Amutha, B., Gordon, D. M., Gu, Y., Lyver, E. R., Dancis, A., and Pain, D. (2008) GTP is required for iron-sulfur cluster biogenesis in mitochondria, *J Biol Chem 283*, 1362-1371.

183. Pandey, A., Yoon, H., Lyver, E. R., Dancis, A., and Pain, D. (2012) Identification of a Nfs1p-bound persulfide intermediate in Fe-S cluster synthesis by intact mitochondria, *Mitochondrion 12*, 539-549.

184. Philpott, C. C., and Ryu, M. S. (2014) Special delivery: distributing iron in the cytosol of mammalian cells, *Front Pharmacol 5*, 173.

185. Havemeyer, A., Bittner, F., Wollers, S., Mendel, R., Kunze, T., and Clement, B. (2006) Identification of the missing component in the mitochondrial benzamidoxime prodrug-converting system as a novel molybdenum enzyme, *J Biol Chem 281*, 34796-34802.

186. Sparacino-Watkins, C. E., Tejero, J., Sun, B., Gauthier, M. C., Thomas, J., Ragireddy, V., Merchant, B. A., Wang, J., Azarov, I., Basu, P., and Gladwin, M. T. (2014) Nitrite reductase and nitric-oxide synthase activity of the mitochondrial molybdopterin enzymes mARC1 and mARC2, *J Biol Chem 289*, 10345-10358.

187. Lill, R., Dutkiewicz, R., Freibert, S. A., Heidenreich, T., Mascarenhas, J., Netz, D. J., Paul, V. D., Pierik, A. J., Richter, N., Stumpfig, M., Srinivasan, V., Stehling, O., and Muhlenhoff, U. (2015) The role of mitochondria and the CIA machinery in the maturation of cytosolic and nuclear iron-sulfur proteins, *Eur J Cell Biol 94*, 280-291.

188. Muhlenhoff, U., Hoffmann, B., Richter, N., Rietzschel, N., Spantgar, F., Stehling, O., Uzarska, M. A., and Lill, R. (2015) Compartmentalization of iron between mitochondria and the cytosol and its regulation, *Eur J Cell Biol 94*, 292-308.

189. Foury, F., and Roganti, T. (2002) Deletion of the mitochondrial carrier genes MRS3 and MRS4 suppresses mitochondrial iron accumulation in a yeast frataxin-deficient strain, *J Biol Chem 277*, 24475-24483.

190. Paradkar, P. N., Zumbrennen, K. B., Paw, B. H., Ward, D. M., and Kaplan, J. (2009) Regulation of mitochondrial iron import through differential turnover of mitoferrin 1 and mitoferrin 2, *Mol Cell Biol 29*, 1007-1016.

191. Chen, W., Paradkar, P. N., Li, L., Pierce, E. L., Langer, N. B., Takahashi-Makise, N., Hyde, B. B., Shirihai, O. S., Ward, D. M., Kaplan, J., and Paw, B. H. (2009) Abcb10 physically interacts with mitoferrin-1 (Slc25a37) to enhance its stability and function in the erythroid mitochondria, *Proc Natl Acad Sci U S A 106*, 16263-16268.

192. Lindahl, P. A., and Moore, M. J. (2016) Labile low-molecular-mass metal complexes in mitochondria: trials and tribulations of a burgeoning field, *Biochemistry 55*, 4140-4153.

193. Chen, O. S., Crisp, R. J., Valachovic, M., Bard, M., Winge, D. R., and Kaplan, J. (2004) Transcription of the yeast iron regulon does not respond directly to iron but rather to iron-sulfur cluster biosynthesis, *J Biol Chem 279*, 29513-29518.

194. Lin, H., Li, L., Jia, X., Ward, D. M., and Kaplan, J. (2011) Genetic and biochemical analysis of high iron toxicity in yeast: iron toxicity is due to the accumulation of cytosolic iron and occurs under both aerobic and anaerobic conditions, *J Biol Chem 286*, 3851-3862.

195. Li, L., Murdock, G., Bagley, D., Jia, X., Ward, D. M., and Kaplan, J. (2010) Genetic dissection of a mitochondria-vacuole signaling pathway in yeast reveals a link between chronic oxidative stress and vacuolar iron transport, *J Biol Chem 285*, 10232-10242.

196. Li, L., Chen, O. S., McVey Ward, D., and Kaplan, J. (2001) CCC1 is a transporter that mediates vacuolar iron storage in yeast, *J Biol Chem 276*, 29515-29519.

197. Liao, G. L., and Palmer, G. (1996) The reduced minus oxidized difference spectra of cytochromes a and a3, *Biochim Biophys Acta 1274*, 109-111.

198. Wofford, J. D., and Lindahl, P. A. (2015) Mitochondrial iron-sulfur cluster activity and cytosolic iron regulate iron traffic in Saccharomyces cerevisiae, *J Biol Chem 290*, 26968-26977.

199. Huang, M. L., Becker, E. M., Whitnall, M., Suryo Rahmanto, Y., Ponka, P., and Richardson, D. R. (2009) Elucidation of the mechanism of mitochondrial iron loading in Friedreich's ataxia by analysis of a mouse mutant, *Proc Natl Acad Sci U S A 106*, 16381-16386.

200. Savary, S., Allikmets, R., Denizot, F., Luciani, M. F., Mattei, M. G., Dean, M., and Chimini, G. (1997) Isolation and chromosomal mapping of a novel ATP-binding cassette transporter conserved in mouse and human, *Genomics 41*, 275-278.

201. Delatycki, M. B., Williamson, R., and Forrest, S. M. (2000) Friedreich ataxia: an overview, *J Med Genet 37*, 1-8.